THE ROLE OF SELECTIVE AUTOPHAGY AND CELL SIGNALING IN FUNGAL DEVELOPMENT AND PATHOGENESIS

YUNLONG HE

NATIONAL UNIVERSITY OF SINGAPORE

2014

DECLARATION

I hereby declare that this thesis is my original work and it has been written by me in its entirety. I have duly acknowledged all the sources of information, which have been used in this thesis.

This thesis has not been submitted for any degree in any university previously.

He yunlong

Yunlong He

February 4, 2015

THE ROLE OF SELECTIVE AUTOPHAGY AND CELL SIGNALING IN FUNGAL DEVELOPMENT AND PATHOGENESIS

YUNLONG HE

A THESIS SUBMITTED

FOR THE DEGREE OF DOCTOR OF PHILOSOPHY

TEMASEK LIFE SCIENCES LABORATORY

and

NATIONAL UNIVERSITY OF SINGAPORE

ACKNOWLEDGEMENTS

First and foremost I would like to thank my supervisor Dr. Naweed Naqvi. It has been my great pleasure to work in his lab on rice blast fungus, *M. oryzae*. I appreciate the contributions of his time, ideas and guidance to make my Ph.D experience wonderful.

The members of the Naweed group have contributed immensely to my personal and professional time. The group has been a source of friendship as well as good advice and collaboration. All the past and present members who assisted me during my Ph.D research are Yang Fan, Qu Ziwei, Deng Yizhen, Kou Yanjun, Patkar Rajesh, Ravikrishma Ramanujam and Selvaraj Poonguzhali.

In regards to mitophagy related work, I thank Deng Yizhen who guided me and helped me during this whole project. In related to image analysis, I would like to thank the TLL confocal training facility for image analysis using ImageJ and how to build up 3D models from stacks of images.

For this dissertation, I would like to thank my thesis committee members: Dr Gregory Jedd, Dr Mohan Balasubramanian and Dr Wang Yue.

My time at Singapore was made enjoyable due to many friends and groups that became a part of my life. I am grateful for the time spent with my friends for our memorable trips into many beautiful places.

Lastly, I would like to thank my family for all their love and encouragement. Without their support, it would have been impossible for me to finish my Ph.D study. Thank you.

TABLE OF CONTENTS

CHAPTER 1. INTRODUCTION 1
1.1 General introduction to mitochondria 1
1.1.1 The structure of mitochondria in eukaryotic cells 1
1.1.2 The fission and fusion machineries of mitochondria 2
1.1.3 The function of mitochondrial dynamics 6
1.1.4 Mitochondria-to-Nucleus signaling 8
1.1.5 Mitophagy 12
1.2 General introduction to *Magnaporthe oryzae* 15
1.2.1 Pathogenic life cycle of *M. oryzae* 15
1.2.2 Metabolic reprograming 21
1.3 Aims and objectives of this study 22
1.4 Significance of this study 23
CHAPTER II MATERIALS AND METHODS 24
2.1 Strains, Growth conditions and Reagents 24
2.1.1 *M. oryzae* and Growth conditions 24
2.1.2 *Agrobacterium tumefaciens* strains and culture medium 27
2.2 Molecular Methods 27
2.2.1 DNA techniques 27
2.2.2 RNA techniques 35
2.3 Staining protocols 39
2.3.1 Vacuolar staining 39
2.3.2 Mitochondrial staining 39
2.3.3 Nuclear staining 39
2.3.4 Trypan blue and aniline blue staining 40
2.4 Protein and immunoblotting related methods 40
2.4.1 Total protein lysates from *M. oryzae* (Denatured) 40
2.4.2 Protein electrophoresis, immunoblots and reprobing protocols. 41
2.5 Infection assays and virulence assessment 42
2.5.1 Barley infection with *M. oryzae* conidia 42
2.5.2 Rice seedling related methods and infection with *M. oryzae* conidia 42
2.5.3 Rice sheath infection assay 43
2.6 Microscopy 43

2.6.1 Epifluorescent Microscopy 43
2.6.2 Confocal Microscopy 44
2.6.3 Imaging analysis 44
CHAPTER III MITOPHAGY IS REQUIRED FOR PROPER PATHOGENESIS IN *M. ORYZAE* 45
3.1 Introduction 45
3.2 Results 47
3.2.1 Generation of *Moatg24*Δ 47
3.2.2 Loss of *MoATG24* leads to decreased aerial hyphae and conidiation 47
3.2.3 Loss of *MoATG24* leads to decreased invasive growth 51
3.2.4 Subcellular localization of MoAtg24-GFP upon starvation induction or in presence of oxidative stress 52
3.2.5 MoAtg24 is essential for mitophagy 53
3.2.6 MoAtg24 is not involved in macroautophagy or pexophagy 54
3.2.7 MoAtg24 colocalizes with mitochondria and RFP-MoAtg8 during mitophagy 55
3.2.8 Domain analysis of PX and BAR domains in MoAtg24 62
3.2.9 Phospholipid PI3P is enriched on mitochondria 62
3.2.10 Mitophagy occurs naturally in foot cells during conidiation 65
3.2.11 Mitophagy occurs naturally during invasive growth 65
3.2.12 GFP-ScAtg32 associates with mitochondria in *M. oryzae* 68
3.2.13 GFP-ScAtg32 partially restored the conidiation defects in *Moatg24*Δ 68
3.2.14 *Moatg24*Δ is hypersensitive to oxidative stresses. 71
3.3 Discussion 71
CHAPTER IV MITOCHONDRIAL DYNAMICS DURING HOST-PATHOGEN INTERACTION IN THE RICE BLAST PATHOGENESIS 75
4.1 Introduction 75
4.2 Results 78
4.2.1 Invasive growth of *M. oryzae* 78
4.2.2 Mitochondrial dynamics during invasive growth in *M. oryzae* 80
4.2.3 Mitochondrial dynamics mediates biotrophy to necrotrophy switch 82
4.2.4 Mitochondrial fission machinery involved in invasive growth 82
4.2.5 Mitochondrial fission is required for pathogenicity 87
4.2.6 Disruption of mitochondrial fission prevents biotrophy to necrotrophy switch 87

4.2.7 Mitochondrial fusion machinery 91
4.2.8 Loss of mitochondrial fusion disrupts maintenance of biotrophy. 93
4.2.9 Effect of anti-oxidants on mitochondrial dynamics in invasive hyphae 95
4.2.10 Effect of carbon metabolism on mitochondrial dynamics 97
4.2.11 Glucose 6-phosphate delays mitochondrial fragmentation 97
4.2.12 Mitochondrial dysfunction during *in planta* growth 100
4.2.13 Mitochondrial dysfunction activates MoRtg2 expression 103
4.2.14 MoRtg2 expression triggers mCherry-MoRtg3 translocation 103
4.2.15 MoRtg2 is required for the biotrophy to necrotrophy switch 106
4.3 Discussion 110
CHAPTER V GENERAL DISCUSSIONS AND CONCLUSIONS 112
REFERENCES 117
APPENDIX 129

SUMMARY

The mitochondrion is a conserved double-membrane bound organelle found in most eukaryotic cells. They provide most of the cellular energy, ATP, through tricarboxylic acid cycle during catabolic growth or glyoxylate cycle during anabolic growth. In addition to ATP generation, mitochondria also fuse and divide actively, in response to various metabolic or environmental stresses, which plays an essential role in quality control and abundance of mitochondria. Mitochondrial dynamics (mitochondrial fission and fusion) has been widely studied in many developmental processes and diseases. However, limited information is available on the function of mitochondrial dynamics during host pathogen interaction.

Magnaporthe oryzae (*M. oryzae*) is a filamentous fungus, which causes the rice blast disease. Its hemibiotrophic *in planta* growth consists of an initial biotrophic stage and a subsequent necrotrophic stage. Although the mechanisms involved in hemibiotrophic growth are unknown, the morphological changes in invasive growth of *M. oryzae* have been clearly documented, which makes it a good model system to understand the mechanisms underlying host interaction with hemibiotrophic pathogens.

In this study, mitochondrial dynamics was first observed at the biotrophy to necrotrophy switch stage during Magnaporthe-Rice interaction. Subsequently, I found that disruption of mitochondrial dynamics by deleting mitochondrial fusion or fission machineries highly reduces the pathogenicity of *M. oryzae*.

Characterization of the *Mofzo1*Δ mutant uncovers that mitochondrial fusion is required to maintain biotrophic growth while mitochondrial fission is required for biotrophy to necrotrophy switch based on the study of the mitochondrial fission mutant *Modnm1*Δ. Furthermore, the mitochondrial dynamics during invasive growth could be delayed by endogenous carbon sources but not antioxidant treatment, which suggest that nutrient limitation regulates mitochondrial dynamics during invasive growth. Subsequently, I identified the metabolic intermediate Glucose-6-phosphate (G-6-P) as a key factor that affects invasive growth and mitochondrial dynamics. A possible pathway that functions downstream of the mitochondrial dynamics during invasive growth, is likely the mitochondria-to-nucleus retrograde signaling based on the translocation of mCherry-Rtg3 from cytosol into the nucleus (this translocation occurs upon activation of mitochondria-to-nucleus retrograde pathway) during mitochondrial fragmentation. The disruption of such retrograde pathway led to highly reduced pathogenicity in *M. oryzae*.

In addition to mitochondrial fusion and fission, mitophagy also regulates the turnover of mitochondria. Atg24 was identified as the mitophagy-specific mediator in *M. oryzae*. Deletion of *MoATG24* resulted in disruption of mitophagy, without affecting macroautophagy or other types of selective autophagy. Highly reduced conidiation and restrained invasive growth were observed in *Moatg24*Δ, which indicates that mitophagy plays important roles in conidiation and invasive growth. Moreover, confocal microscopic images revealed that mitophagy naturally occurs during conidiation and invasive

growth, which were found lacking in the *Moatg24*Δ mutant. Thus, MoAtg24 mediated mitophagy in *M. oryzae* regulates conidiation and invasive growth.

To summarize, mitochondrial dynamics and turnover are required for proper asexual development and pathogenesis in *M. oryzae*.

LIST OF FIGURES

Figure 1. General schematic representation of mitochondrial fission and fusion. **5**

Figure 2. Mitochondrial retrograde pathway. **9**

Figure 3. Schematic representation of *M. oryzae* life cycle. **17**

Figure 4. Generation of *Moatg24*Δ. **49**

Figure 5. Colony growth and conidiation of *Moatg24* mutant. **50**

Figure 6. MoAtg24 is required for proper pathogenicity of *M. oryzae.* **56**

Figure 7. MoAtg24-GFP localizes to mitochondria upon ROS and starvation induction. **57**

Figure 8. MoAtg24-RFP does not localize to the peroxisomes. **58**

Figure 9. Atg24 is required for mitophagy in *M. oryzae*. **59**

Figure 10. MoAtg24 is not essential for macroautophagy or pexophagy. **60**

Figure 11. MoAtg24 colocalizes with mitochondria and RFP-MoAtg8 during mitophagy. **61**

Figure 12. PX and BAR domains are required for mitochondrial anchoring of MoAtg24. **63**

Figure 13. Phospholipid PI3P is enriched on mitochondrial membrane. **64**

Figure 14. Mitophagy occurs in foot cells during Magnaporthe conidiation. **66**

Figure 15. Mitophagy during invasive growth in Magnaporthe. **67**

Figure 16. GFP-ScAtg32 localizes to mitochondria in *M. oryzae*. **69**

Figure 17. Conidiation defect of *Moatg24*Δ is partially repressed by expressing GFP-ScAtg32. **70**

Figure 18. *Moatg24*Δ is hypersensitive to oxidative stress. **72**

Figure 19. Classification of invasive hyphae. **79**

Figure 20. Mitochondrial morphology during host-pathogen interaction. **81**

Figure 21. Biotrophy to necrotrophy switch occurs between 48 hpi and 72 hpi. **84**

Figure 22. Generation of *Modnm1*Δ. **85**

Figure 23. The function of MoDnm1 in mitochondrial fission in *M. oryzae*. **86**

Figure 24. Mitochondrial fission is required for proper pathogenesis of *M. oryzae*. **89**

Figure 25. Mitochondrial fission is required for biotrophy to necrotrophy switch in *M. oryzae*. **90**

Figure 26. Mitochondrial morphology in *Mofzo1*Δ. **92**

Figure 27. Mitochondrial fusion is required for proper pathogenesis of *M. oryzae*. **94**

Figure 28. Antioxidant treatment could not delay mitochondrial dynamics during invasive growth. **96**

Figure 29. Carbon source could delay mitochondrial dynamics *in planta*. **98**

Figure 30. G-6-P could delay mitochondrial dynamics. **99**

Figure 31. mCherry-MoYbh3 translocates into mitochondria during mitochondrial dynamics. **102**

Figure 32 MoRtg2is upregulated at 48 hpi. **104**

Figure 33. MoRtg3 translocates into nucleus at 48 hpi during invasive growth. **105**

Figure 34. Generation of *Mortg2*Δ. **106**

Figure 35. MoRtg2 is required for proper pathogenesis in *M. oryzae*. **107**

LIST OF TABLES

Table 1. The Magnaporthe strains used in this study **25**

Table 2. Oligonucleotide primers used in this study **29**

Table 3. Oligonucleotide primers used for RT-PCR in this study **38**

LIST OF ABBREVATIONS

Atg	Autophagy related gene
PA	Prune agar
CM	Complete medium
BM	Basal medium
MM	Minimal medium
MM-N	Minimal medium minus nitrogen
G-1-P	Glucose 1-phosphate
G-6-P	Glucose 6-phosphate
h	Hour
hpi	Hour post inoculation
ORF	Open reading frame
PAGE	Polyacrylamide gel electrophoresis
RT-PCR	Reverse transcription polymerase chain reaction
SDS	Sodium dodecyl sulphate
WT	Wild type
NAC	N-acetyl-cysteine
RT	Room temperature
CMAC	7-amino-4-chloromethylcoumarin

PUBLICATIONS

First author publication

He, Y., Deng, Y.Z., Naqvi, N.I. **Atg24-assisted mitophagy in the foot cells is necessary for proper asexual differentiation in *Magnaporthe oryzae***. Autophagy 2013; 9: 1818 – 1827.

Co-author publication

Deng, Y.Z., Qu, Z., He, Y., Naqvi, N.I. **Sorting nexin Snx41 is essential for conidiation and mediates glutathione-based antioxidant defense during invasive growth in *Magnaporthe oryzae***. Autophagy 2012; 8: 1058 – 1070.

CHAPTER 1. INTRODUCTION

1.1 General introduction to mitochondria

The mitochondrion, a semi-autonomous double-membrane bound organelle, exists in nearly all eukaryotes (Green 1983). They generate most of the cellular adenosine triphosphate (ATP) through tricarboxylic acid cycle (Azzi & Chance 1969, Cockrell et al 1967, Witter et al 1955). In addition to supplying ATP, mitochondria also function as an important signaling platform, conducting cellular signaling, regulating cell death, controlling cell cycle, and incorporating cell differentiation and cell proliferation (Amuthan et al 2001, Bao et al 2009, Cottrell 1982, Finkel & Hwang 2009, Giorgi et al 2008, Levonen et al 2001, Smaili et al 2003). Mitochondria have also been proposed to be the damaged cellular sites in multiple serious human diseases, such as respiratory disorders and cardiac dysfunction, and to be the key organelles directly involved in ageing (Bodemer et al 1999, Lee & Sokol 2007, Malpass 2013, Moustris et al 2011, Sack & Finkel 2012, Yin et al 2014). Therefore, it is crucial to review the current understandings of mitochondria, in order to study the function of mitochondria in fungal pathogenesis.

1.1.1 The structure of mitochondria in eukaryotic cells

The structure of mitochondria is relatively complicated compared to other organelles, because mitochondria consist of several compartments which execute specialized and unique functions. These compartments are the outer

membrane, the inter membrane space, the inner membrane, the cristae, the matrix and the mitochondrial DNA. The entire organelle is enclosed by the outer mitochondrial membrane that is crucial to transport cytosolic proteins into mitochondria selectively and is essential to mediate ER-mitochondria calcium signaling (Nicholls 2005). The inter membrane space stores cytochrome c which is essential in mitochondrial electron transport and apoptosis (Giege et al 2008, Odinokova et al 2009). The inner mitochondrial membrane anchors proteins which function in oxidative phosphorylation, selective transportation of metabolite into and out of the matrix, ATP synthesis, import of proteins containing mitochondrial targeting sequence (MTS), and mitochondrial fusion and division (Evtodienko et al 2000). The cristae, the compartmentalized inner mitochondrial membrane, enhances the ability to produce ATP. The space encompassed by the inner membrane is a matrix, which accommodates about two-third of the total proteins in a mitochondrion. The matrix is also important for the ATP generation because a part of the ATP synthase is present in the matrix. Mitochondrial DNA encodes some of the essential proteins for mitochondrial replication and proliferation.

1.1.2 The fission and fusion machineries of mitochondria

The machineries of mitochondrial fission and fusion are well conserved from yeast to mammals (Pan & Hu 2011, Polyakov et al 2003). Mitochondrial fission is directly mediated by a cytosolic dynamin-like protein (Dnm1) in yeast (Figure 1). In addition, other important proteins involved in mitochondrial fission are Fis1, the membrane anchor protein, and Mdv1/Caf4,

the adaptor proteins. Fis1 is upregulated upon induction of mitochondrial fission and then transported into the mitochondrial outer membrane, where its C-terminal transmembrane domain anchors Fis1 at the division sites. The cytosolic N-terminal domain of Fis1 forms a six-helix bundle with the tandem tetratricopeptide repeat (TPR) that provides a surface for interaction with the adaptor proteins Mdv1/Caf4 (Zhang et al 2012). Mdv1 and Caf4 share the same domains and perform redundant functions during mitochondrial fission. Mdv1 or Caf4 binds to Fis1 through hetero-oligomeric interaction, which is mediated by a heptad repeat region in Mdv1/Caf4 N-terminal extension. Subsequently, Mdv1 or Caf4 recruits Dnm1 through their C-terminal WD40 repeat domains (Tieu et al 2002, Zhang et al 2012). Afterwards, the Dnm1 forms a spiral ring at the mitochondrial division plate to constrict both inner and outer membranes (Ingerman et al 2005). Overall, the Fis1-Mdv1/Caf4-Dnm1 complex mediates mitochondrial fission through protein-protein interaction. Loss of either Fis1 or Dnm1 results in highly interconnected fishnet-like mitochondria (Bleazard et al 1999, Jakobs et al 2003).

Mitochondrial fusion is mediated by the transmembrane GTPase Fzo1 in yeast (Figure 1). During fusion, two mitochondria approach each other and are tethered in a docking step. Such tethered step is mediated by Fzo1 through its C-terminal heptad repeats which form an intermolecular antiparallel coiled coil (Fritz et al 2001). This antiparallel coiled coil formation is thought to draw the membranes close together and initiate lipid bilayer mixing, during which Fzo1 provides necessary biochemical energy to overcome the membrane fusion barrier. The inner membrane fusion is mainly mediated by a membrane-

anchored dynamin related protein (Mgm1) in yeast (Sesaki et al 2003). To link the outer membrane and inner membrane fusion machineries, a protein named Ugo1 physically interacts with both Fzo1 and Mgm1 to pull the mitochondrial outer and inner membranes fusion machineries together (Sesaki & Jensen 2004). Loss of either Fzo1 or Mgm1 results in numerous small mitochondrial fragments.

Rates of mitochondrial division and fusion are mainly controlled by metabolic status. When mitochondria are forced to use oxidative phosphorylation to generate energy, they become more fused, as the increased fusion maximizes the fidelity for oxidative phosphorylation (Chen & Chan 2010, Zorzano et al 2004). Mitochondrial fusion can also be enhanced by protein synthesis inhibition, starvation-induced autophagy or mTOR inhibition induced autophagy (Zhang et al 2009). Cellular energy is provided more by oxidative phosphorylation in starved cells, which finally leads to increase mitochondrial fusion. Meanwhile, starvation might activate a specific stress response inducing mitochondrial hyperfusion or may inhibit fission to protect mitochondria from mitophagy (Redpath et al 2013, Tondera et al 2009). Similarly, protein synthesis inhibition and mTOR inhibition induced autophagy also trigger stress-induced mitochondrial hyperfusion. Taken together, all of these effects support that mitochondrial dynamics is directly associated with stress conditions and/or cellular metabolic status.

Figure 1. General schematic representation of mitochondrial fission and fusion.

Mitochondrial morphology is largely regulated by the balance of fusion and fission. Schematic representation of mitochondrial fusion and fission is shown and the essential proteins Fis1, Dnm1, Fzo1 and Mgm1 are labeled in different colors.

Figure 1

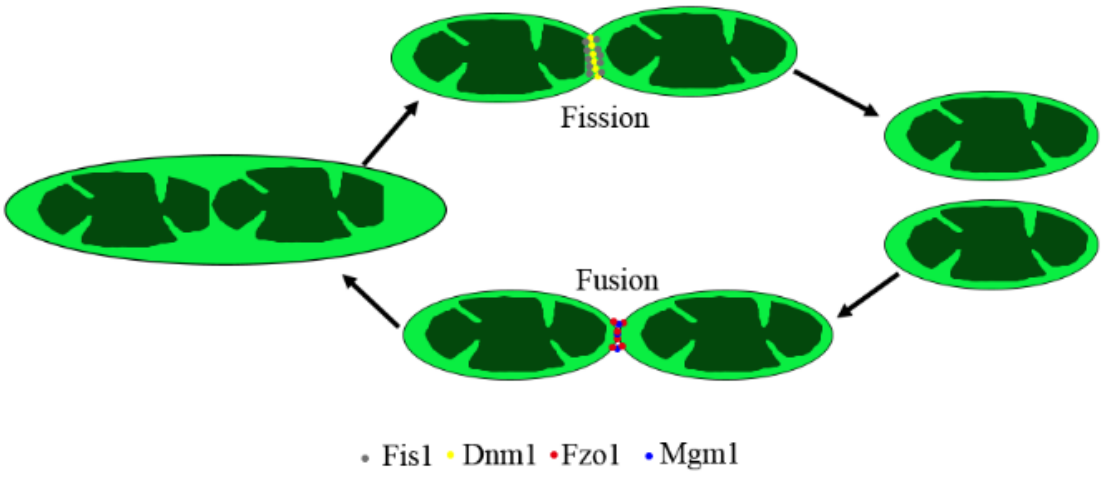

1.1.3 The function of mitochondrial dynamics

During metabolism, highly reactive superoxide anions are produced as byproducts of electron transport during oxidative phosphorylation in mitochondria (Inoue et al 2003, Murphy 2009). In healthy cells, such small amount of reactive oxygen species (ROS) produced by mitochondria can be neutralized by cellular antioxidants. However, if mitochondria are damaged, the amount of ROS produced far exceeds the ability of neutralization by cellular antioxidants, and herein the excessive ROS would damage proteins, lipids, and DNA (Scherz-Shouval & Elazar 2007). Depending on the degree of mitochondrial damage, cells are either rescued by damage-response pathways or by complete elimination of damaged mitochondria through mitophagy (Battersby & Richter 2013, Scherz-Shouval & Elazar 2007). Damage-response pathways do not alter the fission or fusion rate, while mitophagy directly relies on mitochondrial fission and fusion (Novak 2012, Pallanck 2013).

Another very important cellular process involved in mitochondrial fission and fusion is apoptosis. Mitochondrial fission and apoptosis seem to be mutually affected downstream pathways induced by multiple cell stresses. During apoptosis, Bax (the apoptosis regulator) translocates to mitochondria, and helps to lock Drp1 (the homolog of yeast Dnm1) on mitochondrial outer membrane, indicating that mitochondrial fission is involved in apoptosis (Chattopadhyay et al 2010, Edlich et al 2011). The possible role of mitochondrial fission in apoptosis is to accelerate Bax-mediated permeabilization of the mitochondrial outer membrane, although the exact role

of mitochondrial fission in apoptosis is not clear (Upton et al 2007). More interestingly, Bcl-1 family members (apoptosis key regulators) also participate in mitochondrial fusion and division in non-apoptotic cells by affecting autophagy and mitochondrial function (Volkmann et al 2014).

Mitochondrial dynamics also highly correlates with yeast cell death which is either dependent on the yeast caspase 1 (Yca1) or promoted by apoptosis-inducing factor 1 (Aif1) and endonuclease G (Nuc1) in a Yca1 independent manner. Activation of Yca1 results in the release of cytochrome c from mitochondria and herein causes yeast cell death (Guaragnella et al 2006). In the Yca1 independent pathway, Aif1 and Nuc1 are released from mitochondria and then translocate into the nucleus, resulting in the fragmentation of the nuclear genome (Buttner et al 2007, Ludovico et al 2002, Wissing et al 2004). Regardless of the pathways activating yeast cell death, fragmented mitochondria always highly correlate to cell death. The role of mitochondrial dynamics in yeast cell death is further confirmed based on that deletion of Dnm1 or Mdv1 leads to increased resistances against cell death stressors.

Taken these lines of evidence together, mitochondrial dynamics affects ROS production at individual mitochondrion level and is involved in apoptosis at the whole-cell level.

1.1.4 Mitochondria-to-Nucleus signaling

Based on the research reviewed above, it is clear that mitochondrial dynamics is directly linked to stress signals and the metabolic status. The controversial scenario is that mitochondria are the sensors of the stress signals while most genes required to be upregulated to compensate the stresses are present in the nucleus. Therefore, the spatial gap between the place where the stress is sensed and the place where the cell acts upon is undeniable. Thus, there should be some pathways, which close the gap between mitochondrial sensing and nuclear gene regulation. In fact, several mitochondria-to-nucleus signaling pathways have been described. Among them, the most well studied pathway is the retrograde response in the budding yeast *Saccharomyces cerevisiae* (Butow & Avadhani 2004, Jazwinski 2004, Liu & Butow 2006). The initial efforts to uncover this pathway come along with the studies of *CIT2* (Citrate synthase 2), which is involved in the glyoxylate cycle. *CIT2* transcription is upregulated as high as 50- to 60-fold in cells containing dysfunctional mitochondria (Kim et al 1986, Liao et al 1991). And herein the *CIT2* transcription upregulation is initiated by mitochondrial damage. Later on, researchers found that *CIT2* transcription is controlled by three positive regulatory factors, Rtg1, Rtg2 and Rtg3 (retrograde response genes 1, 2 and 3) and four negative regulators, Mks1 (Multicopy Kinase Suppressor 1), Lst8, Bmh1 and Bmh2 (Figure 2) (Guha & Avadhani 2013, Liao & Butow 1993).

Figure 2. Mitochondrial retrograde pathway.

The mitochondrial retrograde pathway is adapted from Jazwinski and Kriete (2012). Upon mitochondrial damage, Rtg1/3 complex is transported into the nucleus to upregulate target genes expression. The Rtg1/3 binding sequence is named as R-box. Mks1 and Lst8 negatively regulate Rtg1/3 translocation from cytosol to nucleus, by phosphorylating Rtg3. Rtg2 negatively regulates Mks1 phosphorylation of Rtg3.

Figure 2

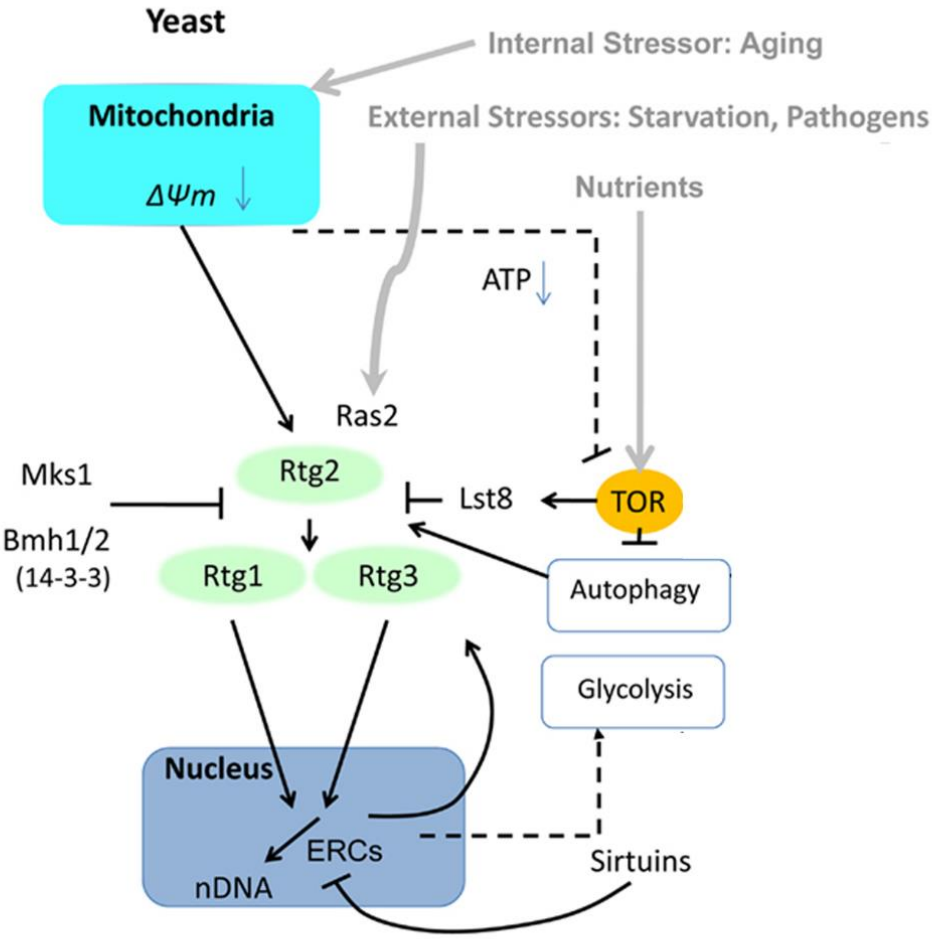
Yeast
Internal Stressor: Aging
Mitochondria
ΔΨm
External Stressors: Starvation, Pathogens
Nutrients
ATP
Ras2
Mks1
Rtg2
Lst8
TOR
Bmh1/2
(14-3-3)
Rtg1
Rtg3
Autophagy
Glycolysis
Nucleus
ERCs
nDNA
Sirtuins

Among such regulators, Rtg2 is the proximal sensor of mitochondrial dysfunction. Although it is unclear how Rtg2 senses mitochondrial damage, Rtg2 activity has been shown to be sensitive to a number of metabolic cues, such as glutamate and nutrient-sensitive kinase target of rapamycin complex I (TORC1) (Chen et al 2010). The most important domain in Rtg2 is its N-terminal ATP binding motif. The integrity of N-terminal ATP binding motif is essential for Rtg2 function, as it monitors the mitochondrial ATP production rate.

Rtg1 and Rtg3 are basic helix-loop-helix-leucine zipper (bHLH-Zip) transcription factors, which bind R boxes, GTCAC, in the promoter region to activate gene expression (Liao & Butow 1993). When the retrograde pathway is off, Rtg1 and Rtg3 are sequestered together in the cytoplasm where Rtg3 is phosphorylated at multiple sites (Sekito et al 2002). When mitochondria are damaged, Rtg2 senses the signal, and then activates Rtg1 and Rtg3 to form a complex. Consequently, the Rtg1/Rtg3 complex translocates into the nucleus to upregulate downstream target genes. In cells lacking Rtg2, Rtg3 becomes hyperphosphorylated and the Rtg1/3 complex is retained in cytosol, no longer responsive to mitochondrial damage signals. Thus, the specific intracellular localization of the Rtg1/3 complex is the key control point of the RTG-dependent retrograde response. And Rtg2 appears to play a unique role in dictating where the Rtg1/3 complex resides. The relevant kinases and phosphatases that modify Rtg3 are discussed below.

The detailed mechanism of Rtg2 regulating the Rtg1/3 complex has been elucidated recently. A key observation of the role of Rtg2 in RTG pathway is that Rtg2 could dynamically interact with Mks1, the negative regulator of RTG pathway (Liu et al 2003). When the RTG pathway is on, Mks1, a phosphoprotein, is captured by Rtg2 and dephosphorylated to form a complex. If Mks1 is phosphorylated by Bmh1 and Bmh2 (the 14-3-3 proteins), it will no longer interact with Rtg2 and consequently terminates the RTG pathway (Figure 2). Although the detailed molecular mechanism of how Mks1 modifies Rtg1/3 to prevent Rtg1/3 nuclear accumulation is unclear, the interaction between Mks1 and Bmh1 or Bmh2 has been shown to function as a negative regulator (Figure 2) (Liu et al 2003). By contrast, the molecular mechanism responsible for Mks1 and Rtg2 interaction is better documented. Such interaction is dependent on the Rtg2 ATP binding motif, which is confirmed from the studies of the Rtg2 point mutations. Mutation in or close to the conserved region of Rtg2 ATP binding motif blocks interaction with Mks1 and inactivates RTG downstream gene expression, because ATP hydrolysis is an essential step of Rtg2 capture of Mks1. Finally, Rtg2 might also directly bind to the CIT2 promoter to activate its expression, which seems unrelated to the retrograde signaling (Liu & Butow 1999).

Inhibition of RTG pathway by altering any key positive regulators of the RTG genes results in highly decreased respiratory rates in cells containing dysfunctional mitochondria. Such decrease of respiratory rates is caused by the repressed TCA activity. In cells with robust respiratory activities, genes responsible for the TCA are under the control of a Hap2/3/4 transcriptional complex. However, as the respiratory activity declines, these genes are regulated by the RTG pathway to maintain respiratory rates at a relative higher level (Figure 2) (Fendt & Sauer 2010, Liu & Butow 1999). If RTG pathway is off, the respiratory rate will further decrease close to zero. Therefore, the role of the RTG pathway in lower respiratory activity cells or respiratory-deficient cells is important.

1.1.5 Mitophagy

During retrograde signaling, damaged mitochondria are delivered into vacuoles for degradation to void the excessive ROS generation. One of the well-studied mechanisms for mitochondrial degradation is mitophagy, a cargo-specific autophagy that mediates the selective removal of mitochondria (Song et al 2014, Youle & Narendra 2011). In yeast and mammalian cells, damaged mitochondrial fragments are first separated out of the whole mitochondria through mitochondrial fission, which also ensures that the size of mitochondrial pieces are manageable for encapsulation during mitophagy (Mao & Klionsky 2013). Afterwards, the damaged mitochondrial compartments are engulfed by autophagic membranes to form autophagosomes. Finally, such autophagosomes fuse with the vacuoles to

deliver cargos for degradation. Beyond quality control, mitophagy has also been shown to be required to regulate the number of mitochondria in response to metabolic requirements during development of specific cell types, such as during the red blood cell differentiation and the fermentation in yeast (Ding & Yin 2012, Youle & Narendra 2011).

1.1.5.1 Autophagy

To understand the molecular mechanism of mitophagy, it is important to review the autophagy pathway since mitophagy shares the core machinery with the autophagy pathway. Autophagy, by terms, describes cell self-eating. Autophagy is a multistep cellular process, including pre-autophagosomal structure (PAS) formation, PAS expansion, cargo recognition, autophagosome-vacuole fusion (Kanki & Klionsky 2010, Stromhaug & Klionsky 2001, Wang & Klionsky 2003, Yang & Klionsky 2009). PAS formation is initiated by the accumulation of Phosphatidylinositol 3-phosphate (PI3P) on the ER or mitochondrial membranes (Hailey et al 2010, Matsunaga et al 2010). Subsequently, PI3P recruits Atg9, the membrane transporter, onto the site to form the PAS. Meanwhile, Atg8 is processed by the Atg12-Atg5 complex to couple to phosphatidylethanolamine (Atg8-PE). Atg8-PE formation is the critical step to anchor the membrane fragments to PAS and then mediates the expansion and elongation of PAS. During this process, cytoplasmic contents are engulfed non-selectively. However, if specific cargos are required to be degraded through this process, the cargos are selectively brought to the PAS by cargo-specific mediators. Mature autophagosomes

finally fuse with vacuoles, which is mediated by the Atg18 complex. Finally, the contents of the autophagosomes are degraded by the vacuolar enzymes. Disruption of any of the aforementioned steps blocks the autophagy pathway.

1.1.5.2 Molecular mechanism of mitophagy

The molecular mechanism of mitophagy has recently been studied in yeast and mammalian cells. Briefly, upon mitophagy induction, a mitophagy specific mediator is translocated onto mitochondrial outer membrane, suggesting that such mitophagy mediator should have the ability to bind to mitochondrial outer membrane. Besides, the mediator should interact with the core machinery of autophagy, which includes Atg8 and Atg11. In yeast, this mediator is shown to be Atg32, which contains a mitochondrial outer membrane domain and a WXXL-like Atg8-binding motif (Kanki et al 2009, Okamoto et al 2009). In red blood cells, this mediator is NIX (NIP3-like protein X), which localizes to OMM and also contains a WXXL-like motif facing the cytosol and the WXXL-like motif indeed binds to LC3 (Atg8 homologue), and the LC3 related, GABA receptor-associated protein (GABARAP), in vitro and in vivo (Ding et al 2010b). Depletion of Atg32 in yeast or NIX in mammalian cells does not affect the function of mitochondria, indicating that mitophagy does not play any direct roles in mitochondrial function *per se* (Jin & Youle 2012, Kanki et al 2009). However, excessive mitochondria and mitochondrial damage automatically induce mitophagy (Kurihara et al 2012), which suggests that mitophagy is required for mitochondrial quality and quantity control.

Since mitochondria are such important organelles in cells, mitophagy should also play an important physiological role. However, the yeast Atg32 defective mutant does not show any phenotype (Kanki et al 2009). Moreover, mitochondria in the Atg32 defective mutant also seem to have comparable functions as the mitochondria in WT under normal growth conditions. However, under starvation conditions, mitochondria in Atg32 defective mutants produce much higher ROS compared to WT (Kurihara et al 2012), which suggests that degradation of damaged mitochondria indeed helps to maintain the cellular ROS at a lower or tolerable level.

1.2 General introduction to *Magnaporthe oryzae*

Magnaporthe oryzae (*M. oryzae),* a filamentous fungus, causes rice blast disease (Liu et al 2013, Wilson & Talbot 2009). Recently, researchers found that *M. oryzae* also causes wheat blast, which raises the importance and urgency of the basic and applied research towards control of *M. oryzae* (Tosa et al 2006, Tufan et al 2012).

1.2.1 Pathogenic life cycle of *M. oryzae*

The infection life cycle of *M. oryzae* is composed of several distinct developmental and morphogenetic events (Figure 3). The rice blast is initiated by a three-celled conidium, which is produced at the tip of aerial hypha upon light induction (Wilson & Talbot 2009). Following the release of conidium from aerial hypha, the conidium sticks to the leaf surface by secreting

adhesives. In proper conditions, conidia start to germinate, during which if the germ tube senses some host cues, such as hydrophobicity and hardness, appressorium formation pathway gets activated (Liu et al 2007). Afterwards, appressorium is formed at the tip of germ tube, and it is shown to be essential for infection as appressorium provides a huge turgor pressure to assist the blast fungus to break the rigid rice cell wall (Wang et al 2005). In addition, a septin ring structure is formed at the base of the mature appressorium by assembling F-actin and septin together, to provide the rigidity and negative membrane curvature needed for protrusion of the penetration peg into the rice leaf (Dagdas et al 2012, Ryder et al 2013). Following the penetration, the fungus ramifies intra- and inter-cellularly in susceptible host tissues. The rapid proliferation results in the lesion formation around 4 to 5 days after infection. During this infection life cycle, conidiation (the process to form conidium) and invasive growth are crucial.

1.2.1.1 Conidiation

Aerial conidiophores (the structures to produce asexual spores) produce a sympodial arrangement of spores in response to environmental cues. The most important cue is the light induction, as illustrated by Barksdale et al (2002).

Figure 3. Schematic representation of *M. oryzae* life cycle.

Mycelia grow vegetatively on rich medium, and differentiate into aerial hyphae. Upon light induction, aerial hyphae produce spores or conidia at their tips. Infection process initiates when conidia land on rice leaf surface. The spore germinates when it senses proper signals in the environment, such as hydration and/or nutrients. After germination, if the germ tube senses the hardness and hydrophobicity surface signals, appressorium formation is initiated at the tip. The germ tube grows vegetatively if proper surface signal is not sensed. At early stages of infection, the blast fungus grows inside the rice epidermal cells without killing the plant cells. At later stages, the fungus starts to kill the plant cells.

Figure 3

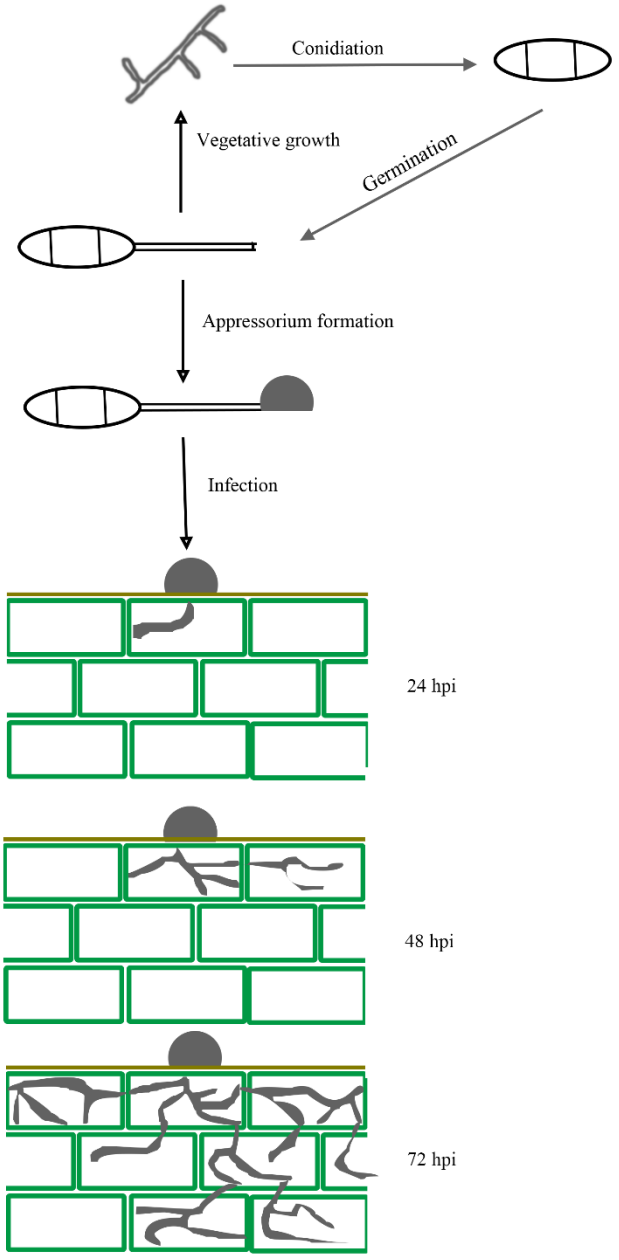
Conidiation
Vegetative growth
Germination
Appressorium formation
Infection
24 hpi
48 hpi
72 hpi

However, recent reports showed that the constant blue light inhibits aerial hyphae development and conidiation (Lee et al 2006), which suggests that darkness is required for induction of conidia. Furthermore, the requirement of darkness in conidiation was confirmed by the results from a *MoWC-1* mutant (*MoWC-1* is the ortholog in *M. oryzae* of the blue light-responsive transcription factor *White Collar-1* of *Neurospora crassa*). Conidiation does not require a period of darkness in *MoWC-1* defective mutants (Kim et al 2011), which suggests the *MoWC-1* is an essential regulator in the darkness-induced pathway.

Apart from light and darkness, autophagy was recently found to play important roles in conidiation. Disruption of autophagy in *M. oryzae* by deletion of *MoATG8* leads to highly reduced conidiation (Deng et al 2009a, Deng et al 2009b). This conidiation defect is due to a lack of sufficient G-6-P for metabolism and could be repressed by exogenous glucose, which suggests that the primary function of autophagy in conidiation is to generate sufficient G-6-P through hydrolysis of glycogen (Deng et al 2009a, Deng et al 2009b).

1.2.1.2 Invasive growth

The interaction of rice blast fungus with its susceptible host is largely biotrophic at the early stage of infection, and an important recent study documents more details of invasive growth (Kankanala et al 2007). Rice cells are alive after 5 hours post penetration, when *M. oryzae* still grows slowly in

the primary infected plant epidermal cells. Once the fungal hyphae start to move from one plant cell to another, the rice cells are killed, which suggests that biotrophic growth only lasts till the host cell is full of fungal hyphae. Another very important finding to be noted is that during invasive growth, fungal hyphae are surrounded by the plant plasma membrane, which has been identified by FM4-64 staining (Kankanala et al 2007). FM4-64 can only stain the rice plant plasma membrane close to the plant cell wall. By contract, the fungal membrane cannot be stained by FM4-64, which clearly suggests that FM4-64 cannot pass the four layers of phospholipids (two layers of phospholipids in the fungal cell and two layers of phospholipids in the plant cell). *M. oryzae* appears to penetrate the plant cell wall at very specific sites when moving from cell to cell (Kankanala et al 2007). The first evidence came from the live cell imaging of invasive hyphae that continually search for preferred sites of penetration. The second evidence that supports this theory is that the sites of cell-to-cell movement are the sites of plasmodesmata formation (Kankanala et al 2007). The third evidence is that the hyphal diameter at the sites of cell-to-cell movement is remarkable narrow and it is the same or similar as the size of the plasmodesmata.

Another study found that the plant plasma membrane is extremely active during *M. oryzae* colonization. Considering that invasive hyphae are surrounded by fungal and plant-derived membranes, it would be difficult for the fungus to secrete proteins directly into the plant. Therefore, *M. oryzae* utilizes plant plasma membranes and ER membranes to form a specialized

structure, the Biotrophic Interfacial Complex (BIC), which is essential for secretion of effectors into the plant cells (Giraldo et al 2013, Khang et al 2010). However, the mechanism of BIC formation is still unclear. Based on the secretory pathway utilized by the effectors, they can be classified into two groups, cytoplasmic effectors and apoplastic effectors (Giraldo et al 2013). Apoplastic effectors are actively secreted through the conventional ER-Golgi secretory pathway and accumulated at the extra-invasive-hyphal membranes (EIHM). By contrast, conventional secretory pathways are not required for cytoplasmic effectors secretion and such effectors only accumulate at the BIC. It was later found that the exocyst complex is required for proper secretion of such cytoplasmic effectors (Giraldo et al 2013).

Other genes affecting colonization are classified into two groups, metabolism related genes and stress response genes. The stress response genes include, *MoPDE1* gene, a homolog to aminophospholipid translocases, and *MoLSH1*, a homolog to the ER heat shock protein Lhs1 in yeast, *MoPDEH* and *MoPDEL*, homologs to the cAMP phosphodiesterase in yeast (Balhadere & Talbot 2001, Ramanujam & Naqvi 2010, Yi et al 2009). These genes mainly affect the core or essential pathways in *M. oryzae*, and herein disruption of these genes reduces the tolerance of fungi to certain stresses. During in planta growth, these mutants could not tolerate the high stresses generated by the plant to inhibit *M. oryzae*. Therefore, higher host response is the typical symptom of these kinds of mutants. And the enhancement of the tolerance of fungi to certain stresses could rescue the abilities of infection in these mutants. For

example, *MoLSH1* deletion shows very high ER stresses, which lead to the infection defects. Reduction of ER stresses by overexpression of *MoKAR2* could highly enhance the pathogenicity of this mutant (Yi et al 2009). The metabolism related genes would be discussed below in more details.

1.2.2 Metabolic reprogramming

The metabolism-related genes are highly related to the *M. oryzae* pathogenesis. The most possible reason is that the plant cellular environment contains limited and variable resources, which makes the fungus to use different metabolic pathways to survive in fluctuating nutritional conditions. To further understand the importance of metabolism during invasive growth, it is important to emphasize that *M. oryzae* is a hemibiotrophic fungus (Marcel et al 2010). In other words, at the initial stage of infection, *M. oryzae* takes up nutrients from plant cells without killing the host cells. Only after 72 h does *M. oryzae* enter its necrotic phase, starts to kill plant cells and obtains nutrients from dead plant cells. During this biotrophic-necrotrophic growth, global regulatory systems in *M. oryzae* must couple with carbon source sensing, gene regulation, acquiring nutrients by stealth during biotrophy and by absorption during necrotrophy and must respond spatially to the fluctuations in nutrient quality and quantity encountered throughout the host leaf.

One of the evidences found recently to support this hypothesis comes from the study of a trehalose-6-phosphate synthase (MoTps1) (Wilson et al 2010). *MoTPS1* deletion mutant was blocked at the early stage of infection. MoTps1 is a glucose-6-phophate (G-6-P) sensor, which might be important for sensing the nutrition levels to decide whether to enter necrotrophic stage or not. Furthermore, MoTps1 regulates the downstream genes through a novel NADPH-dependent genetic switch. However, no new study on regulation of metabolic reprogramming is reported recently, as it is difficult to study the invasive growth stage.

1.3 Aims and objectives of this study

As invasive growth is such a crucial stage for *M. oryzae* pathogenesis, it would be important to understand the mechanism of fungal adaptation to host environment and the pathways that regulate metabolic reprogramming. Therefore, in this study, I set out to decipher mitochondrial function and dynamics in fungal development and pathogenesis. Since mitochondria are involved in many important metabolic processes, I set out to first understand the role of mitochondria in pathogenesis from the mitochondrial dynamics angle (mitochondrial fusion, fission and turnover). As mitochondrial dynamics is highly related to metabolism, it is possible that mitochondrial dynamics might have important functions in the biotrophy-necrotrophy transition in the rice blast fungus. The role of mitochondrial dynamics herein was studied in detail during biotrophy-necrotrophy transition. Moreover, mitochondrial quality control might also play an important role in *M. oryzae* pathogenesis. I

first tried to identify a specific mitophagy mediator, similar to yeast Atg32 function, in *M. oryzae.* Subsequently, the role of mitophay during biotrophy-necrotrophy transition was characterized in depth.

Overall, the function of mitochondrial dynamics and mitophagy was studied during asexual differentiation and pathogenesis in *M. oryzae*.

1.4 Significance of this study

Although mitochondrial dynamics and mitophagy have been well studied in yeast and mammalian cells, little information can be found in filamentous fungi. This study is the first to explore the function of mitochondrial dynamics and mitophagy during fungal invasive growth. Based on the results of this study, further experiments can be designed to understand more about the metabolic reprogramming, which is an important question in the host-pathogen interaction field.

CHAPTER II MATERIALS AND METHODS

2.1 Strains, Growth conditions and Reagents

2.1.1 *M. oryzae* and Growth conditions

M. oryzae strains used in this study are shown in Table 1. *M. oryzae* was cultured in prune agar medium (PA: Yeast Extract 1 g/L, Prune Juice 40 mL/L, Lactose 5 g/L , Agar 20 g/L, pH 6.5) or complete medium (CM: Casein Hydrolysate 6 g/L, Sucrose 10g/L, Yeast Extract 6 g/L, Agar 20 g/L, pH 6.5) at 23°C. Mutants generated by *Agrobacterium tumefaciens* Transferred-DNA (T-DNA) mediated Transformation were selected on either CM containing Hygromycin (250 μg/ml) or Basal medium (BM: Yeast Nitrogen Base 1.6 g/L, Asparagine 2.0 g/L, NH_4NO_3 1.0 g/L, Glucose 10 g/L, Agar 20g/L, pH 6.0) containing Ammonium Glufosinate (50 μg/ml) or BM containing Chlorimuron-ethyl (50 μg/ml). Total genomic DNA, RNA or proteins were extracted from mycelia grown in liquid CM for 2 d.

Table 1. The Magnaporthe strains used in this study

Name	Genotype	Source
B157	WT	This study
*Moatg8*Δ	*atg8*::*hph*$^+$	Deng et al (2009a)
*Moatg24*Δ	*atg24*::*hph*$^+$	This study
MoATG24Δ-comp	*ATG24*:*bar*$^+$ *atg24*::*hph*$^+$	This study
MoAtg24-GFP	*ATG24-GFP*:*hph*$^+$	This study
Mito-GFP	PRO_{GPD}:*Mito-GFP*:*hph*$^+$	Patkar et al (2012)
*Moatg24*Δ with GFP-ScAtg32	*atg24*::*hph*$^+$ *GFP-ATG32*:*bar*$^+$	This study
GFP-2xFYVE	PRO_{RP27}:*GFP-2xFYVE*:*hph*$^+$	This study
MoATG24$_{1\text{-}190}$-GFP	PRO_{TRPC}:*ATG24*$_{1\text{-}190}$-*GFP*:*hph*$^+$	This study
MoATG24$_{190\text{-}495}$-GFP	PRO_{TRPC}:*ATG24*$_{190\text{-}495}$-*GFP*:*hph*$^+$	This study
MoATG24-GFP/RFP-MoATG8	*ATG24-GFP*:*hph*$^+$ *RFP-ATG8*:*bar*$^+$	This study
*Modnm1*Δ/Mito-GFP	*dnm1*::*ilv2*$^+$ PRO_{GPD}:*Mito-GFP*:*hph*$^+$	This study
*Mofzo1*Δ/Mito-GFP	*dnm1*::*bar*$^+$ PRO_{GPD}:*Mito-GFP*:*hph*$^+$	This study
Mito-roGFP	PRO_{GPD}:*Mito-roGFP*:*hph*$^+$	This study
mCherry-MoYbh3/Mito-GFP	PRO_{RP27}:*mCherry-YBH3*:*hph*$^+$ PRO_{GPD}:*Mito-roGFP*:*hph*$^+$	This study
mCherry-MoRtg3	PRO_{FOX2}:*mCherry-RTG3*:*hph*$^+$	This study
*Mortg2*Δ	*rtg2*::*ilv2*$^+$ PRO_{GPD}:*Mito-GFP*:*hph*$^+$	This study

To induce mitophagy, mycelia collected from two-day old liquid CM were transferred into BM with glycerol (BM-G; 1.6 g/L yeast nitrogen base, 2 g/L asparagine, 1 g/L NH_4NO_3, 1.5% V/V glycerol, pH 6.5) for 30 h. Subsequently, mycelia were cultured in minimal medium lacking nitrogen containing 3 mM PMSF (MM-N; 0.5 g/L KCl, 0.5 g/L $MgSO_4$, 1.5 g/L KH_2PO_4, 0.1% V/V trace elements, 10 g/L glucose, pH 6.5) for indicated time to induce mitophagy. For biochemical analysis, mycelia were starved in MM-N for 12 h, while for imaging analysis mycelia were starved in MM-N for 6 h. To induce nonselective autophagy, mycelia collected from two-day old liquid CM were immediately transferred into MM-N and incubated for indicated time (~ 4, 6 or 12 h). To induce pexophagy, mycelia collected from two-day old liquid CM were immediately transferred into BM with oleate (BM-O; 1.6 g/L yeast nitrogen base, 2 g/L asparagine, 1 g/L NH_4NO_3, and 1% V/V oleate) for 24 h. Subsequently, mycelia were then collected and transferred back to CM (with 3 mM PMSF) for 12 h.

Conidiation were assessed by subculturing dedicated strains on PA plates. The PA plates were incubated in constant dark for two days and the plates were subsequently exposed to light for another five days. Aerial hyphae were then collected in presence of water (3 ml - 10 ml). The water containing fungal mass and conidia was transferred into Falcon Conical Tubes. The mixture was then vortexed for 30 s to ensure that conidia were separated from the hyphae, and then the mycelia were filtered out through two lays of Miracloth. Conidia were collected by centrifuging the suspension and washed twice to remove all nutrients and ions. Then conidia production by experimental Magnaporthe

strain was counted by using a hemocytometer, and conidia are used for infection assays as described below.

2.1.2 *Agrobacterium tumefaciens* strains and culture medium

Agrobacterium tumefaciens (A.tumefaciens) was cultured in liquid Luria-Bertani broth medium (LB; Tryptone 10 g/L, Yeast Extract 5 g/L, NaCl 5 g/L) overnight at room temperature (RT). To activate *A.tumefaciens*, acetosyringone (ACS) was added into the liquid induction medium (IM: K salts 10 mL/L, M salts 20 mL/L, NH_4NO_3 (20%) 2.5 mL/L, $CaCl_2$ (1%) 1 mL/L, Glucose 5 mM, MES 40 mM, Glycerol 0.5% W/V; K salts: K_2HPO_4, 20.5%, KH_2PO_4 14.5%; M salts: $MgSO_4$-$7H_2O$ 3%, NaCl 1.5%, $(NH_4)_2SO_4$ 2.5%). The transformation of *M. oryzae* with *A. tumefaciens* was performed on solid IM containing ACS, based on the methodology described by de Groot et al (1998). To selectively kill *Agrobacterium* after the cocultivation with *M. oryzae,* 200 μM Cefotaxime was added into the indicated medium.

2.2 Molecular Methods

2.2.1 DNA techniques

2.2.1.1 PCR amplification

Routine PCR amplification was performed using genomic or plasmid DNA as templates with *Taq* DNA polymerase. To express gene or peptide in *M. oryzae, Pfu* DNA polymerase or KAPA HiFi DNA polymerase (#KK2502, Kapa Biosystem Inc) was used for PCR amplification. Oligo nucleotide

primers used in my research are shown in Table 2, and the restriction enzyme sites are underlined. The optimal annealing temperature and the PCR reaction extension time were set according to the primers and the length of target fragment, respectively. All other components for PCR reaction were added based on the manufacturer's instruction.

2.2.1.2 Agarose gel electrophoresis and gel purification of nucleic acid fragments

Agarose gels (1%) containing 0.1 μg/ml SYBR Green (#S9430, Sigma-Aldrich) were prepared by dissolving agarose (Bio-rad) in 1X TAE buffer (89 mM Tris base, 89 mM boric acid, 2.6 mM EDTA, pH8.3). Gels were submerged in a running tank containing 1X TBE buffer. The DNA samples from PCR amplification or enzyme digestion were mixed with 6X DNA loading buffer (50% sucrose, 10% SDS and 0.2% Orange G), and loaded into preset agarose gel wells. Five volt per cm of gel length current was applied to run the gels. Nucleic acid bands separated on agarose gels were visualized by UV transillumination, and fragment sizes were compared to that of a 1 kb DNA marker (#N3232L, NEB). The desired bands were cut out and DNA purifications were performed by using QIAGEN quik kits (#28704, Qiagen Corp.) following manufacturer's instructions.

Table 2. Oligonucleotide primers used in this study

Primer	Sequence
ATG24-1	F CCGGAATTCCGGTTGCTACGATGTGCTTCAGG
	R TCCCCCGGGGGAGGTTTCGGCTGTGATCTGTT
ATG24-2	F GAGAGTGTTCTGCAGCTTACTTTTGGGGGCACTTG
	R GAGAGTGTTAAGCTTTGACTGGCGACGTGAAGTAG
ATG24-3	F GAGAGTGTTGAATTCGCACCCGGTGCTCCGTCG
	R GAGAGTGTTCCATGGAGCAGCCACGGCGCCCTC
ATG24-4	F GAGAGTGTTCCATGGATGGTGAGCAAGGGCGAG
	R GAGAGTGTTGGTACCTTACTTGTACAGCTCGTC
ATG24-5	F GAGAGTGTTCCATGGGGGGAATCGACCAAGACAACTT
	R GAGAGTGTTGAATTCAGCAGCCACGGCGCCCTC
ATG24-6	F GAGAGTGTTGAATTCATGGGGGGAATCGACCAAG
	R GAGAGTGTTGGTACCGGCTCGTGATCTCATCGTG
ATG24-7	F GAGAGTGTTGGTACCATGAGTAGGAGCGTCTCTATGAG
	R GAGAGTGTTACTAGTAGCAGCCACGGCGCCCTCCTT
DNM1-1	F GAGAGTGTTGAATTCCTCACGGGATGGGCTTCTG
	R GAGAGTGTTGGTACCGGCGAAAATCGGTTCCGTGGTC
DNM1-2	F GAGAGTGTTGTCGACTGAAGCTGTTTGCGCCATG
	R GAGAGTGTTGCATGCTACCTATGATCAGCCCGC
FZO1-1	F GAGAGTGTTGAATTCACTCGGCCGCGATACGCTGC
	R GAGAGTGTTGGATTCCGTGATCGATTTCGTCCAGTC
FZO1-2	F GAGAGTGTTCTGCAGGCAGAACCATCCTCGTCGTC
	R GAGAGTGTTAAGCTTCCTGGCGGCGGCGACATCAAC
roGFP-1	F GAGAGTGTTGGTACCATGGTGAGCAAGGGCGAGGAG
	R GAGAGTGTTTCTAGATTACTTGTACAGCTCGTCCATG

RTG3-1	F GAGAGTGTTTCTAGAATGGCGCAACACGGCTTCAACCAAATTGC
	R GAGAGTGTTTCTAGACTAGTTCAAGTCCATGTACTCATCCTCTTCCTTG
YBH3-1	F GAGAGTGTTACTAGTGCTGCAAATGCCAAGTACAC
	R GAGAGTGTTTCTAGATTAATTCTGCTGCTGGCTG
RTG2-1	F GAGAGTGTTGAATTCGTGTCCATGATCTGTACTG
	R GAGAGTGTTGGTACCTTTGTTGTTTCGTCAGACG
RTG2-1	F GAGAGTGTTCTGCAGAACTAATGCACATCCCGTC
	R GAGAGTGTTAAGCTTGCACTCGTCCATGCCCGAGTC

F: Forward primer R: Reverse primer

2.2.1.3 Recombinant DNA techniques

Restriction and modifying enzymes were purchased from Promega Bioscience Inc (USA), New England biolabs (Beverly, MA, USA), Roche Diagnostics (Mannheim, Germany) or Thermo Scientific (USA), and used according to the manufacturer's instructions. Restriction digestion of DNA was carried out at the optimal temperature using recommended buffers depending on the restriction enzyme used. DNA ligation was performed at RT for 0.5 h or 16°C overnight, respectively. High-Speed Plasmid Mini Kit **(#**PD300**,** Geneaid Biotech**)** was used to extract and purify the plasmid. Standard procedures were employed based on the regent's instruction. The reliability of the recombinant DNA was examined by nucleotide sequence analysis using the Applied Biosystems Prism 377 DNA Sequencer (Forster, CA, USA).

2.2.1.4 Genomic DNA extraction from *M. oryzae*

This method is modified from the protocol used for rice genomic DNA extraction as described by Naqvi and Chattoo (1996). The procedures are described below briefly.

Mycelial plugs were cut from PA plates and then were cultured in liquid CM at 28 ºC for around 48 h with shaking speed around 160 rpm. Mycelia were then harvested by filtering through sterilized Mirocloth and washed with distilled water twice till clean. Mycelia then were ground into fine powders in presence of liquid nitrogen, which protects DNA from degradation. The mycelial fine powder (100-200mg) was re-suspended in 300ml yeast cell lysis buffer. To completely break down cells, the mixture was incubated at 65 °C

for 30 min. To precipitate proteins, 150 µL protein precipitation buffer was added into the mixture. Subsequently, the mixture was centrifuged at 12000 rpm at 4 °C for 15 min. Later on, the supernatant was transferred into a fresh 1.5 ml sterilized tube. To precipitate the DNA, equal volume of isopropanol was added into the supernatant and the mixture was centrifuged at 12000 rpm at 4 °C for 15 min. After centrifugation, the supernatant was removed and the remained DNA pellet was washed with 1 ml 70% ethanol and centrifuged at 12000 rpm at 4 °C for 15 min to remove the residual isopropanol. The DNA pellet was then air dried for 15-30 min till no ethanol remained, and re-dissolved in 100-200 µl water or TE buffer (pH 8.0) at 37 °C for 1 h. The DNA solution was ready for future experiments.

2.2.1.5 Southern Blotting

The procedure of southern blotting was modified based on the manufacturer's instruction (Amersham Pharmacia Biotech) and is described briefly below. The ECL kit was used for direct nucleic acid labeling and detection was purchased from GE (USA).

Around 10 µg genomic DNA was digested with the selected restriction enzymes at the appropriate temperatures overnight. Later on, the digested DNA was purified and then loaded into wells of 0.8% agarose gel. To completely separate DNA fragments, lower voltage was applied to run the gel. The gel was photographed and then incubated in depurination solution (22 mL/L HCl) at RT for 14 min or until the bromophenol blue dye turned into yellow. The gel was subsequently rinsed in the distilled water three times and

then incubated in denaturation solution (1.5 M NaCl and 0.5 M NaOH) at RT for 45 min. Once the denaturation process was complete, the denaturation solution was discarded and the gel was subsequently rinsed with distilled water three times to remove the residual denaturation solution. To neutralize the denaturation, the gel was incubated in neutralization solution (1.5 M NaCl, 0.5 M Tris HCl, pH 7.5) at RT for 45 min. During neutralization of the gel, Hybond-N+ (Amersham) nylon membrane (pre-wet in distilled water and then soaked in 10X SSC for 10 min) and 3 pieces filter paper were prepared. After neutralization, DNA was transferred from the gel to Hybond-N+ nylon membrane through capillary blot transfer. The membrane carrying DNA was then exposed to 1200 UV for auto-cross linking. Later on, the membrane was pre-hybridized in hybridization buffer at 42 °C for 20-60 min. To generate DNA labeling probe, a total amount of 350 ng DNA (30 ng/μL) was denatured for 8 min in a heater block (100 °C) and immediately cooled down on ice for 7 min. Subsequently, an equivalent volume of labeling reagent was added and mixed thoroughly. Later on, the same volume of glutaraldyhyde solution was then added and mixed thoroughly. To enhance the labeling quality, the mixture is incubated at 37 °C for 10 min. The mixture (the probe) was then stored on ice for 10 -15 min or in 50% glycerol at -15 °C for 6 months before use. The labeled probe was added to the pre-hybridized membrane to start hybridization (at least 8 h at 42 °C). Once the hybridization finished, the hybridization buffer was discarded and the blot was washed with the primary wash buffer (0.4% SDS and 0.5 X SSC) at 55 °C for 10 min three times to remove the residual probe. The membrane was then washed in the secondary wash buffer (2 X SSC) to remove SDS at RT for 5 min three times. To detect

the signal, the blot was covered with an equal volume of detection reagent 1 and reagent 2 in dark and incubated at RT for 1.5 min. The blot was placed in an X-Ray cassette and covered with a sheet of autoradiography film to expose for an appropriate length of time. The film was removed and developed.

2.2.1.6 Transformation of competent *E. coli* by the heat shock method

Chemically competent cells (*E. coli, Escherichia coli*) were thawed on ice for 10 min. Purified plasmid DNA (0.5 μg) was added into the competent cells, mixed well by pipetting and then incubated on ice for 5 min. The DNA-bacteria mixture was heat-shocked at 42 °C for 60 - 90 seconds and cooled down on ice immediately. *E. coli* cells were recovered by using 1 ml LB medium and incubating at 37 °C for 1 h. *E. coli* cells were spread onto LB plates containing appropriate antibiotics for selection and incubated at 37 °C overnight.

2.2.1.7 Transformation of *Agrobacterium* by electroporation method

Around 45 μL Electrocompetent cells (*Agrobacterium*) were thawed on ice. The selected T-DNA plasmid was added into the Electrocompetent cells and mixed well by pipetting. The mixture was transferred to a pre-chilled electroporation cuvette (gap 0.1 cm) (Bio-rad, USA). A 5 ms electric pulse (Micropulser, Bio-rad) at a field strength of 5 kv/cm was applied to transform the *Agrobacterium*. *Agrobacterium* cells were immediately incubated with 1 ml of LB medium at 28 °C for 1 h and then plated onto selective medium to grow at 28 °C until the colonies appeared.

2.2.2 RNA techniques

2.2.2.1 RNA extraction from *M. oryzae*

Mycelia plugs were cut from PA plates and then were cultured in liquid CM at 28 ºC for around 48 h with shaking speed at 160 rpm. Mycelia were then harvested by filtering through sterilized Mirocloth and washed with distilled water twice. Mycelia then were ground into fine powders in presence of liquid nitrogen, which could protect RNA from degradation. The mycelial fine powder (no more than 30mg) was re-suspended in 600 mL buffer RLT (spin at 12,000 rpm at 4 °C for 5 min). The supernatant was then transferred into a fresh 2 mL sterilized tube. 1 mL 70% ethanol was added to the supernatant, mix well by pipetting immediately. A maximum of 700 µL of the mixture was transferred into RNeasy spin column, placed in a 2 mL tube and centrifuged for 15 s at 10,000 rpm. The RNeasy spin column containing RNA was washed with 700 µL buffer RW1 (spin 30 s at 12,000 rpm). Subsequently, the RNeasy spin column containing RNA was washed with 500 µL buffer RPE (spin 30 s at 12,000 rpm). The RNeasy spin column containing RNA was again washed with 500 µL buffer RPE (spin 2 min at 12,000 rpm). To elute the RNA in RNeasy spin columm, 30-50 µL RNase-free water was added in and the RNeasy spin columm was centrifuged for 1 min at 12, 000 rpm. RNAase-free DNAase was then added into the eluted RNA solution to degrade any DNA contamination from genome. The RNA was ready for qRT-PCR or could be stored at -20 °C for 2 weeks.

2.2.2.2 RNA extraction from rice sheath

RNA extraction method for rice sheath was very similar to that for *M. oryzae*, except for the difference in the sample preparation.

Rice sheath was cut and prepared from 4 - 5 weeks old rice seedlings based on the method described by the Valent lab (2010). Conidia were drop-inoculated onto the surface of rice sheath. To make sure that the drops do not roll down the rice sheath, 0.01% gelatin was added to the conidia solution before inoculation. Invasive growth at selected time points in rice sheath was recorded by microscope and the rice sheath was grounded into fine powder in presence of liquid nitrogen. The rest of the procedures are the same as the RNA extraction from *M. oryzae*.

2.2.2.3 RT-PCR and qRT-PCR

Tissue specific mRNA was extracted with RNeasy Plant Mini Kit (Qiagen, Japan). The DNA in the final mRNA solution was removed by digestion with DNase I purchased from Thermo Scientific. cDNA synthesis was carried out following the manufacturer's instruction (RevertAid First Strand cDNA Synthesis Kit, Thermo Scientific #K1622). Oligo nucleotide primers used for qRT-PCR are listed in Table 3.

qRT-PCR was performed as per the manufacturer's instruction (KAPA SYBR FAST qPCR Kits). Briefly, 24 μL master mix was made from 12.5 μL 2 x iQ SYBR green, 0.5 μL forward primer (10 μM), 0.5 μL reverse primer (10 μM) and 10.5 μL sterile distilled water. The mixture was briefly vortexed and

centrifuged to remove any bubbles. The master mix (72 μL) was added into each tube with 3 μL of each template individually. Each sample (5 or 10 μL) was placed in the appropriate wells in a 384-well plate and ran in an ABI 7900 RT-PCR machine as per the manufacturer's instructions.

Table 3. Oligonucleotide primers for RT-PCR used in this study

Primer	Sequence
PBZ1	F CTACTATGGCATGCTCAAGAT
	R ATAGAAAGGCACATAAACACAA
PR5	F GAGGATCGGGAGATTGCAAA
	R CTCCACGGCAGCAATATTGA
RTG2	F CTAAGCATCGGGCTAACCTC
	R ATGACCTTGCCCTCCATTAG

F: Forward primer R: Reverse primer

2.3 Staining protocols

2.3.1 Vacuolar staining

Cell Tracker Blue CMAC (Molecular Probes, C2110) was diluted to a final working concentration of 10 μM, and then the biological material was incubated for 30 min at room temperature (25 °C) prior to microscopic observation. CMAC staining for Rice sheath involved an incubation time of 2 h at 37 °C prior to microscopic observation.

2.3.2 Mitochondrial staining

MitoFluor Red 589 (Molecular Probes, M22424) was diluted to a final working concentration of 1 μM. The biological sample was incubated in the working solution for 30 min at RT and washed with fresh medium or dedicated buffer to remove the residual MitoFluor Red dye prior to microscopic observation. Rice sheath samples were stained for 2 h at 37 °C prior to microscopic observation.

2.3.3 Nuclear staining

Hoechst 33342 (Molecular Probes) was diluted into final working concentration of 1 μM. The tissue samples were stained in the working solution for 30 min at RT and then washed with fresh medium or dedicated buffer to remove the residual Hoechst dye prior to microscopic observation. Rice sheath samples were stained for 2 h at 37 °C prior to microscopic observation.

2.3.4 Trypan blue and aniline blue staining

Inoculated rice sheaths were incubated with clearing solution A (acetic acid: ethanol = 1: 3, V/V) at RT for overnight, followed by treatment with clearing solution B (acetic acid: ethanol: glycerol = 1: 5: 1, V/V/V). Such pre-treated rice sheaths were immersed in the staining solution (0.01% trypan blue in lactophenol) at RT for at least 4 h. The stained rice sheaths were stored in 60% glycerol before observation.

2.4 Protein and immunoblotting related methods

2.4.1 Total protein lysates from *M. oryzae* (Denatured)

Mycelia from required *M. oryzae* strains were cultured in liquid CM at RT for 2 d. Later on, mycelia were harvested and washed with NP40 buffer (with proteinase inhibitor mixture: 2 mM PMSF, 2 mM Benzamidine, 50 mM NaF, 100 μM Na_3VO_4, 4 μg/mL leopeptin) to remove residual CM. To break the mycelial cells, the washed mycelia were ground into powder in presence of liquid nitrogen, which could protect protein from degradation. To further break down the cells, SDS lysis buffer (3 μL/ mg; 10 mM Na_3PO4, 0.5% SDS, 1 mM DTT, 1 mM EDTA, pH7.0) was added to the ground mycelial powder. The mixture was first incubated on ice for 10 min prior to incubation at 100ºC for 3-5 min. The boiled mixture was then centrifuged at 14, 000 rpm 4° C for 15 min. The supernatant was then collected and stored at 4 ºC for following experiments.

2.4.2 Protein electrophoresis, immunoblots and reprobing protocols.

Protein concentration was measured by Bio-Rad protein assay (#500-0006) to ensure equivalent sample loading to SDS-PAGE. The SDS-PAGE gel was prepared based on the molecular weight of predicated protein size. Electrical transfer of the proteins in the SDS-PAGE onto the nitrocellulose membrane was performed at 90 V for 2 h or at 40 V overnight.

The nitrocellulose membrane was then first blocked in the freshly prepared PBST buffer (0.05% Tween 20, 1% PBS, 5% nonfat dry milk V/V) for 1 h. Subsequently, the nitrocellulose membrane was incubated in the primary antibody solution at RT for 2 h or at 4ºC for overnight. To remove the unbound residual primary antibody, the nitrocellulose membrane was washed in the fresh PBST buffer five times for 10 to 15 minutes each. Later on the nitrocellulose membrane was incubated in the secondary antibody solution (HRP conjugated, 1:10000 dilution in PBST buffer) at RT for 1 h or at 4ºC for overnight. To remove the unbound residual secondary antibody, the nitrocellulose membrane was washed with the fresh PBST buffer five times for 10 to 15 minutes each. The membrane was then developed/processed with the enhanced chemiluminescence system (ECL, Amersham) to detect the signal.

To reprobe the immunoblots, a standard stripping buffer (2% SDS, 62.5 mM Tris-HCl pH 6.8, 100 mM β-mercaptoethanol) was applied to strip the

nitrocellulose membrane at 70ºC for 1 h. The nitrocellulose membrane was reprobed by repeating the aforementioned method.

2.5 Infection assays and virulence assessment

2.5.1 Barley infection with *M. oryzae* conidia

Leaf pieces from a three-week old healthy seedling were cut, rinsed in 40% ethanol twice for 1 min each and then washed with the fresh distilled water three times to remove any ethanol from the leaf surface. To hold the leaves from rolling during incubation, both ends of the surface-sterilized leaf pieces were inserted into the agar medium (100 µg/mL streptomycin, 100 µg/mL ampicillin and 2 µg/mL kinetin). Such leaf pieces were drop-inoculated with twenty µl of conidial suspension and incubated in a growth chamber (22°C, 80-95% humidity and 16 h/8 h light/dark cycle) for 5-7 days. The infection results were recorded by scanning the leaves.

2.5.2 Rice seedling related methods and infection with *M. oryzae* conidia

Three-week old healthy rice seedlings of the compatible rice line were sprayed with conidial suspension containing 0.01% Gelatin, and incubated in a growth chamber (22°C, 80-95% humidity and 16 h/8 h light/dark cycle) for 5-7 d prior to disease symptoms evaluation. The infection results were recorded by scanning the leaves.

2.5.3 Rice sheath infection assay

Healthy rice seedlings at the 4- to 6-leaf stage were selected for sheath preparation. After careful slicing, the intact rice sheath pieces were inoculated with the conidial suspension, and incubated in a moist chamber for the required time period. The rice sheath pieces were then observed under a confocal microscope at selected time points.

In a parallel experiment, heat killed yet structurally intact rice sheath was used as a control to evaluate the function of host response to fungal infection. Heat-killed rice sheaths were prepared by immersing selected sheath pieces into sterile water at 75°C for 30 min.

2.6 Microscopy

2.6.1 Epifluorescence Microscopy

Light microscopic examination was performed using a Zeiss Axioplan 2 microscope with appropriate filters (438nm, 488nm and 534 nm). Images were captured with a Photometrics CoolSnap cf CCD camera (Muskogee, OK) and Metamorph software (Molecular Devices, Sunnyvale). Images were processed in ImageJ and Adobe photoshop CS6.

2.6.2 Confocal Microscopy

Infected rice sheaths were observed under a Zeiss 510 Meta inverted Confocal System (Carl Zeiss MicroImaging) based on Zeiss Axiovert 200M. 488-nm (eGFP) was excited by 30-mW argon lasers, while 543-nm (RFP) was excited by 1-mW helium:neon lasers.

In order to observe the biological events occuring in foot cells, a fresh mycelial plug was inserted into a thin layer of 1% water agar plate. And then the plate was cultured in constant dark for 2 days. Subsequently, the plate was shifted to constant illumination to induce conidiation. Conidiation was assessed after 12-24 h of photo induction.

2.6.3 Image analysis

The standard package (ImageJ program) for biological image analysis was downloaded from National Institutes of Health (http://rsb.info.nih.gov/). The ImageJ software was used to quantify the fluorescence signal and to analyze co-localization. 3-D reconstruction, visualization and analysis were performed in Bitplan Imaris (Zurich, Switzerland).

CHAPTER III MITOPHAGY IS REQUIRED FOR PROPER PATHOGENESIS IN *M. ORYZAE*

3.1 Introduction

When mitochondria are damaged, downstream pathways are activated to rescue cells from excessive oxidative stress. As mentioned in Chapter I, the retrograde pathway protects cells by upregulation of metabolic genes. Alternately, cells are protected from such a damage by selectively removing the damaged mitochondria through autophagy (termed as mitophagy) (Ashrafi & Schwarz 2013). Although the molecular mechanism underlying mitophagy has been explored in yeast, little is known about that in filamentous fungi, partially due to the lack of specific orthologues. Since mitochondria are such important organelles, it would be interesting to see whether mitophagy occurs naturally during filamentous fungal development. If so, it would be important to identify the protein(s) or protein complexes serving specific functions in mitophagy in filamentous fungi.

During pathogenesis, two developmental processes are very important, conidiation and invasive growth. Conidiation is a developmental process shared by many filamentous fungi, and has been extensively studied (Kim et al 2009, Springer & Yanofsky 1989). Conidiation is the term used to describe the asexual development in filamentous fungi. This process mainly occurs at the tips of aerial hyphae that grow from vegetative mycelia. Upon light induction, the tip of an aerial hypha starts to enlarge to form a swollen structure, the conidiophore. Finally, about 3 to 5 conidia are formed in a sympodial pattern per conidiophore. During conidiation, carbon and nitrogen sources are

transported to conidiophores from vegetative mycelia through the foot cells (Adams et al 1998). The foot cell is a thick-walled vegetative cell, which connects the vegetative hypha to the aerial hypha.

Conidiation is regulated by multiple environmental factors, such as the circadian rhythm and the metabolic status. Furthermore, glycogen autophagy is required for conidiation (Deng et al 2009a), as glycogen hydrolysis provides necessary energy for conidiation. Disruption of autophagy highly represses the condiation, and such defect can be restored by exogenous carbon sources. However, whether any selective autophagy is required for conidiation is unknown. The selective autophagy pathways have not been studied in detail in filamentous fungi. Until now, pexophagy has been reported to be essential for conidiation in *Colletotrichum* sp. (Asakura et al 2009); and infection-associated nuclear degradation in *M. oryzae* is through non-selective macroautophagy (He et al 2012). Therefore, it would be very interesting to study whether mitophagy occurs naturally during conidiation.

In this study, MoAtg24 was identified as a specific mediator of mitophagy. Furthermore, I show the role of mitophagy in the foot cells during conidiation, and in the invasive hyphae during host colonization. I describe effect of loss-of Atg24 function on total conidiation and invasive growth in *M. oryzae*.

3.2 Results

3.2.1 Generation of *Moatg24*Δ

The full-length *M. oryzae ATG24* was identified through BLAST with yeast *ATG24* as the query sequence (http://blast.ncbi.nlm.nih.gov/). Based on the BLASTP search, *MGG_03638.6*, containing a Phox homology (*PX*) and a BAR (*Bin–Amphiphysin–Rvs*) domain, was considered as the likely ortholog of *ScATG24* (Figure. 4A). The PX domain is a phosphoinositide-binding domain involved in targeting proteins to dedicated cell membranes (Ellson et al 2002). The BAR domain is capable of sensing membrane curvature and binds to the curved membrane through its concave face (Peter et al 2004). The *MoATG24* gene was deleted by one-step locus specific replacement with the hygromycin-resistance marker cassette (*HPH1*; Figure 4B) using *Agrobacterium* Transfer DNA-mediated transformation. The requisite gene replacement event for *MoATG24* was confirmed by Southern blotting (Figure. 4C). Three independent strains thus identified were then characterized for various aspects of vegetative growth, colony formation and pathogenesis.

3.2.2 Loss of *MoATG24* leads to decreased aerial hyphae and conidiation

The *Moatg24*Δ exhibited a reduced growth rate and decreased aerial hyphae formation (Figure 5A and 5B). The total number of conidia produced by the mutant was merely 0.26% of that in WT (Figure 5C). These results suggested that the reduced aerial hyphae most likely led to the highly reduced conidiation in the mutant. To determine how reduced aerial hyphae affect

condiation of *Moatg24*Δ, conidiation process was examined carefully in the WT and *Moatg24*Δ. Aerial hyphae of *Moatg24*Δ were significantly shorter than those of the WT when cultured in the dark (Figure 5A). After a 24 h light induction, conidia were still difficult to be detected at the tips of aerial hyphae in *Moatg24*Δ (Figure 5D). By contrast, at least three conidia per conidiophore would be easily found at the tip of an aerial hypha at the same time point in WT (Figure 5D). These results indicate that the highly reduced conidiation in *Moatg24*Δ is mainly due to the decreased aerial hyphae and impaired condiophore formation. To confirm that the phenotypes observed in *Moatg24*Δ are due to loss of MoAtg24 function, a complementary strain *Moatg24*Δ-Comp was made by expressing PRO$_{MoATG24}$:MoATG24 in the *Moatg24*Δ strain. Importantly, the growth rate, the aerial hyphae formation and conidiation were fully restored in the complemented strain *Moatg24*Δ-Comp (Figure 5A, 5B and 5C), which suggests that the phenotypes observed in *Moatg24*Δ are because of loss of MoAtg24 function. Therefore, MoAtg24 function is essential for proper initiation of asexual development in *M. oryzae*.

Figure 4. Generation of *Moatg24*Δ.

(A) Domain organization of the MoAtg24 protein. The two domains of MoAtg24 are labeled grey, and numbers below the domains represent amino acid residues.

(B) Schematic representation of the *MoATG24* locus in *M. oryzae* B157. Dashed lines, solid bars and short open boxes represent the 1 kb flanking region, the coding region and introns respectively. The *Moatg24*Δ mutant was generated by homology based relacement with hygromycin-resistance cassette (*HPH1*). NcoI restriction enzyme sites are labeled.

(C) Southern blot results of wild type and the *Moatg24*Δ mutant. Genomic DNA from the indicated strains was digested by *Nco*I. The appearance of the 1.9 kb band in the *Moatg24*Δ strain, with the concomitant loss of the wild-type 5 kb *MoATG24* fragment, was diagnostic of the correct gene replacement event.

Figure 4

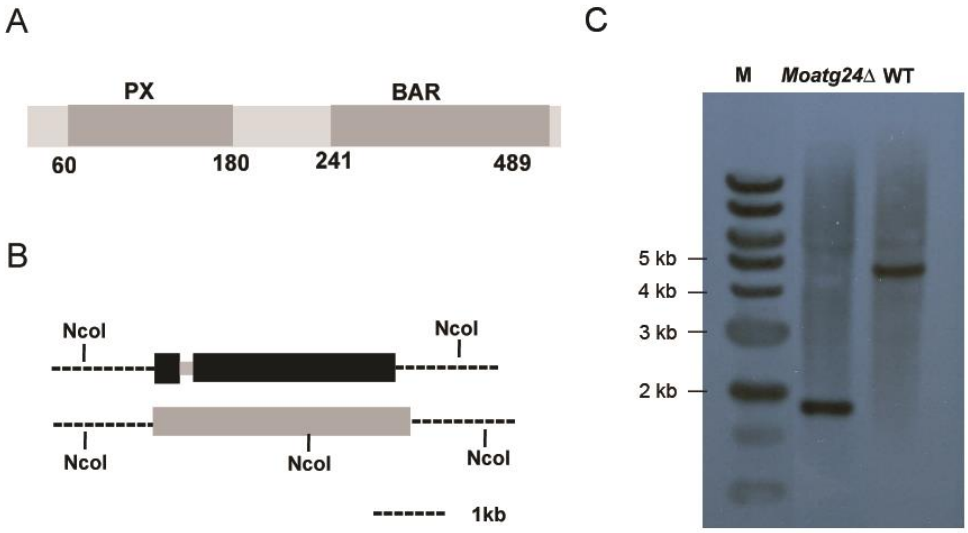
A
PX
BAR
60
180
241
489
B
NcoI
NcoI
NcoI
NcoI
NcoI
1kb
C
M
Moatg24Δ
WT
5 kb
4 kb
3 kb
2 kb

Figure 5. Colony growth and conidiation of *Moatg24* mutant

(A) Aerial hyphal growth in *Moatg24*Δ. Indicated strains were cultured in constant darkness for 7 d. Subsequently, the colonies were sectioned at the median region and documented.

(B) Colony diameters of the indicated strains, grown on PA solid medium for 4 d, were compared.

(C) Conidiation comparison between *Moatg24*Δ, wild type and *Moatg24*Δ-comp. To compare the conidiation, indicated strains were cultured on PA solid medium for 2 d in constant darkness and following a 5 d light induction. Mean values (±SE) presented as percentage points were derived from three independent experiments (3 colonies for each instance).

(D) Microscopic image of conidiation of wild type and *Moatg24*Δ. To observe the conidiation formation in plates, indicated strains were cultured on PA solid medium for 1 d in constant darkness and then under constant light for 24 h.

Figure 5

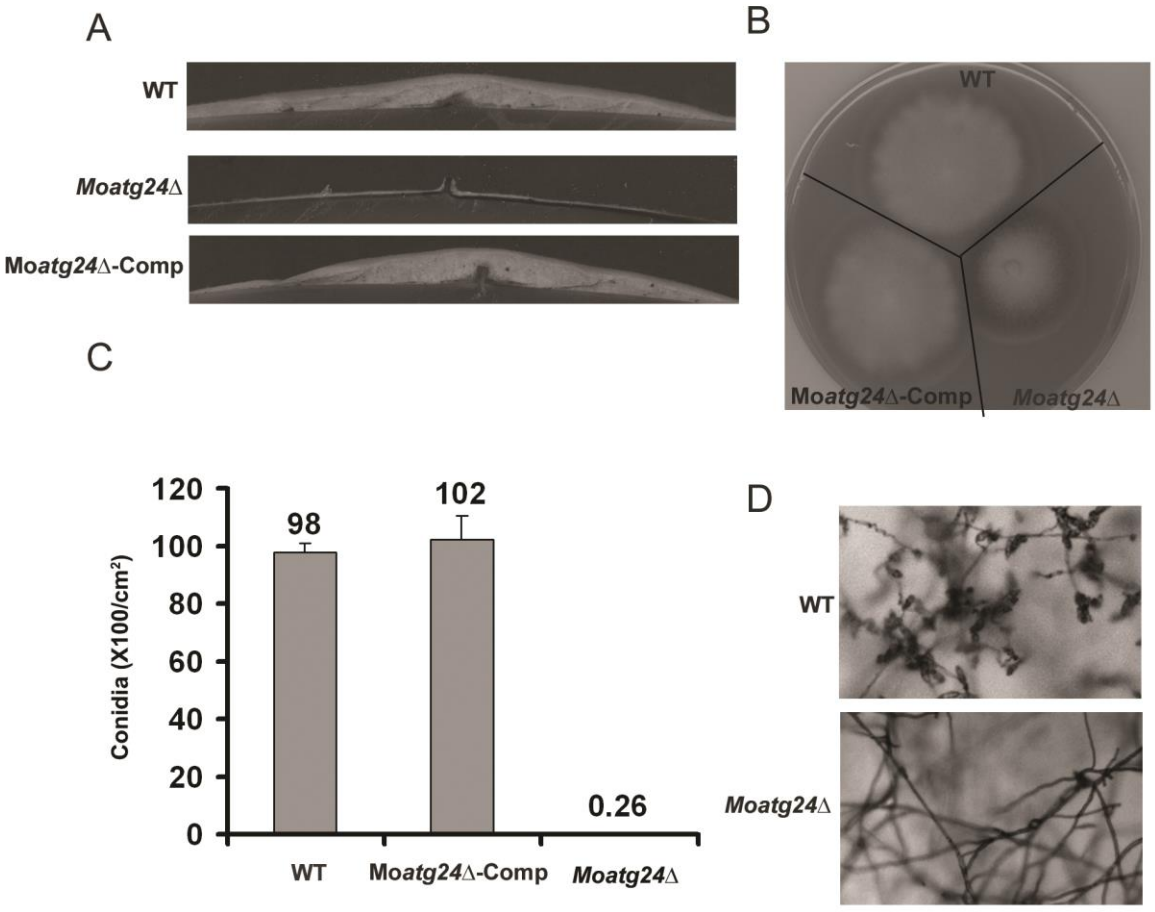
A
WT
Moatg24Δ
Moatg24Δ-Comp
B
WT
Moatg24Δ-Comp
Moatg24Δ
C
Conidia (X100/cm²)
120
100
80
60
40
20
0
98
102
0.26
WT
Moatg24Δ-Comp
Moatg24Δ
D
WT
Moatg24Δ

3.2.3 Loss of *MoATG24* leads to decreased invasive growth

To test the role of MoAtg24 in infection, infection assays were performed on a susceptible rice cultivar (CO39) and a barley cultivar. Disease symptoms were assessed 5 dpi and 7 dpi on barley and rice, respectively. Compared to the wild type, which caused rice blast disease with characteristic spindle shaped lesions with gray centers, the *Moatg24*Δ showed highly reduced pathogenicity in both rice and barley (Figure 6A and 6B). Typical rice blast lesions could not be observed in the susceptible rice cultivar inoculated with *Moatg24*Δ conidia, while only small dark spots could be occasionally observed (Figure 6A). To understand the differences between the infection of *Moatg24*Δ conidia and the infection of WT conidia, the invasive hyphae of WT and *Moatg24*Δ were examined at 30 hpi, 48 hpi, and 72 hpi (Figure 6C). At 30 hpi, nearly 40% of WT appressoria had successfully penetrated the rice sheath. By contrast, less than 5% of *Moatg24*Δ conidia had penetrated rice sheath successfully (Figure 6C and 6D left panel). At 48 hpi, although the penetration rates of appressoria in WT and *Moatg24*Δ were comparable, the secondary invasive hyphae were highly reduced in *Moatg24*Δ (less than 2%) compared to WT (around 60%) (Figure 6C and 6D right panel). At 72 hpi, the differences of invasive hyphae between *Moatg24*Δ and WT were more dramatic. The invasive hyphae of WT had successfully grown out into 5 to 7 plant cells, whereas the invasive hyphae of *Moatg24*Δ was mainly limited in the primary infected rice epidermal cell (Figure 6C right panel). In rare cases, the invasive hyphae of *Moatg24*Δ could be found at the neighboring cells surrounding the primary infected rice epidermal cell. Based on these results, it is clear that the highly reduced pathogenicity of *Moatg24*Δ is a result of invasive hyphae spreading defects.

3.2.4 Subcellular localization of MoAtg24-GFP upon starvation induction or in presence of oxidative stresses

To figure out the molecular mechanism in which MoAtg24 is involved, its subcellular localization was examined in a strain expressing MoAtg24-GFP under native regulation. To detect the MoAtg24-GFP signal, mycelia were first cultured in liquid CM for 2 d. However, no GFP signal could be detected (Figure 7A and 7B). By contrast, the MoAtg24-GFP signal intensified and appeared as aggregates or punctate structures in presence of oxidative stresses or under nitrogen starvation (Fig. 7A and 7B). Intracellular ROS is known to be produced by mitochondria and peroxisomes, and thus the MoAtg24-GFP punctae could be peroxisomal and/or mitochondrial origin. To verify this, I examined the colocalization rates of MoAtg24-GFP with peroxisomes or mitochondria. In presence of ROS stress or upon starvation, MoAtg24-GFP and mitochondria (stained with MitoFluor red) showed significant colocalization (nearly 100% MoAtg24-GFP overlaps with mitochondria; Figure 7C). To rule out the possibility that some of MoAtg24-GFP might colocalize with peroxisomes under ROS or starvation conditions, MoAtg24-GFP and peroxisomes colocalization analysis was performed. There was no overlap between MoAtg24-GFP and peroxisomes (Figure 8). Based on these data, it is clear that MoAtg24-GFP is induced and associates with mitochondria under starvation or oxidative stress condition.

3.2.5 MoAtg24 is essential for mitophagy

As MoAtg24-GFP colocalizes with mitochondria in presence of ROS stresses or upon starvation, it is possible that MoAtg24 plays a key role in mitophagy. Mitophagy is a subtype of autophagy and degrades damaged or excessive mitochondria during ROS stresses or upon starvation induction (Ding & Yin 2012, Song et al 2014, Youle & Narendra 2011). To verify the function of MoAtg24 in mitophagy, a mitophagy assay was first established. In yeast, mitophagy occurs during aging process after cultured in lactate or glycerol medium for an extended period of time or during nitrogen starvation after growth in acetate or glycerol medium for a short period. Similarly, to induce mitophagy in *M. oryzae*, mycelia were cultured in CM for 3 d to obtain a sufficient amount of biomass, a subsequent step for accelerating mitochondria biogenesis was performed in BM-G for 30 h (Damsky 1976, Ibrahim et al 1973). Mycelia were then starved in MM-N to induce mitophagy. A mito-GFP strain was used to verify this assay. After 6 h of starvation in MM-N, vacuolar mito-GFP signals were detected in WT mycelia, suggesting that mitochondria were indeed transported into vacuoles for degradation (vacuoles were stained by CMAC; Figure 9A). By contrast, vacuolar mito-GFP signals could not be detected in the mycelia of *Moatg8*Δ (Figure 9A), which is expected as MoAtg8 is essential for nearly all types of autophagy, including mitophagy. The differences of vacuolar mito-GFP signals between WT and *Moatg8*Δ suggest that the mitophagy assay works well in *M. oryzae*. Afterwards, the same mitophagy assay was performed to identify the function of MoAtg24 in mitophagy. After induced mitophagy in *Moatg24*Δ, similar to that in *Moatg8*Δ, vacuolar mito-GFP signal was undetectable, implying that

mitophagy was likely repressed in *Moatg24*Δ. Besides the microscopic observation, the activity of mitophagy was assessed by a biochemical assay. In wild type, total Porin (a mitochondrial protein) showed a time-course dependent degradation, and the difference in levels was most obvious between time 0 h and 12 h (Figure 9B). Such time-course dependent reduction of Porin was inhibited in WT cells incubated with PMSF, a small inhibitor of vacuolar proteases, suggesting that the time-course dependent degradation of mitochondria occurs inside the vacuoles. The levels of Porin were stabilized at the selected time points in *Moatg24*Δ, similar to the results in *Moatg8*Δ (Figure 9C). Based on these data, I therefore conclude that Atg24 is essential for mitophagy in *M. oryzae*.

3.2.6 MoAtg24 is not involved in macroautophagy or pexophagy

As MoAtg8 is required for both selective and nonselective autophagy, to rule out the possibilities that MoAtg24 is also a key regulator for macroautophagy and/or involves in any other types of selective autophagy. Macroautophagy and pexophagy were performed as described (Klionsky et al 2012). To measure the activity of macroautophagy, the level of RFP-MoAtg8 lipidation was assessed. I found that MoAtg8 lipidation was not altered in *Moatg24*Δ, compared to the WT (Figure 10A). Furthermore, vacuolar RFP-MoAtg8 in *Moatg24*Δ could also be detected, which was similar to RFP-MoAtg8 in WT (Figure 10B). Till now, pexophagy is the selective autophagy that has been studied in filamentous fungi and it was also found to occur naturally in *M. oryzae.* Therefore, I decided to examine the requirement of MoAtg24 in

pexophagy. To evaluate pexophagy, the level of a peroxisome protein Pex14 after pexophagy induction was measured in WT, *Moatg8*Δ and *Moatg24*Δ. The degradation of Pex14 in *Moatg24*Δ was similar to that in WT and was significantly higher than that in *Moatg8*Δ (Figure 10C). Based on these microscopic observations and biochemical data, I conclude that MoAtg24 is not required for macroautophagy or pexophagy.

3.2.7 MoAtg24 colocalizes with mitochondria and RFP-MoAtg8 during mitophagy

Although MoAtg24-GFP localization was examined upon starvation and in presence of oxidative stresses, it is still unclear whether it localizes to mitochondria upon mitophagy induction. As expected, MoAtg24-RFP localized to mitochondria, marked by mito-GFP, upon mitophagy induction (Figure 11A). The colocalization of MoAtg24-RFP and mito-GFP could be found in vacuoles, punctate and filamentous structures. Based on the morphology, the small punctate structures could be fragmented mitochondria and the filamentous structures are likely to be filamentous mitochondria. Meanwhile, RFP-MoAtg8 could also be found to colocalize to filamentous and fragmented mitochondria (Figure 11B). Furthermore, MoAtg24-GFP also colocalized with RFP-MoAtg8 (Figure 11C). These results confirm that MoAtg24 indeed functions on the mitochondria during mitophagy.

Figure 6. MoAtg24 is required for proper pathogenesis of *M. oryzae*.

(A) Pathogenicity of *Moatg24*Δ is highly reduced based on rice infection. To test the pathogenicity of *Moatg24*Δ, 20 mL $1x10^7$/mL conidia were spray-inoculated on the 3-week rice seedlings. And the symptoms were checked at 7 dpi.

(B) Pathogenicity of *Moatg24*Δ is highly reduced based on barley infection. To test the pathogenicity of *Moatg24*Δ, 20 μL $1x10^7$/mL conidia were inoculated on the 2-week leaves from barley. And the symptoms were examined at 5 dpi.

(C) Invasive growth of *Moatg24*Δ is stopped at 48 hpi. To observe the invasive growth of *Moatg24*Δ, 20 μL $1x10^3$ /mL conidia was inoculated on the pre-cut rice sheath. The inoculated rice sheath was observed under confocal microscope at the indicated time points.

(D) The quantitative data correlated to the images in panel C. Mean values (±SE) presented as percentage points were derived from three independent experiments (100 appressorium for each instance).

Figure 6

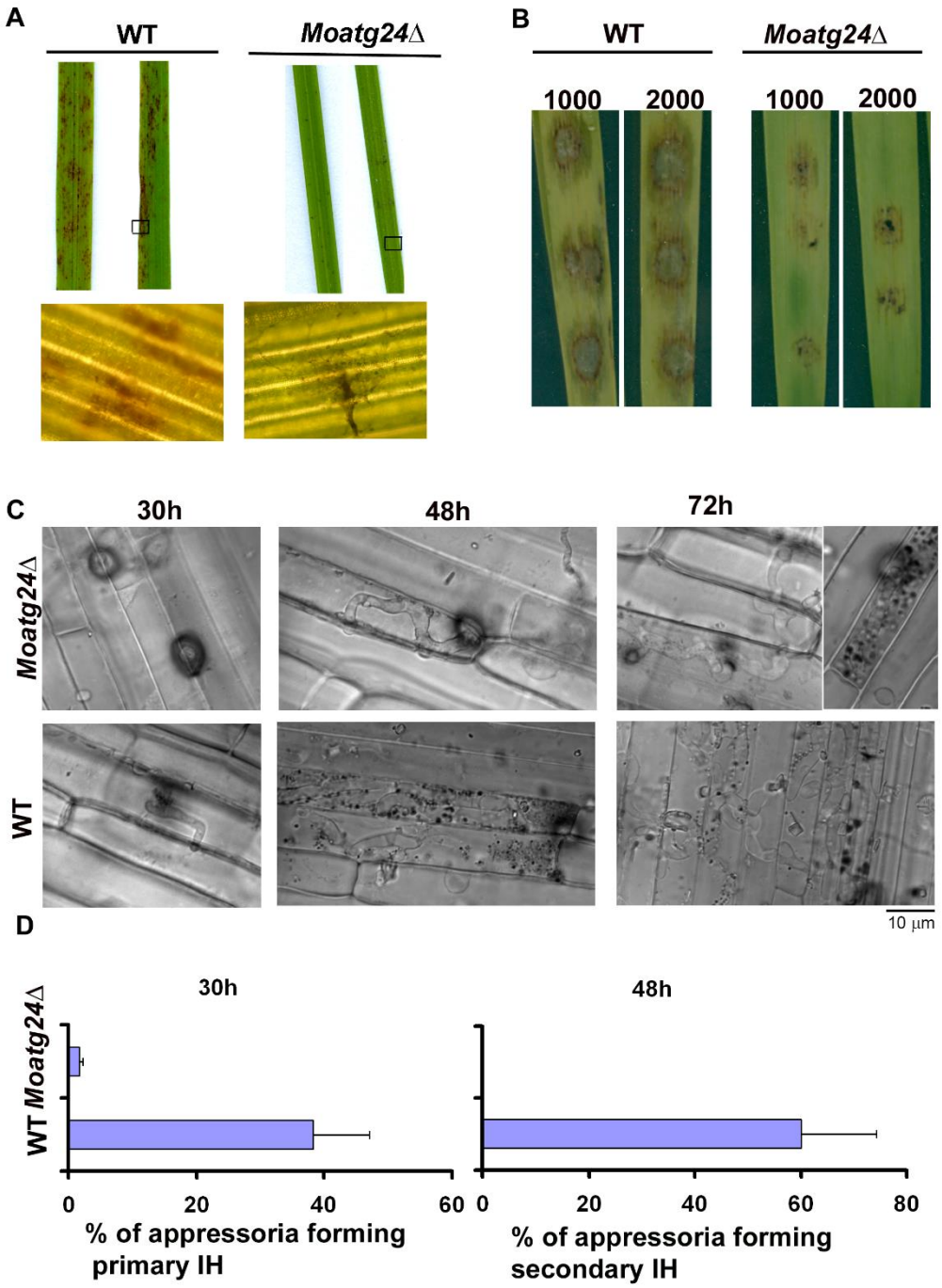
A
WT
Moatg24Δ
B
WT
Moatg24Δ
1000
2000
1000
2000
C
30h
48h
72h
Moatg24Δ
WT
10 μm
D
30h
48h
WT Moatg24Δ
0
20
40
60
0
20
40
60
80
% of appressoria forming primary IH
% of appressoria forming secondary IH

Figure 7. MoAtg24-GFP localizes to mitochondria upon ROS and starvation induction.

(A) MoAtg24-GFP appears aggregated on cytoplasmic punctate structures upon oxidative stress induction. MoAtg24-GFP strain was cultured in liquid CM for 48 h. Subsequently, 3 mM H_2O_2 was added into the medium 1 h before observation. Imaging was performed on Zeiss Widefield Fluorescence inverted microscope.

(B) MoAtg24-GFP appears aggregated on cytoplasmic punctate structures induced by glycerol/MM-N starvation. 48 h old mycelia from CM were transferred into BM-glycerol medium for another 30 h incubation. Subsequently, the mycelia from BM-glycerol medium were shifted to MM-N for 6 h prior to microscopy. Imaging was then carried out on Zeiss Widefield Fluorescence inverted microscope.

(C) MoAtg24-GFP localizes to mitochondria. MoAtg24-GFP strain was firstly cultured in liquid CM for 48 h. To induce MoAtg24-GFP expression, two-day old mycelia from CM were shift into CM with 3 mM H_2O_2. Mitochondria were then stained with MitoFluor Red prior to observation.

Figure 7

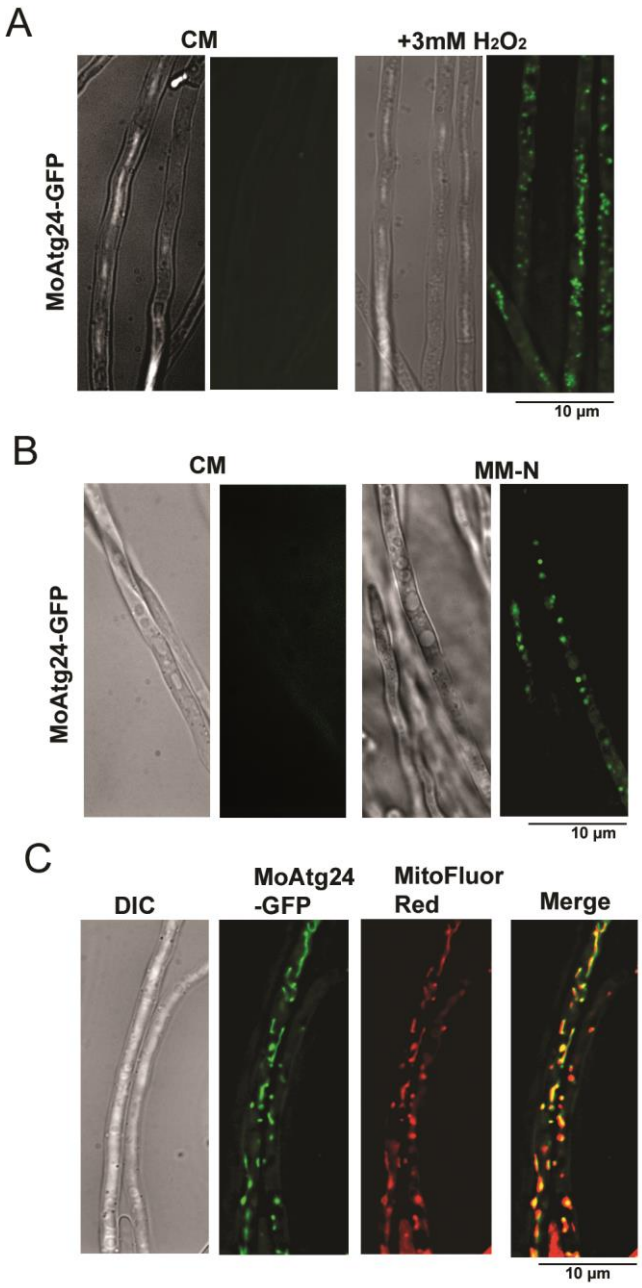
A
CM
+3mM H2O2
MoAtg24-GFP
10 μm
B
CM
MM-N
MoAtg24-GFP
10 μm
C
DIC
MoAtg24
-GFP
MitoFluor
Red
Merge
10 μm

Figure 8. MoAtg24-RFP does not localize to the peroxisomes

MoAtg24-RFP/GFP-SRL strain was cultured in liquid CM for 48 h. To induce MoAtg24-RFP expression, two-day old mycelia from CM were shifted to CM with 3 mM H_2O_2. Peroxisomes are marked by GFP-SRL.

Figure 8

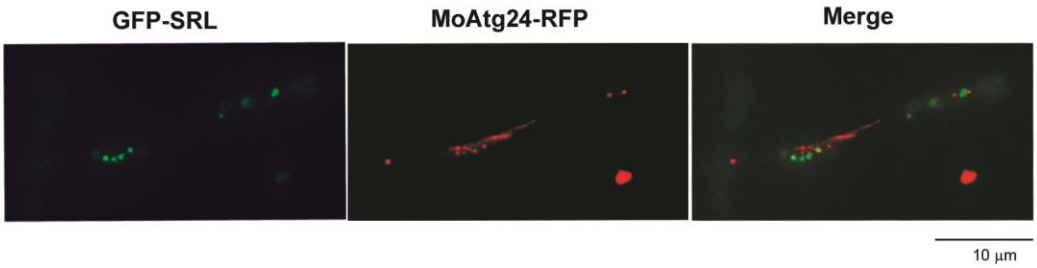

Figure 9. Atg24 is required for mitophagy in *M. oryzae*.

(A) Vacuolar mito-GFP could not be detected in *Moatg8*Δ or *Moatg24*Δ strains upon mitophagy induction. Glycerol/MM-N starved mycelia from indicated strains were incubated with 10 μM CMAC for 30 min. Imaging was immediately performed on Zeiss inverted confocal microscope.

(B) Vacuolar degradation of Porin in wild type upon mitophagy induction. Mitophagy induction was carried out as the process described in Methods and Materials. Mycelia were then collected at the indicated time points to extract the total cellular protein for immuno-blot analysis. Coomassie blue staining served as loading control.

(C) Comparison of vacuolar degradation of Porin in wild type, *Moatg24*Δ or *Moatg8*Δ strains. Loading control comprised staining the gel with Coomassie blue.

Figure 9

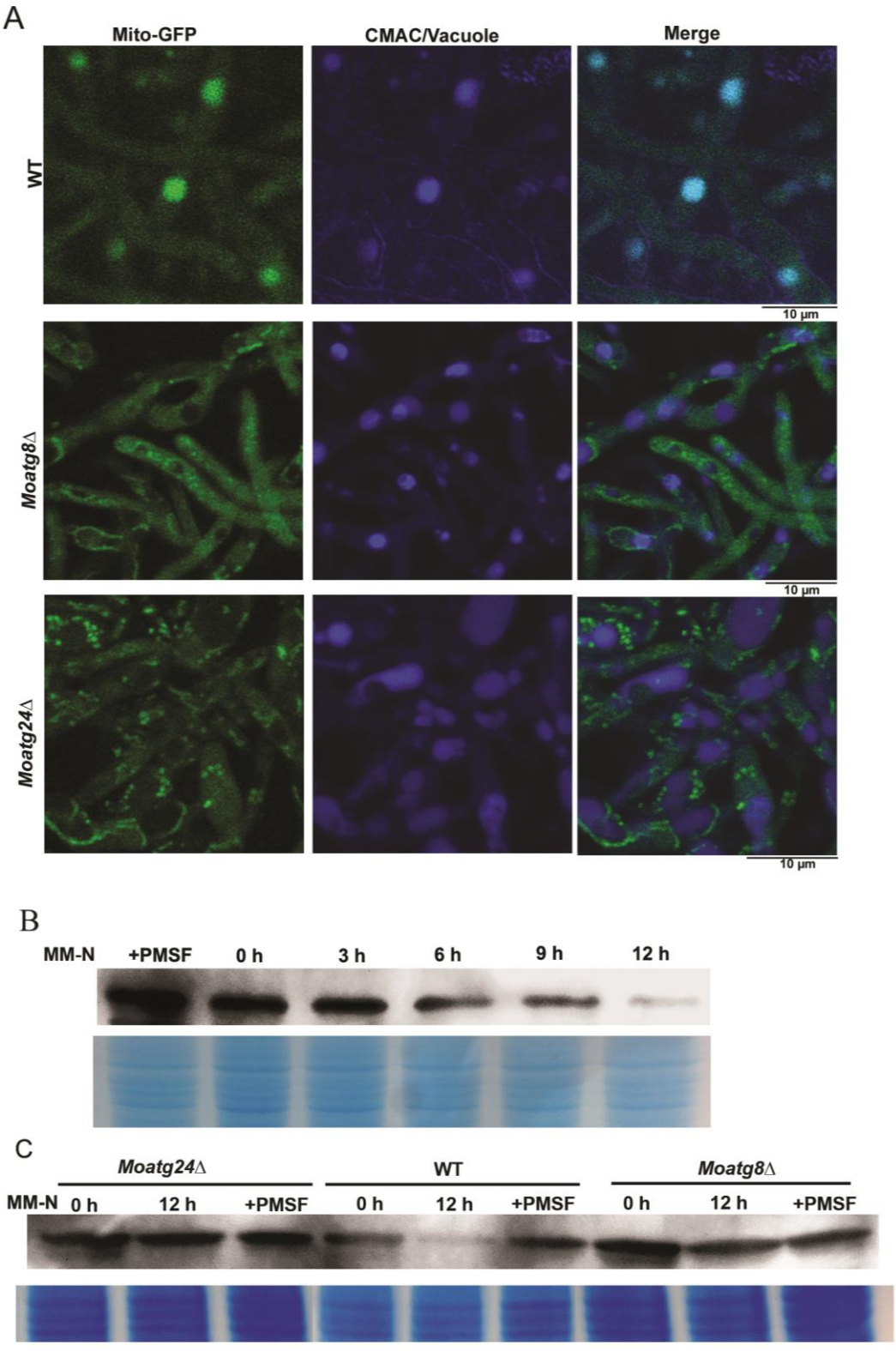
A
Mito-GFP
CMAC/Vacuole
Merge
WT
Moatg8Δ
Moatg24Δ
10 μm
10 μm
10 μm
B
MM-N
+PMSF
0 h
3 h
6 h
9 h
12 h
C
Moatg24Δ
WT
Moatg8Δ
MM-N
0 h
12 h
+PMSF
0 h
12 h
+PMSF
0 h
12 h
+PMSF

Figure 10. MoAtg24 is not essential for macroautophagy or pexophagy.

(A) Macroautophagy in *Moatg24*Δ is not affected. Indicated strains were cultured in CM for 2 days and then starved in MM-N for indicated time. Mycelia were then harvested and immunoblot analysis with anti-RFP antibody was carried out.

(B) Indicated strains expressing RFP-MoAtg8 were cultured in CM for 2 days and then starved in MM-N for 8 h prior to confocal microscopy. The vacuolarRFP-MoAtg8 is denoted by arrowheads.

(C) To induce pexophagy, two-day old mycelia from indicated strains were transferred into BM-O for 20 h. Subsequently, the mycelia were transferred into CM for 12 h. Immunoblot analysis was performed with anti-Pex14 antibody. Coomassie blue staining serves as loading control.

Figure 10

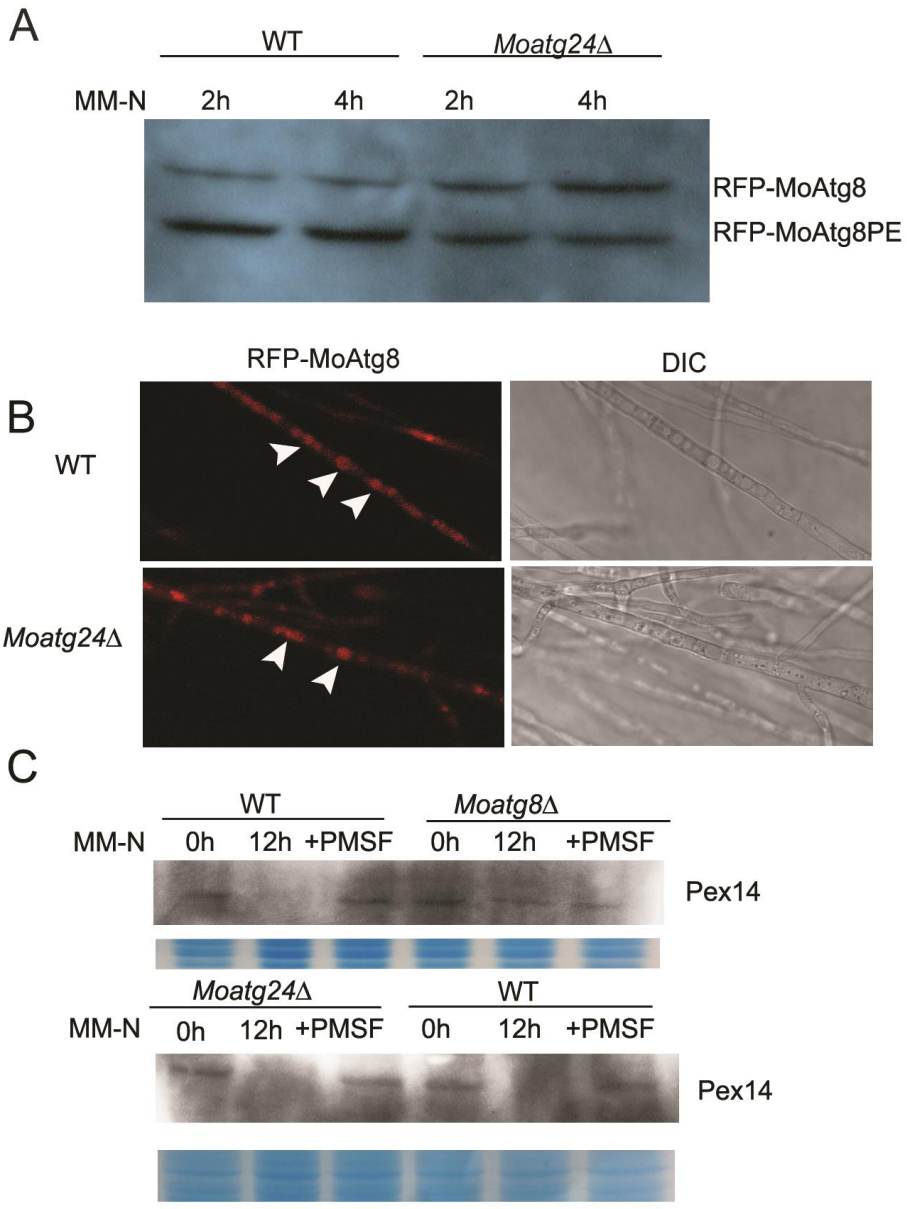
A
WT
Moatg24Δ
MM-N
2h
4h
2h
4h
RFP-MoAtg8
RFP-MoAtg8PE
B
RFP-MoAtg8
DIC
WT
Moatg24Δ
C
WT
Moatg8Δ
MM-N
0h
12h
+PMSF
0h
12h
+PMSF
Pex14
Moatg24Δ
WT
MM-N
0h
12h
+PMSF
0h
12h
+PMSF
Pex14

Figure 11. MoAtg24 colocalizes with mitochondria and RFP-MoAtg8 during mitophagy.

(A) Colocalization between mito-GFP and MoAtg24-RFP was observed in fragmented/punctate (upper panel) and filamentous (lower panel) mitochondria, as denoted by arrowheads.

(B) RFP-MoAtg8 colocalizes with mito-GFP (Mitochondria). Colocalization between RFP-MoAtg8 and mito-GFP could be found in spherical vacuoles (upper panel), filamentous mitochondria and/or vacuoles (middle panel) and fragmented/punctate mitochondria (lower panel), as denoted by the arrowheads.

(C) MoAtg24-GFP colocalized with RFP-MoAtg8 during mitophagy.

Figure 11

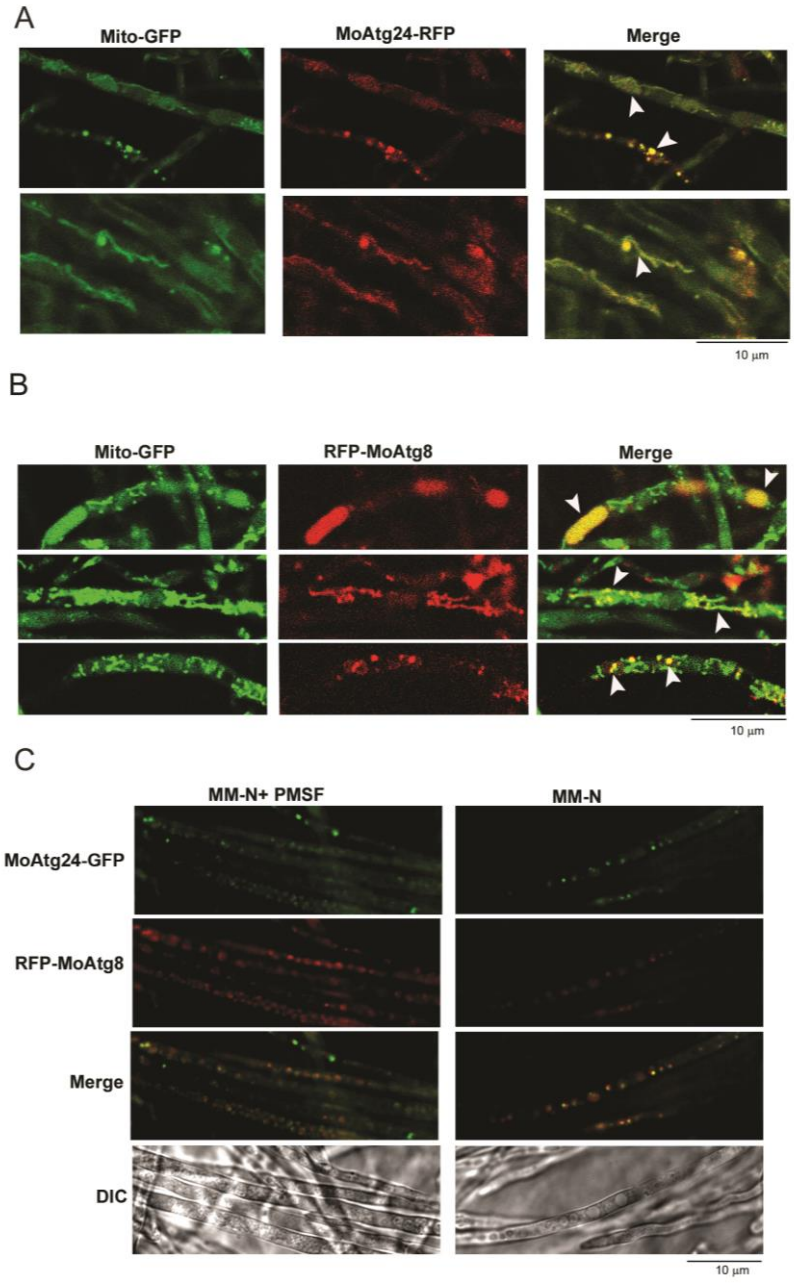
A
Mito-GFP
MoAtg24-RFP
Merge
10 μm
B
Mito-GFP
RFP-MoAtg8
Merge
10 μm
C
MM-N+ PMSF
MM-N
MoAtg24-GFP
RFP-MoAtg8
Merge
DIC
10 μm

3.2.8 Domain analysis of PX and BAR domains in MoAtg24

To understand the function of MoAtg24 in mitophagy, it is important to analyze the functions of the two domains in MoAtg24, namely the PX and BAR domains. To characterize these two domains, MoAtg24-GFP without PX domain and MoAtg24-GFP without BAR domain were generated (Figure 12A). The PX domain truncated MoAtg24$_{190\text{-}495}$-GFP displayed cytosolic localization upon mitophagy induction (Figure 12B). This cytosolic localization was also observed in the BAR domain truncated variant, MoAtg24$_{1\text{-}190}$-GFP (Figure 12B). Considering that MoAtg24-GFP colocalizes with mitochondria, these results indicate that the PX and BAR domains are both required to anchor MoAtg24 to mitochondria.

3.2.9 Phospholipid PI3P is enriched on mitochondria

Although PX and BAR domains need to cooperate together to anchor MoAtg24 to mitochondria, it is possible that PX domain plays a more important function in targeting, since PX domain is shown more to target proteins to membrane microdomains while the BAR domain strengthens the protein-membrane binding. GFP-2xFYVE was used to monitor PI3P, a known PX domain binding phospholipid. In normal physiological conditions, about 15% of total mitochondria colocalize with GFP-2xFYVE puncta (Figure 13A left panel and 13B). However, this colocalization increases dramatically to near 100% in presence of ROS stresses (Figure 13A right panel and 13B). Based on these observations, PI3P is enriched on mitochondria in presence of ROS stresses.

Figure 12. PX and BAR domains are required for mitochondrial anchoring of MoAtg24.

(A) Schematic representation of truncated versions of MoAtg24, tagged with GFP.

(B) Stains expressing indicated truncated MoAtg24-GFP were cultured in CM. To induce the truncated MoAtg24-GFP expression, the mycelia were then transferred into CM with 2 mM H_2O_2. To visualize mitochondria, mycelia were incubated with MitoFluor Red for 30 min prior to confocal imaging.

Figure 12

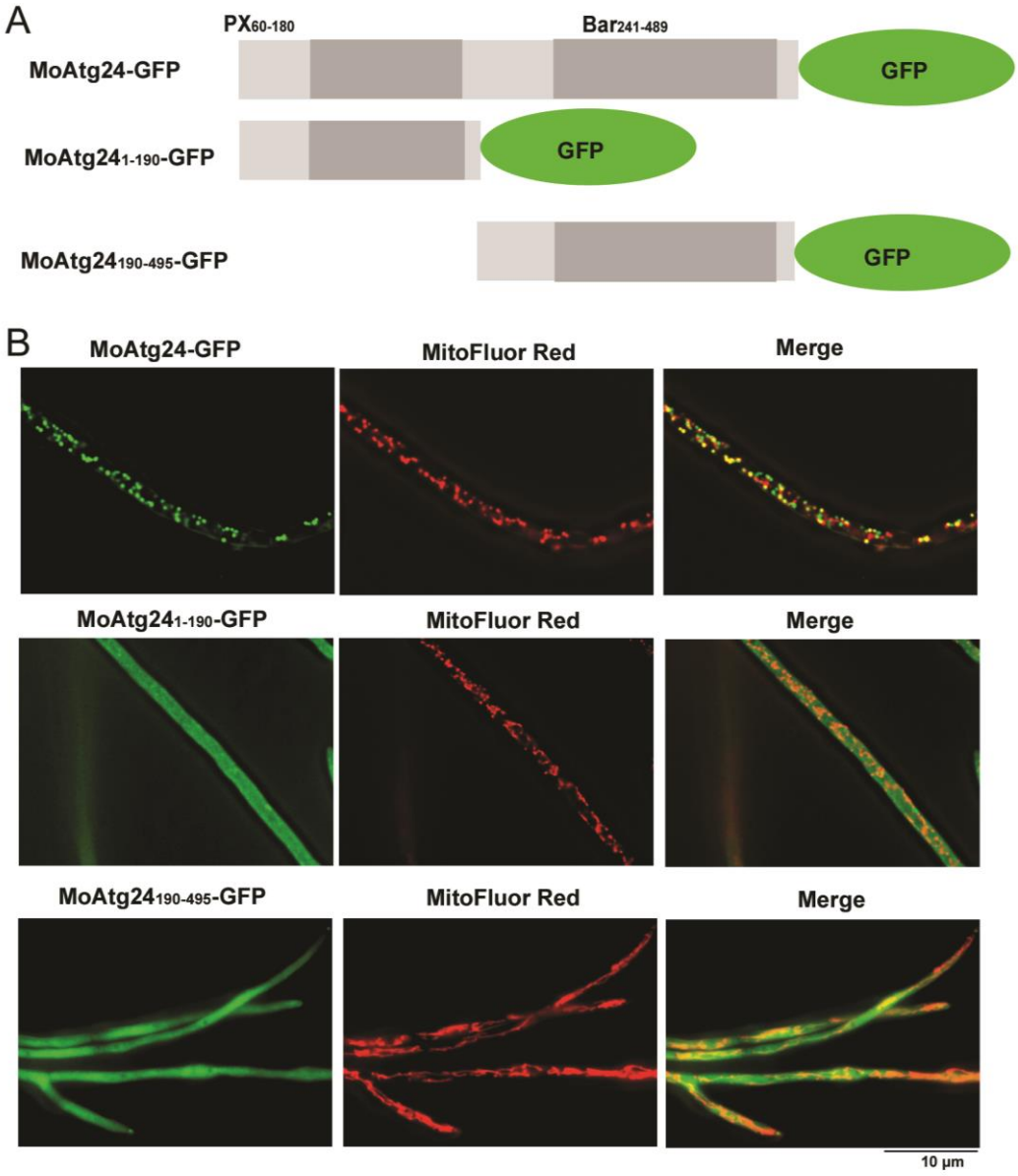
A
PX60-180
Bar241-489
MoAtg24-GFP
GFP
MoAtg241-190-GFP
GFP
MoAtg24190-495-GFP
GFP
B
MoAtg24-GFP
MitoFluor Red
Merge
MoAtg241-190-GFP
MitoFluor Red
Merge
MoAtg24190-495-GFP
MitoFluor Red
Merge
10 μm

Figure 13. Phospholipid PI3P is enriched on mitochondrial membrane.

(A) To visualize PI3P, GFP-2xFYVE was expressed in the WT strain. The 2 d old mycelia of such strain from CM were incubated in CM with 5 mM H_2O_2 for 30 min prior to observation.

(B) Quantification of co-localization between MitoFluor Red (mitochondria) and GFP-2xFYVE (PI3P). To calculate the co-localization rate, 30 images were taken for each instance. Subsequently, the number of mitochondria partially or completely colocalzied with GFP signal was quantified with ImageJ (http://rsb.info.nih.gov/ij/).

Figure 13

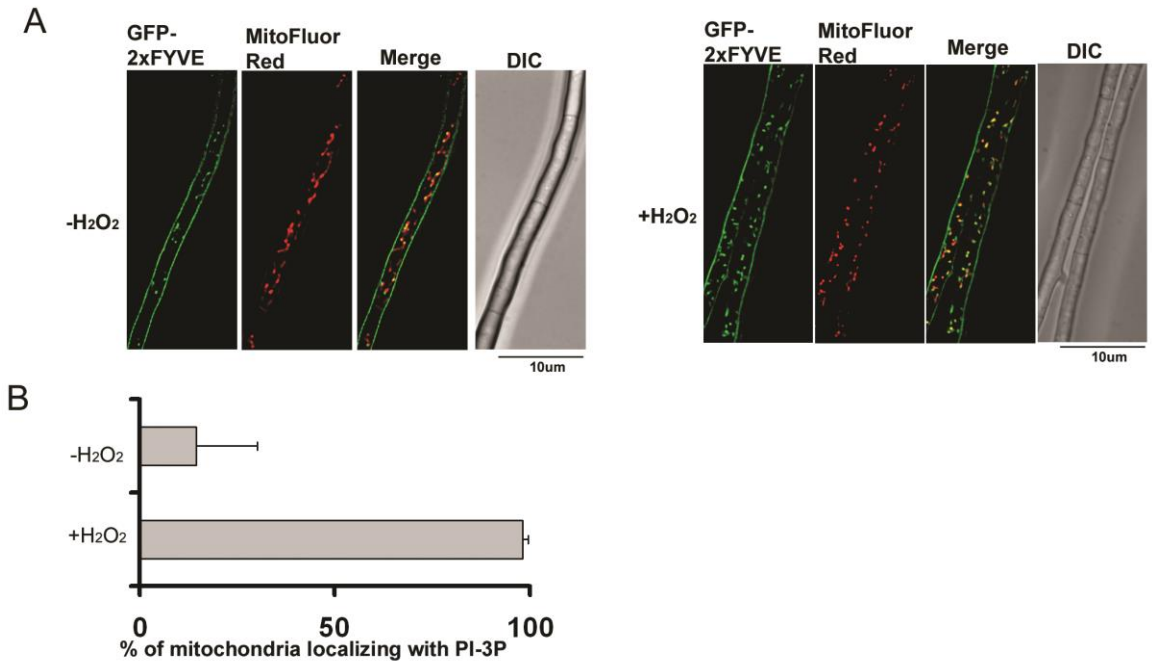
A
GFP-
2xFYVE
MitoFluor
Red
Merge
DIC
-H2O2
+H2O2
10um
B
-H2O2
+H2O2
0
50
100
% of mitochondria localizing with PI-3P

3.2.10 Mitophagy occurs naturally in foot cells during conidiation

Based on the data mentioned above, MoAtg24 affects aerial growth and conidiation and is also essential for mitophagy. However, it is not clear whether the role of MoAtg24 in conidiation is dependent on its function in mitophagy or not. To address this question, I investigated the existence of mitophagy during conidiation. Mito-GFP was clearly detected in vacuoles in the foot cells during conidiation (Figure 14B and 14E; n=30). In contrast, such vacuolar mito-GFP signal was unable to detect in aerial hyphae (Figure 14C and 14F; n=30). In the *Moatg24*Δ mutant, mito-GFP could not be detected in vacuoles in either foot cells or aerial hyphae (Figure 14H and 14I; n=30). Based on these results, it is clear that mitophagy occurs naturally in foot cells during *M. oryzae* conidiation, while MoAtg24 is essential for that.

3.2.11 Mitophagy occurs naturally during invasive growth

Since MoAtg24 is essential in mitophagy and *Moatg24*Δ shows highly reduced invasive growth, it is important to study whether MoAtg24-based mitophagy occurs naturally in invasive hyphae. Vacuolar mito-GFP signal could be detected at 48 hpi in invasive hyphae (Figure 15, upper panels; vacuoles were stained by CMAC). By contrast, such vacuolar mito-GFP signal was undetectable in invasive hyphae in *Moatg24*Δ (Figure 15, lower panels). Considering the MoAtg24 mutant is defective in invasive growth, these results suggest that MoAtg24 mediated mitophagy plays an important role in invasive growth.

Figure 14. Mitophagy occurs in foot cells during Magnaporthe conidiation.

Foot cells observation was prepared as the methods described in Methods and Materials. Confocal microscopy was carried out at 20 h post photo-induction to observe foot cells (FC) and aerial hyphae (AH).

Mitophagy observation was performed in FC and the connected AH. Two cases of such observation are shown in panels (A-C) and (D-F) individually. Panel (B) and (E) depict the mitophagy in FC, while Panel (C) and (F) describe the mitophagy in AH. The mitophagy defects in *Moatg24*Δ could be observed in panel (G-I). (H) and (I) show enlarged FC and AH respectively from the boxed regions in (G). Vacuoles based on DIC images were identified and marked by arrowheads in fluorescent images.

Figure 14

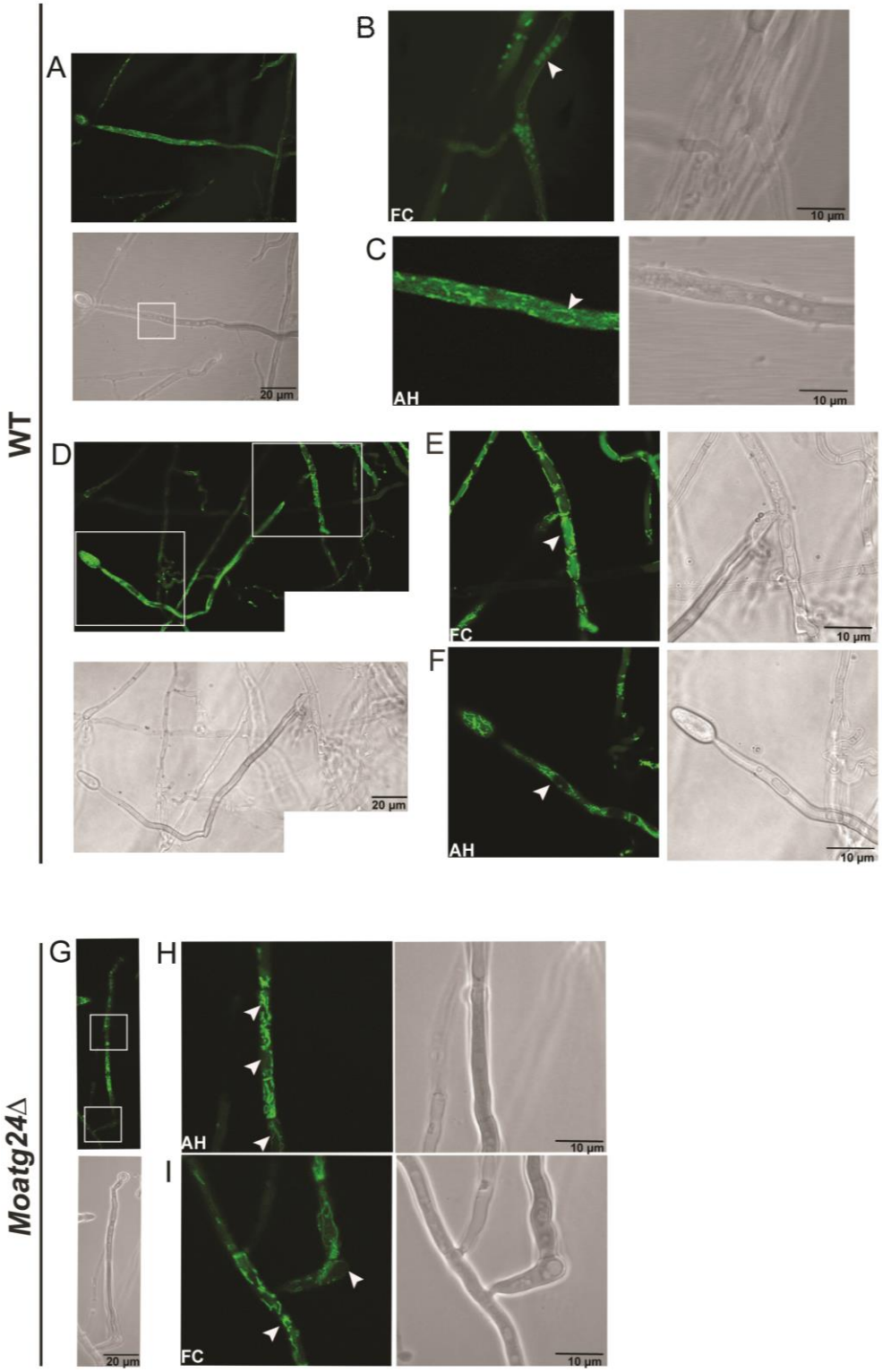
WT
A
B
FC
10 μm
20 μm
C
AH
10 μm
D
E
FC
10 μm
20 μm
F
AH
10 μm
Moatg24Δ
G
H
AH
10 μm
20 μm
I
FC
10 μm

Figure 15. Mitophagy during invasive growth in *M. oryzae*.

Wild type or *Moatg24*Δ expressing mito-GFP was inoculated on rice sheaths. Confocal microscopy was performed at 48 hpi. The vacuoles in invasive hyphae were stained by CMAC.

Figure 15

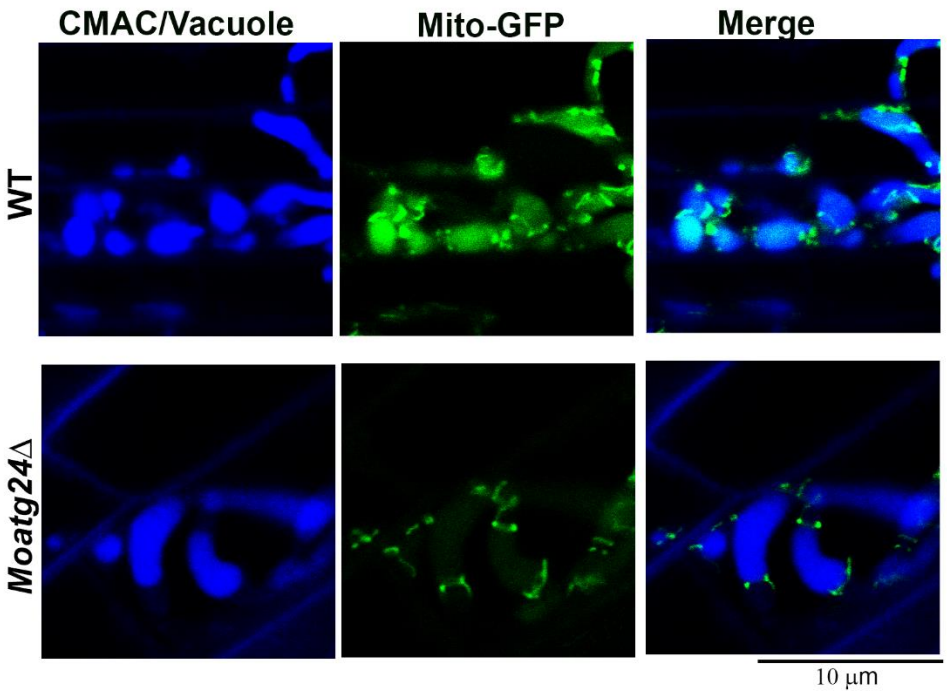

3.2.12 GFP-ScAtg32 associates with mitochondria in *M. oryzae*

In yeast, ScAtg32 specifically mediates mitophagy, and it is translocated onto mitochondria upon mitophagy induction (Kanki et al 2009, Okamoto et al 2009). Both MoAtg24 and ScAtg32 contain a WXXL motif and a mitochondrial targeting domain, thus it is highly possible that MoAtg24 might share some similar functions as ScAtg32 in mitophagy. If they do share some common functions, it is highly possible that the conidiation defects of *Moatg24*Δ could be at least partially rescued by ScAtg32. To test this hypothesis, I first expressed GFP-ScAtg32 under a strong constitutive promoter (RP27 promoter) in *Moatg24*Δ. The localization of GFP-ScAtg32 was first examined. As predicted, GFP-ScAtg32 nicely colocalized with mitochondria stained by Mito-Fluor Red (Figure 16), which indicates that the GFP-ScAtg32 might function in mitophagy in *M. oryzae.*

3.2.13 GFP-ScAtg32 partially restored the conidiation defects in *Moatg24*Δ.

After the localization of GFP-ScAtg32 was examined, I next checked whether *Moatg24*Δ defects could be repressed by yeast ScAtg32. Conidiation was significantly increased in *Moatg24*Δ expressing the $RP27_{PRO}$:GFP-ScAtg32 (Figure 17A). After two day induction by light, *Moatg24*Δ expressing the $RP27_{PRO}$:GFP-ScAtg32 produced an equivalent number of conidia as WT (Figure 17B). However, the number of conidia collected in *Moatg24*Δ with GFP-ScAtg32 strain after five days light induction was significantly smaller than that in WT (Figure 17B).

Figure 16. GFP-ScAtg32 localizes to mitochondria in *M. oryzae*.

To visualize the localization of GFP-ScAtg32, the strain expressing GFP-ScAtg32 was cultured in CM for 2 d. Subsequently, the mycelia were incubated with MitoFluor Red for 30 min prior to confocal microscopy.

Figure 16

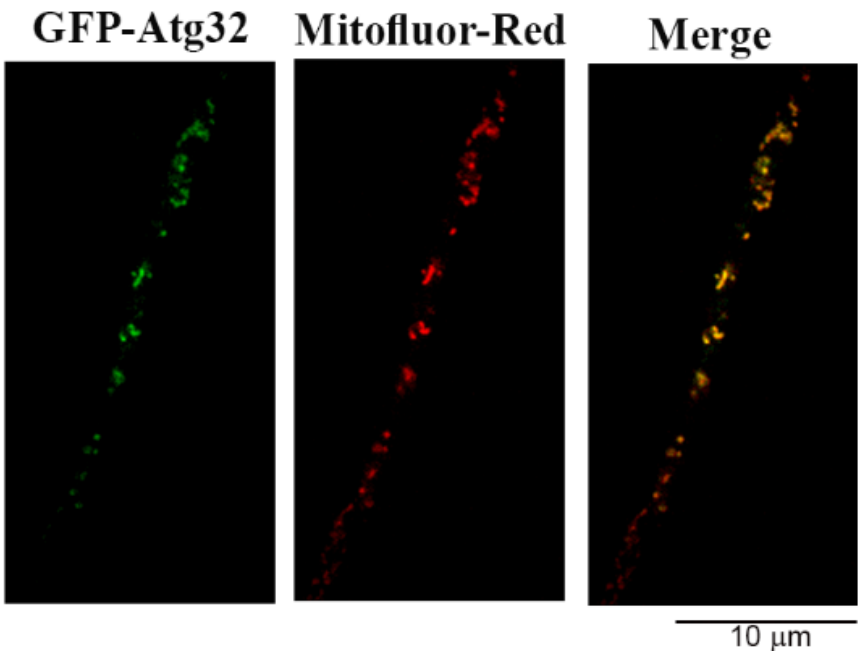

Figure 17. Conidiation defect of *Moatg24*Δ is partially repressed by expressing GFP-ScAtg32.

(A) Improved conidiation was observed in the *Moatg24*Δ mutant expressing GFP-ScAtg32.

(B) Quantification of conidiation in wild type, *Moatg24*Δ or *Moatg24*Δ with GFP-ScAtg32 strain. Mean values (±SE) presented as percentage points were derived from three independent experiments (three colonies for each sample).

(C) Conidia collapsed in *Moatg24*Δ with GFP-ScAtg32. The collapsed conidia are indicated by arrowheads.

Figure 17

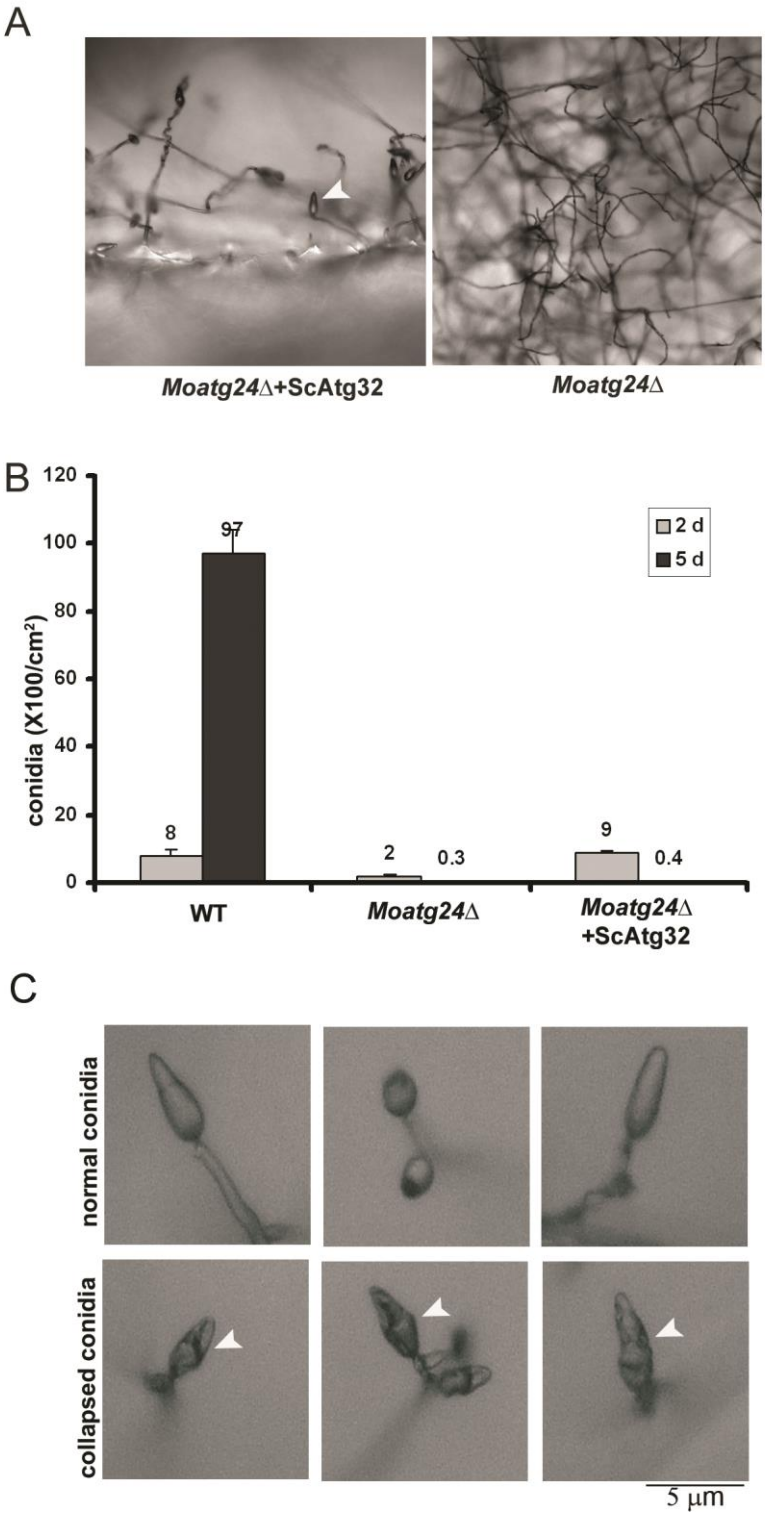
A
Moatg24Δ+ScAtg32
Moatg24Δ
B
conidia (X100/cm²)
120
100
80
60
40
20
0
97
8
2
0.3
9
0.4
2 d
5 d
WT
Moatg24Δ
Moatg24Δ
+ScAtg32
C
normal conidia
collapsed conidia
5 μm

To understand the controversial results of conidiation upon short (two days) versus long photo-induction (five days), the process of conidiation was analyzed in more details. I found that conidia produced by *Moatg24*Δ with the GFP-ScAtg32 failed to mature and subsequently collapsed (Figure 17C). Since the quality and viability of conidia produced in *Moatg24*Δ with the GFP-ScAtg32 strain were compromised, such conidia could not be used in infection assays. Based on these data, I conclude that MoAtg24 shares common functions with ScAtg32 in mitophagy.

3.2.14 *Moatg24*Δ is hypersensitive to oxidative stresses.

Since mitochondria are important organelles for controlling the cellular ROS levels, I tested whether the defects in mitophagy affects the sensitivity to ROS. The sensitivities of *Moatg24*Δ to mitochondrial respiratory complex inhibitors (menadione and paraquat) were increased compared to WT (Figure 18A). By contrast, the sensitivity of *Moatg24*Δ to a whole-cellular ROS generator (H_2O_2) was comparable to WT (Figure 18A). Furthermore, the conidiation defects of *Moatg24*Δ could be partially restored by antioxidants such as NAC and GSH (Figure 18B). I conclude that MoAtg24 plays a key role in cellular redox homeostasis during conidiation in *M. oryzae*.

3.3 Discussion

In this chapter, I identified that mitophagy is conserved in *M. oryzae*, which extends the research of mitophagy in yeast and mammalian cells.

Figure 18. *Moatg24*Δ is hypersensitive to oxidative stress.

(A) The sensitivity of wild type, *Moatg24*Δ and *Moatg8*Δ to H_2O_2, Menadione and Paraquat.

(B) Effects of antioxidants NAC, Ascorbate or GSH on conidiation in *Moatg24*Δ. Mean values (±SE) presented as percentage points were derived from three independent experiments (3 colonies for each instance).

Figure 18

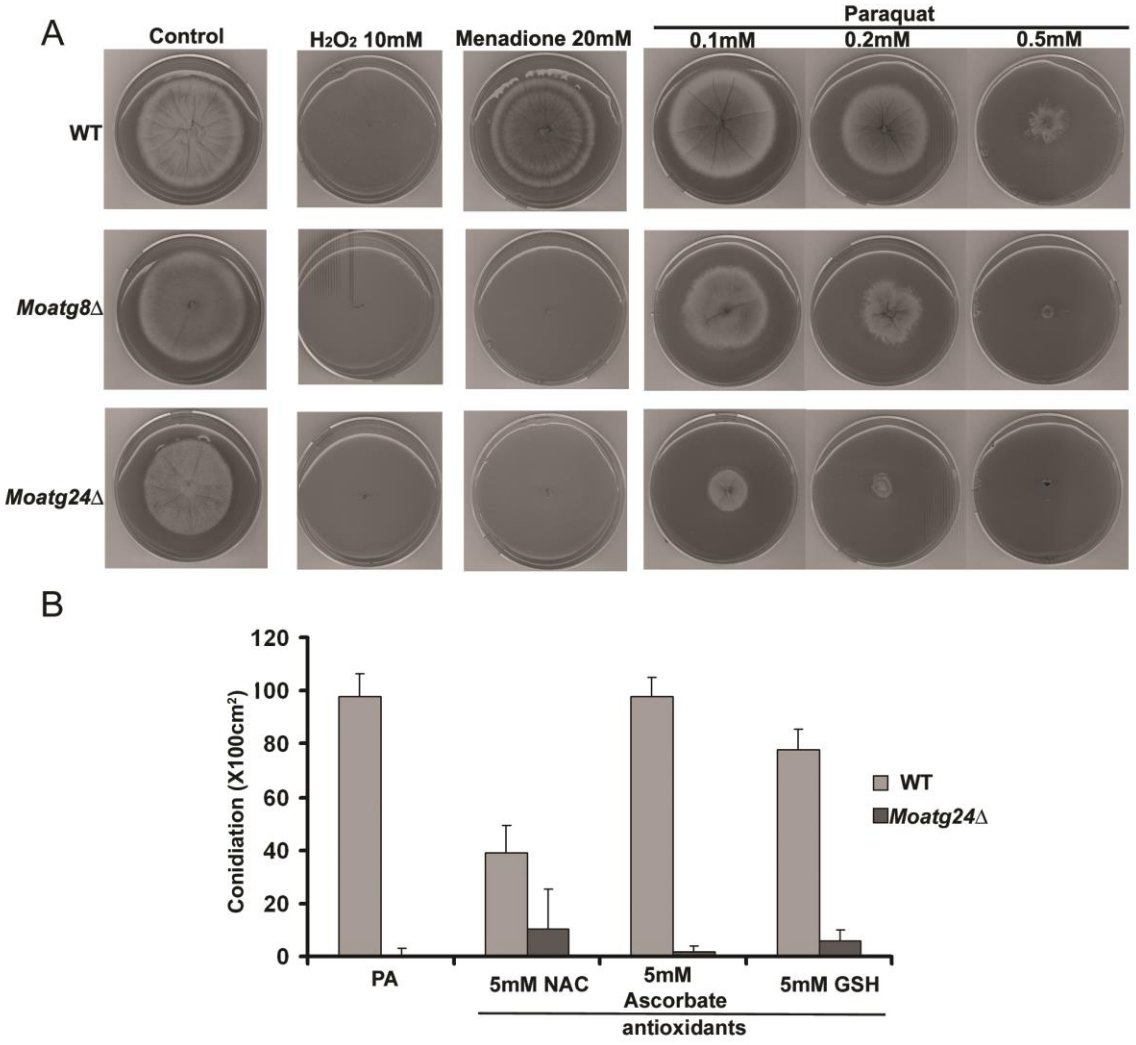
A
Control
H2O2 10mM
Menadione 20mM
Paraquat
0.1mM
0.2mM
0.5mM
WT
Moatg8Δ
Moatg24Δ
B
Conidiation (X100cm2)
120
100
80
60
40
20
0
WT
Moatg24Δ
PA
5mM NAC
5mM Ascorbate
5mM GSH
antioxidants

It is clear that mitophagy has important functions in conidiation and involves in oxidative stress regulation. More importantly, I confirmed that MoAtg24 specifically mediates mitophagy and is not required for macroautophagy and/or pexophagy, which could be used to understand the physiological function of mitophagy in *M. oryzae*.

Based on my biochemical and cell biological examination, mitophagy could be induced by nitrogen starving of two days old mycelia from the glycerol medium (Kanki et al 2009). Upon mitophagy induction, MoAtg24 was induced and translocated onto mitochondria dependent on its PX and BAR domains. The induced expression and translocation are similar to ScAtg32 in mitophagy in yeast (Okamoto et al 2009). Based on these similarities, I speculate that MoAtg24 reflects an aspect of adaptive evolution as the yeast mitophagy mediator, since ScAtg32 is not conserved in filamentous fungi including *M. oryzae*. And this hypothesis is partially confirmed based on the restoration of conidiation in *Moatg24*Δ upon exogenous expression of ScAtg32.

Another interesting observation was that mitophagy only occurs in foot cells but not in aerial hyphae. Since foot cells and aerial hyphae are inter-connected and cooperate to transfer carbon sources and other necessary nutrients during conidiation, how is mitophagy differently regulated in these two compartments is an interesting question. Future studies will be designed to explore such distinct regulation during asexual reproduction in the rice blast development.

To understand the relationship between mitophagy and cellular ROS, the sensitivity of mitophagy defective strains to ROS was tested. *Moatg24*Δ was highly sensitive to menadione and paraquat but not exogenous peroxides/H_2O_2. Exogenously added menadione and paraquat could inhibit mitochondrial respiratory chain complex IV and II respectively, and herein enhance the mitochondrial ROS specifically (Cocheme & Murphy 2008, Criddle et al 2006). Taken together, *Moatg24*Δ shows increased sensitivity specifically to mitochondrial ROS. This observation reaffirms the functions of MoAtg24 in mitophagy and redox regulation. However, *Moatg8*Δ does not show any increased sensitivity specifically to mitochondrial ROS compared to *Moatg24*Δ. Therefore, MoAtg24 might serve some additional functions in mitochondria.

To summarize, the sorting nexin Atg24 in *M. oryzae* shows likely adaptive function in mitochondrial targeting as an important step towards mitophagic regulation of organelle integrity and function towards likely modulation of nutrient and/or redox homeostasis.

CHAPTER IV MITOCHONDRIAL DYNAMICS DURING HOST-PATHOGEN INTERACTION IN THE RICE BLAST PATHOGENESIS

4.1 Introduction

The pathogenic life cycle in *M. oryzae* consists of conidiation, appressorium formation and maturation, penetration and invasive growth. Conidiation and appressorium formation can occur naturally without interaction with host cells. However, penetration and invasive growth could not be studied alone without host cells, which makes them difficult to research. Therefore invasive growth has not been studied carefully until recently, although there are numerous reports on mutations leading to invasive growth defects (Deng et al 2012, Ding et al 2010a, Patkar et al 2012, Yi et al 2009). Briefly speaking, around 24- 28 hpi, penetration hyphae are formed in a primary infected plant epidermal cell. Another 5 h later, bulbous hyphae were formed at the tips of penetration hyphae. Large vacuoles are the typical signatures of the bulbous hyphae and count more than 90% of the total volume. About 10 h later, the bulbous hyphae start to spread into neighboring cells through plasmodesmata (Khang et al 2010, Zhang & Xu 2014). Once the bulbous hyphae colonize the neighboring cells around the primary infected rice epidermal cell, they would grow rapidly into more plant cells to establish rice blast symptom. Because such morphological change of invasive hyphae has only been documented in recent studies (Giraldo et al 2013, Khang et al 2010), the molecular mechanisms or the molecular pathways involved in the invasive growth are largely unknown.

Based on lifestyles of invasive growth, nearly all known fungal pathogens of plants can be classified into three groups, biotrophic plant pathogens, necrotrophic plant pathogens and hemibiotrophic plant pathogens (Oliver & Solomon 2010). Whereas biotrophic pathogens require living host cells to support their obligate parasitism, necrotrophic plant pathogens are facultative parasites that may actively kill their host during the disease process by secretion of toxins (Laluk & Mengiste 2010). Hemibiotrophs establish themselves in host cells by eluding detection and forming associations with living cells, much like biotrophs. Later during the infection process, these pathogens more closely resemble necrotrophs, since they may spread rapidly and actively kill host cells (Laluk & Mengiste 2010). During a compatible interaction, biotrophs have evolved the means to evade recognition or to suppress plant defense responses while colonizing living tissue (Greenberg 1997). For these organisms, cell death becomes an unwanted consequence of the disease process that occurs late in infection. Conversely, elicitation of plant resistance during an incompatible interaction occurs with host recognition of pathogen-specific signal molecules that trigger multifaceted defense responses (Dangl et al 1996). Commonly associated with plant resistance is the induction of a hypersensitive response (HR), a rapid and localized cell death that restricts microbial growth to the site of ingress. It has been proposed that necrotrophs may even manipulate plant cell death programs such as HR for their own advantage (Dickman et al 2001, Mayer et al 2001). However, very little is known about the hemibiotrophs and the mechanisms underlying the transition from biotrophic to necrotrophic growth.

Regardless of the lifestyle of pathogen invasive growth, host responses to pathogen attack share several common features. The well-known feature of host responses is the dramatically increased ROS levels during host-pathogen interaction (Vellosillo et al 2010, Zurbriggen et al 2010). Considering mitochondria are the main sources of cellular ROS, more clearly understanding of mitochondrial function during invasive growth might provide useful information for the mechanisms underlying the transition from biotrophic to necrotrophic growth during rice blast development (Torres 2010). Mitochondria are able to dynamically fuse and divide in response to environmental factors, especially nutrients availability. The essential proteins involved in mitochondrial fusion and division in yeast have been described in Chapter I, and these proteins are evolutionarily conserved.

In this chapter, I provide evidence to support that mitochondrial dynamics and function are directly involved in invasive growth during the rice blast development. Furthermore, the mitochondrial dynamics correlates with the biotrophy-to-necrotrophy transition. More importantly, I demonstrate that genetic disruption of mitochondrial dynamics via loss of *MoDNM1* or *MoFZO1* leads to a failure in mediating the biotrophy-to-necrotrophy transition and to loss of the ability to maintain biotrophic growth respectively, thus suggesting that the mitochondrial dynamics is critical for invasive growth in the rice blast pathogen.

4.2 Results

4.2.1 Invasive growth of *M. oryzae*

In the initial efforts to understand the invasive growth, invasive hyphae were carefully observed at selected time points, 24 hpi, 30 hpi, 48 hpi, 72 hpi and 96 hpi. At 24 hpi, about 28% of the appressoria successfully penetrated the rice sheath, and primary hyphae could be clearly observed in plant cells (Figure 19A). Bulbous hyphae could be found in plant cells around 30 hpi. At this time point, 66% appressoria successfully penetrated the rice sheath. And among them 26% appressoria have formed bulbous invasive hyphae (Figure 19B). At 48 hpi, 76% appressoria successfully penetrated the rice sheath. And among them 22% and 33% appressoria have formed bulbous invasive hyphae and grown out into neighboring plant cells respectively (Figure 19C). At 72 hpi, 82% appressoria successfully penetrated the rice sheath. And among them 22%, 29% and 23% appressoria have formed secondary invasive hyphae, grown out into neighboring plant cells and spread into more than three neighboring plant cells respectively (Figure 19D).

As it is difficult to synchronize appressorium formation and penetration, the following patterns were used to describe the invasive growth at the selected timepoint: 1) Appressoria with primary hyphae around 24 hpi, 2) appressoria with bulbous hyphae only around 30 hpi, 3) appressoria with invasive hyphae grown out into neighboring plant cells at 48 hpi, 4) appressoria with invasive hyphae spread into more than three neighboring plant cells at 72 hpi.

Figure 19. Classification of invasive hyphae

The schematic represent the three types of invasive hyphae. The outlines of the plant cells are depicted in green, while the fungus is labeled greyish blue. The percentages of the different types of invasive hyphae observed at the selected time points, 24 hpi **(A)**, 30 hpi **(B)**, 48 hpi **(C)** and 72 hpi **(D)** were calculated. Mean values (±SE) presented as percentage points were derived from three independent experiments (around 200 invasive hyphae were counted in each independent experiment). Asterisks denote the appressorium.

Figure 19

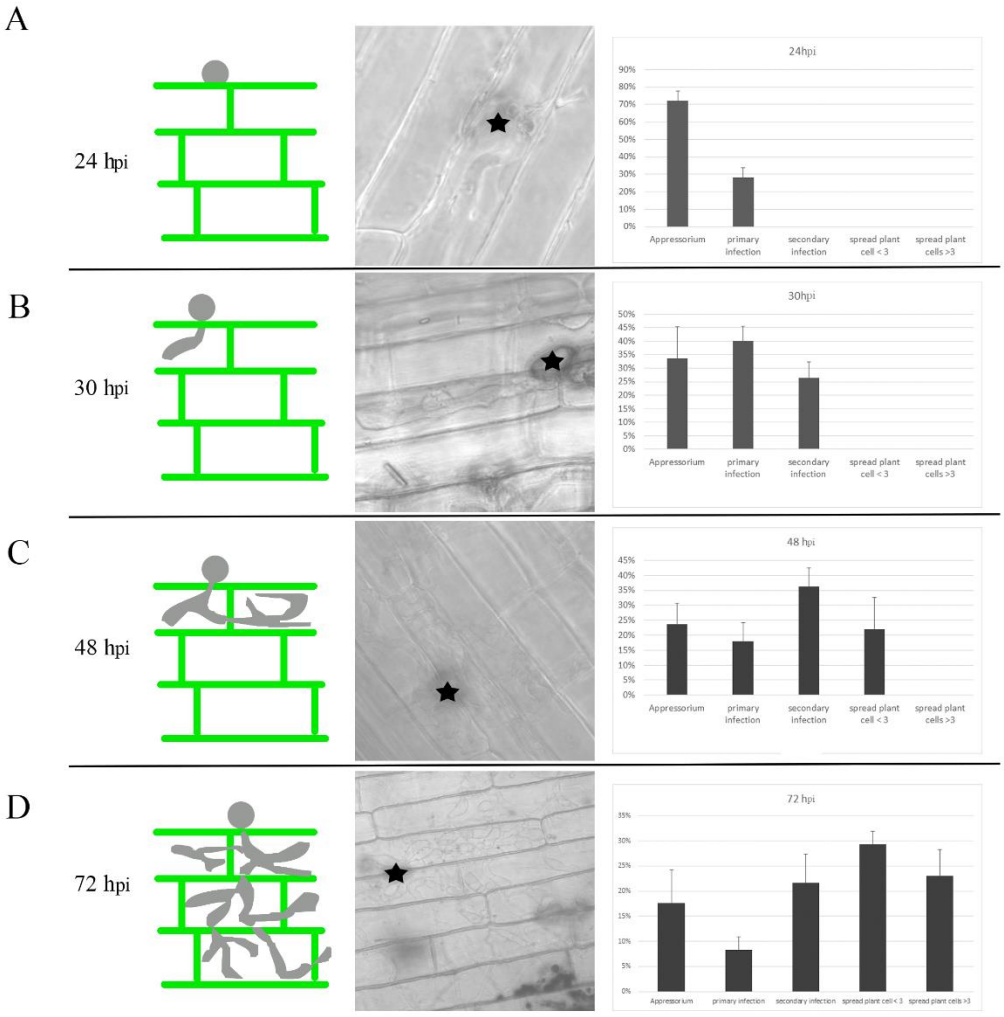
A
24 hpi
24hpi
90%
80%
70%
60%
50%
40%
30%
20%
10%
0%
Appressorium
primary infection
secondary infection
spread plant cell < 3
spread plant cells >3
B
30 hpi
30hpi
50%
45%
40%
35%
30%
25%
20%
15%
10%
5%
0%
Appressorium
primary infection
secondary infection
spread plant cell < 3
spread plant cells >3
C
48 hpi
48 hpi
45%
40%
35%
30%
25%
20%
15%
10%
5%
0%
Appressorium
primary infection
secondary infection
spread plant cell < 3
spread plant cells >3
D
72 hpi
72 hpi
35%
30%
25%
20%
15%
10%
5%
0%
Appressorium
primary infection
secondary infection
spread plant cell < 3
spread plant cells >3

4.2.2 Mitochondrial dynamics during invasive growth in *M. oryzae*

Mitochondria are essential organelles involved in many metabolic processes. Previous studies have shown that mitochondria actively fuse and divide in response to fluctuating metabolic status (Westermann 2010). To study the mitochondrial function during invasive growth of *M. oryzae*, I first examined the mitochondrial morphology during the first 72 hpi utilizing the mito-GFP strain, which was used in my previous study (He et al 2013). In all observations, Z-stack images were taken by a Zeiss inverted confocal microscope and 3-D reconstruction and measurements were done in Imaris (Bitplan). Briefly, at 30 hpi (the early stage of invasive growth), mitochondria (more than 90%) were mainly tubular or filamentous (Figure 20A, the 3D reconstruction was shown in the right panel). However, at 48 hpi (invasive hyphae just spread to neighbouring cells), most of the mitochondria (more than 90%) in invasive hyphae appeared punctate (Figure 20B, the 3D reconstruction was shown in the right panel). More interestingly, at 72 hpi (invasive hyphae spreads to at least three plant cells), around 50% mitochondria became filamentous or tubular again (Figure 20C, the 3D reconstruction was shown in Figure 20C right panel). Such time-course dependent dramatic changes of mitochondrial morphology suggest that the rice blast fungus might face dynamical environmental or cellular conditions during invasive growth at the first 72 hpi.

Figure 20. Mitochondrial morphology during host-pathogen interactions

The mitochondrial morphology was observed under a confocal microscope at 30 hpi **(A)**, 48 hpi **(B)** and 72 hpi **(C)**. The percentages of the fragmented and tubular mitochondria were observed and calculated at the selected time points. Mean values (±SE) presented as percentage points were derived from three independent experiments (around 100 invasive hyphae were observed and counted in each independent experiment).

Figure 20

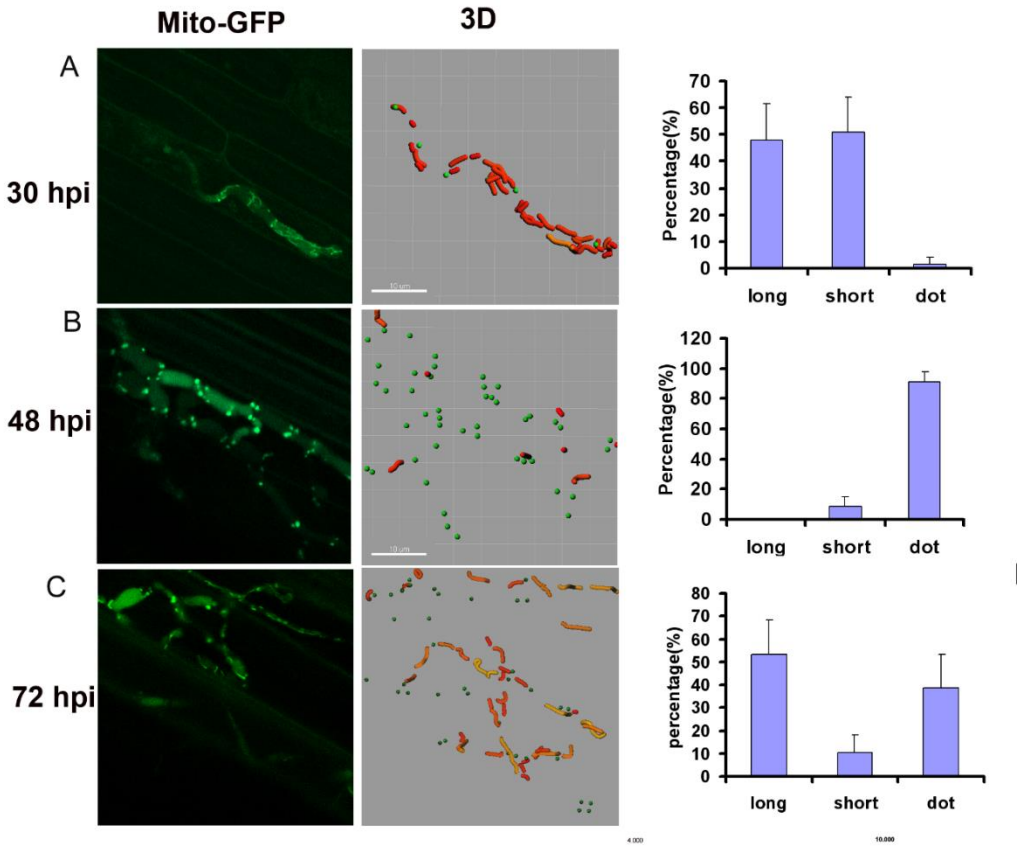
Mito-GFP
3D
A
30 hpi
B
48 hpi
C
72 hpi
Percentage(%)
70
60
50
40
30
20
10
0
long
short
dot
Percentage(%)
120
100
80
60
40
20
0
long
short
dot
percentage(%)
80
70
60
50
40
30
20
10
0
long
short
dot

4.2.3 Mitochondrial dynamics mediates biotrophy to necrotrophy switch

To understand the role of mitochondrial dynamics observed, invasive growth was herein examined carefully. Very interestingly, previous studies reported that lesion could be seen at 72 hpi, which suggests that necrotrophic growth is evident before 72 hpi (Samalova et al 2013). Although there are little data of the molecular mechanisms in controlling biotrophy to necrotrophy switch, it is highly possible that mitochondrial dynamics might be involved in this process as the time point at which mitochondrial fragmentation (48 hpi) occurs is before the observation of necrotrophy. To test whether mitochondrial dynamics correlates to biotrophy to necrotrophy switch, trypan blue staining was performed with the infected rice sheath. Only dead cells could be stained by trypan blue as live cells possess intact cell membranes that exclude trypan blue (van Wees 2008). As expected, cell death could only be found at 72 hpi, but not at 30 hpi or 48 hpi (Figure 21). These results affirm that mitochondrial fragmentation occurs before necrotrophic invasive growth and it is highly possible that mitochondrial dynamics is one of the key events triggering biotrophic to necrotrophic growth transition.

4.2.4 Mitochondrial fission machinery involved in invasive growth

To understand the role of mitochondrial dynamics in invasive growth, I investigated the role of mitochondrial fission. Based on the research in yeast and mammalian cells, the punctate mitochondria are mainly derived from tubular mitochondria through division (Benard & Karbowski 2009). To

investigate the role of mitochondrial fission in mitochondrial dynamics during host-pathogen interaction, the *Modnm1*Δ mutant was generated and characterized. Initially, the full-length *M. oryzae MGG_06361.6* was identified through BLAST as the orthologue of *ScDNM1*. Similar to ScDnm1, MoDnm1 contains the conserved GTPase, Dynamin central and GTPase effector domains (Figure 22A). Between Dynamin central and GTPase effector domains, a small region called Insert B is also conserved and plays very important roles in the Dnm1/Mdv1 interaction. The *Modnm1*Δ mutants were then generated by replacing the entire *MGG_06361.6* open reading frame with the Sulfonylurea-resistance marker cassette (*ILV2*, Figure 22B) in the mito-GFP strain. The deletion strains were then confirmed by Southern blotting (Figure 22C). Two independent strains were then characterized for various aspects of pathogenesis.

As expected, mitochondria in *Modnm1*Δ formed interconnected fishnet-like structures in vegetative mycelia, while the WT still showed punctate and filamentous mitochondria (Figure 23A). The differences of the mitochondrial network between *Modnm1*Δ and WT were more obvious during invasive growth (Figure 23B). Based on these results, I conclude that MoDnm1 is required for mitochondrial fission during vegetative growth and invasive growth in *M. oryzae*.

Figure 21. Biotrophy to necrotrophy switch occurs between 48 hpi and 72 hpi.

Rice sheath inoculated with water (in panel **A**) or wild type *M. oryzae* conidia ($1x10^6$/mL, in panel **B**) was stained by trypan blue. Rice sheath at indicated time point was then processed as described in methods and materials**.** Conidia droplets are outlined by the dashed lines. The asterisks mark the dead plant cells because of precutting during preparation of rice sheath.

Figure 21

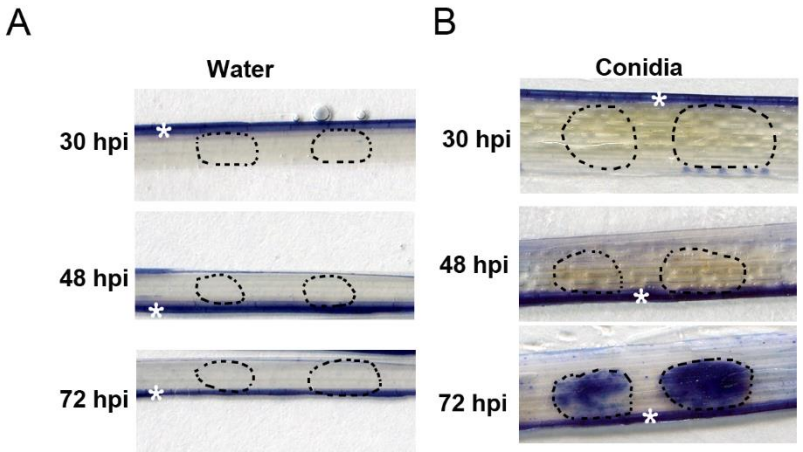

Figure 22. Generation of *Modnm1*Δ.

(A) Domains organization of MoDnm1.

(B) Schematic representation of *MoDNM1* locus with an approximate 1 kb flanking region (dashed lines). Solid bars and open boxes indicate the coding regions of *MoDNM1* and the sulfonylurea-resistance cassette (*IVL2*) respectively. The strategy of homology based gene replacement is also described. Restriction enzyme sites *SacI* used for genomic DNA digestion have been depicted.

(C) *Modnm1*Δ mutants were confirmed by southern blotting. Genomic DNA from wilds type or Modnm1Δ was digested with *SacI*. Southern blotting was performed as described in methods and materials. The appearance of the 1.9 kb band in the *Modnm1Δ* strain, with the concomitant loss of the wild-type 5 kb *MoDNM1* locus, was diagnostic of the correct gene replacement event. Transformants number 1, 3 and 4 are *Modnm1*Δ mutants.

Figure 22

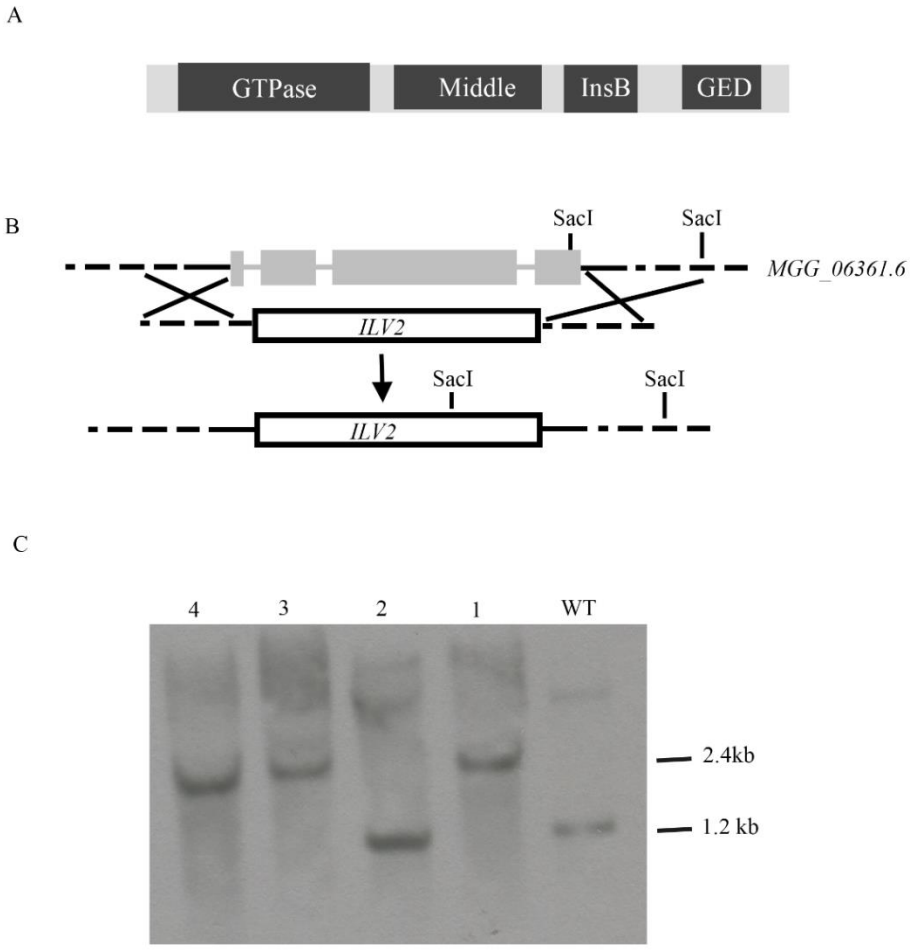
A
GTPase
Middle
InsB
GED
B
SacI
SacI
MGG_06361.6
ILV2
SacI
SacI
ILV2
C
4
3
2
1
WT
2.4kb
1.2 kb

Figure 23. The function of MoDnm1 in mitochondrial fission in *M. oryzae*.

(A) Mitochondrial morphology in vegetative hyphae of *Modnm1*Δ and WT. Vegetative hyphae of *Modnm1*Δ and WT expressing mito-GFP were cultured in CM for 2 days before observation. The inter-connected network of mitochondria in mycelia of *Modnm1*Δ is enlarged for easy visualization.

(B) Mitochondrial morphology in invasive hyphae of *Modnm1*Δ and WT. Mitochondrial morphology was observed in invasive hyphae of *Modnm1*Δ and WT at 36 hpi.

Figure 23

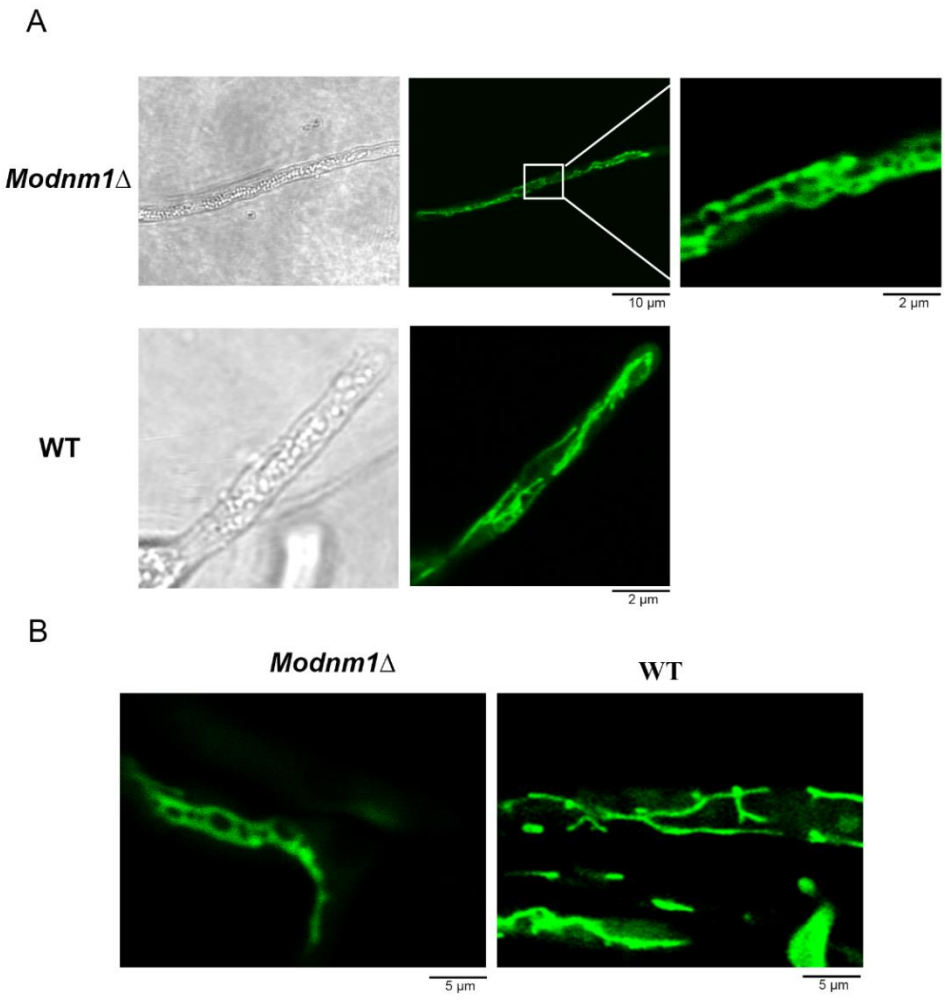

4.2.5 Mitochondrial fission is required for pathogenicity

Vegetative growth, colony formation, conidiation and appressorium formation of the *Modnm1*Δ mutant were comparable to those of WT. However, pathogenicity of the *Modnm1*Δ mutant was highly reduced. In spray inoculation of WT conidia on 3-week old seedlings, typical blast disease lesions could be found on rice leaves at 7 dpi (Figure 24A). However, only small black puncta or dots could be found on leaves of rice seedlings inoculated with *Modnm1*Δ conidia (Figure 24B). Based on these data, I conclude that MoDnm1 indeed plays a crucial role in *M. oryzae* pathogenesis, which infers the importance of mitochondrial fission during *in planta* growth of *M. oryzae*.

4.2.6 Disruption of mitochondrial fission prevents biotrophy to necrotrophy switch

To further understand the reason of reduced pathogenicity in *Modnm1*Δ mutants, time course detailed analysis was performed based on rice sheath infection assay. The infection of *Modnm1*Δ at 30 hpi was comparable to the WT and both of them grew well in the primary infected plant cells (Figure 25A). The HR responses were similar in the rice sheath infected by *Modnm1*Δ and WT (Figure 25A, DIC image). The infection of *Modnm1*Δ at 48 hpi was also similar to the WT and showed invasion/spread into neighbouring plant cells (Figure 25A). There were also no differences in the HR responses in the rice sheath infected by *Modnm1*Δ and WT (Figure 25A, DIC image). However, the invasive growth differed at 72 hpi. The spread of invasive

hyphae was similar to that observed at 48 hpi (2-3 plant cells) in *Modnm1*Δ, while the invasive hyphae grew into 5-7 plant cells at 72 hpi in WT (Figure 25A). The accumulation of dark puncta in the plant cells inoculated with *Modnm1*Δ indicated that the HR was dramatically enhanced (Figure 25A, white asterisk). Since biotrophy to necrotrophy switch occurs between 48 hpi and 72 hpi, the invasive growth defects of *Modnm1*Δ might be a result of a failure of biotrophy to necrotrophy switch.

To further confirm this observation, cell death in rice sheath infected by WT or *Modnm1*Δ was detected by trypan blue staining. The time point of cell death observed was same in *Modnm1*Δ or WT infected tissue (Figure 25B). Cell death could be detected at 72 hpi, other than 48 hpi. However, based on the invasive growth analysis, the cell death inoculated with WT conidia was caused by necrosis, while cell death inoculated with*Modnm1*Δ conidia might be caused by HR, as the HR signature, accumulation of small black dots, could only be found in the rice sheath infected by *Modnm1*Δ (Figure 25A, white asterisk). To test whether HR is increased in *Modnm1*Δ, transcriptional level of two HR genes, *PBZ1* and *PR5*, was measured. The transcriptional level of *PBZ1* and *PR5* was significantly increased in rice sheath infected by conidia from *Modnm1*Δ (Figure 25C). Therefore, the cell death observed in rice sheath infected by *Modnm1*Δ is indeed a result of HR. Based on these results, I conclude that mitochondrial fission is required for biotrophy to necrotrophy switch.

Figure 24. Mitochondrial fission is required for proper pathogenesis of *M. oryzae*.

Pathogenicity of mitochondrial fission defective mutant, *Modnm1*Δ, was highly reduced based on rice infection assays. Whereas, pathogenicity in the *Modnm1*Δ-Comp was comparable to the WT strain. Conidia from the WT, *Modnm1*Δ or *Modnm1*Δ-Comp strains were used to inoculate the seedlings of rice cultivar CO39. Disease symptoms for both experiments were assessed 7 days post inoculation.

Figure 24

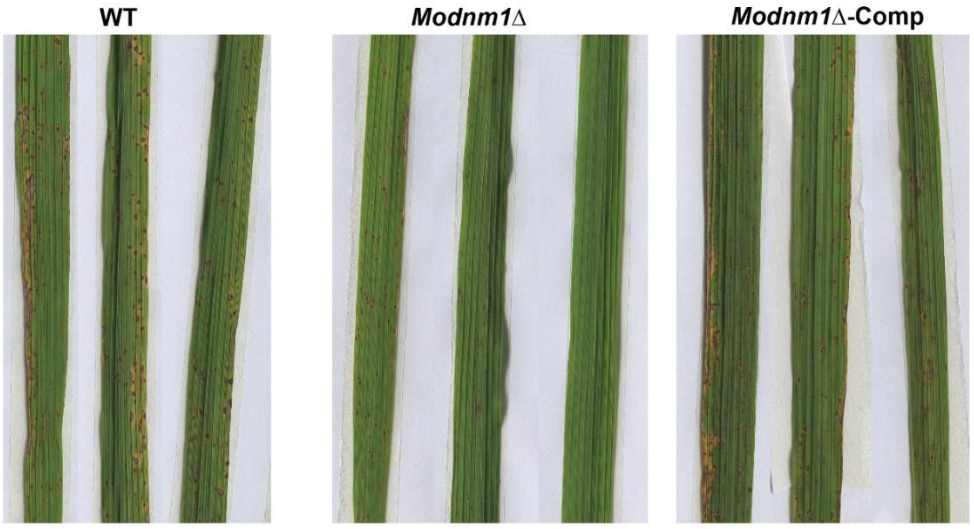

Figure 25. Mitochondrial fission is required for biotrophy to necrotrophy switch in *M. oryzae*.

(A) Invasive growth of *Modnm1*Δ is slowed at 72h. To test the invasive growth of *Modnm1*Δ, 20 µL conidia ($1x10^3$ /mL) were inoculated on the pre-cut rice sheath. The inoculated rice sheath was observed under confocal microscope at the indicated time points. The asterisk denotes the HR.

(B) Trypan blue staining reveals that cell death occurs in *Modnm1*Δ between 48 hpi and 72 hpi. To test the cell death induced by WT or *Modnm1*Δ infection, 20 µL conidia ($1x10^6$ /mL) was inoculated on the pre-cut rice sheath. The trypan blue staining was performed at the indicated time points as described in the Materials and Methods section. Conidial droplets are marked using dashed lines.

(C) *PR5* and *PRZ1* transcription levels are significantly increased at 72 hpi in rice sheath inoculated with *Modnm1*Δ.

Figure 25

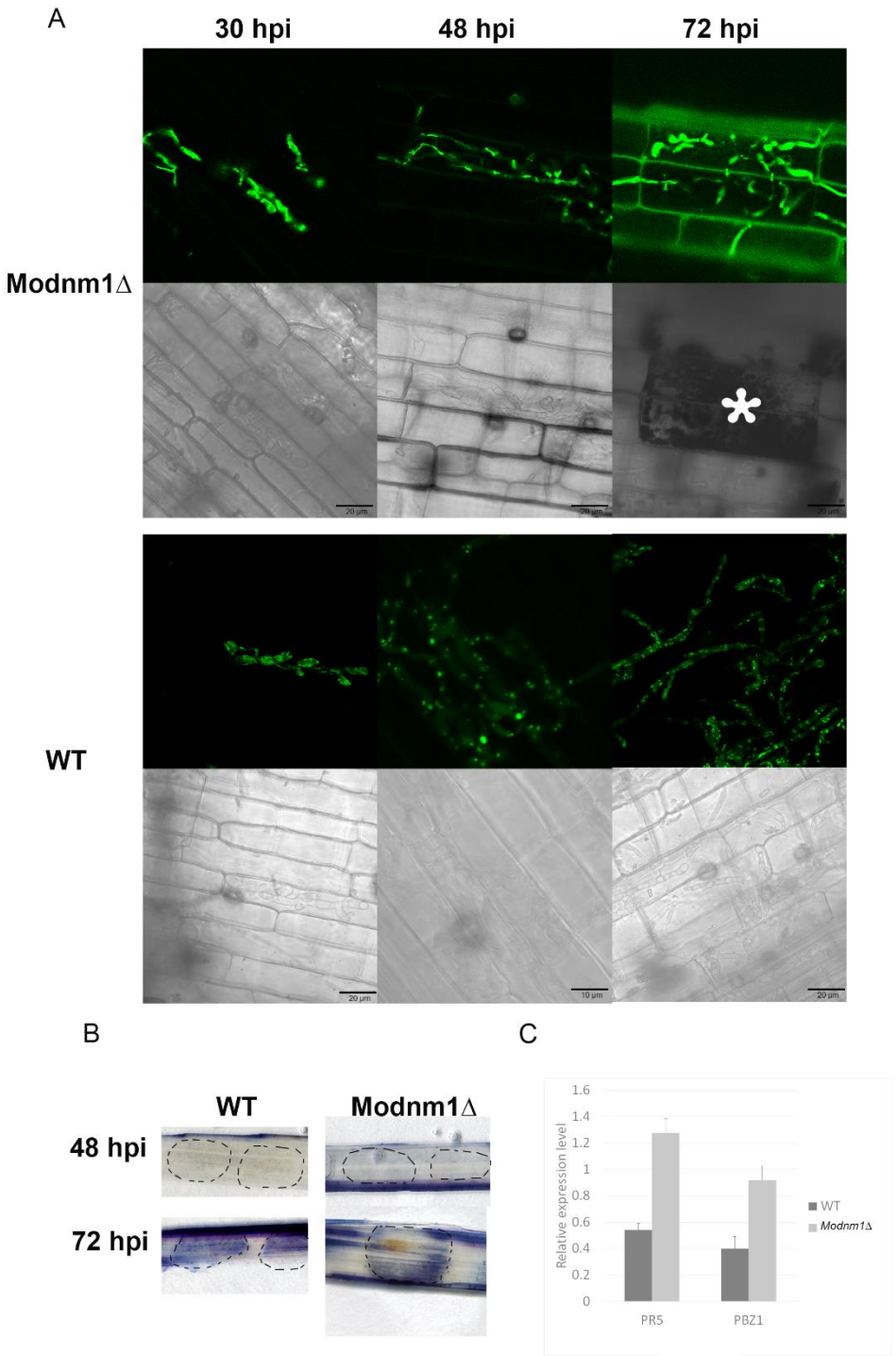
A
30 hpi
48 hpi
72 hpi
Modnm1Δ
WT
B
C
WT
Modnm1Δ
48 hpi
72 hpi
Relative expression level
1.6
1.4
1.2
1
0.8
0.6
0.4
0.2
0
PR5
PBZ1
WT
Modnm1Δ

4.2.7 Mitochondrial fusion machinery

Since mitochondrial fission is required for proper *M. oryzae* pathogenesis, mitochondrial fusion might also play an important role during invasive growth. To further address this question, a mitochondrial fusion defective mutant was generated and characterized. The *Mofzo1*Δ mutant was generated by replacing *MGG_05209.6* ORF with the bialaphos-resistance marker cassette (*BAR*, Figure 26A) in the mito-GFP strain. The deletion strains were confirmed by Southern blotting (Figure 26B). Two independent strains were then characterized for various aspects of pathogenesis.

To examine whether the function of MoFzo1 in mitochondrial fusion is conserved, the mitochondrial morphology in *Mofzo1*Δ was first studied. Most of the mitochondria remained punctate or fragmented in *Mofzo1*Δ, while most of mitochondria were filamentous or tubular mitochondria in WT (Figure 26C). Unlike the *Scfzo1*Δ, of which all the mitochondria became punctate (Hermann et al 1998), only about 70% mitochondria became punctate in *Mofzo1*Δ, which is similar to the mammalian mitochondrial fusion defective mutant (Santel & Fuller 2001). These results indicate that Fzo1 is required for mitochondrial fusion in *M. oryzae*.

Figure 26. Mitochondrial morphology in *Mofzo1*Δ

(A) Homology based gene replacement with the Bar-resistance cassette (*BAR*) was used to create the *Mofzo1*Δ mutant. The coding regions of *MoFZO1* and *BAR* are depicted in gray and white boxes respectively. Restriction enzyme site *SpeI* used for genomic DNA digestion is depicted. The 1 kb 3'UTR of *MoFZO1* served as the probe.

(B) Southern blot analysis of WT and the *Mofzo1*Δ mutant. The appearance of the 4.5 kb band in the *Mofzo1*Δ strain, with the concomitant loss of the wild-type 5.4 kb *MoFZO1* locus, was diagnostic of the correct gene replacement event.

(C) Mitochondrial morphology in WT and the *Mofzo1*Δ mutant. The mycelia from indicated strains were cultured in CM for 2 d prior to confocal microscopy.

Figure 26

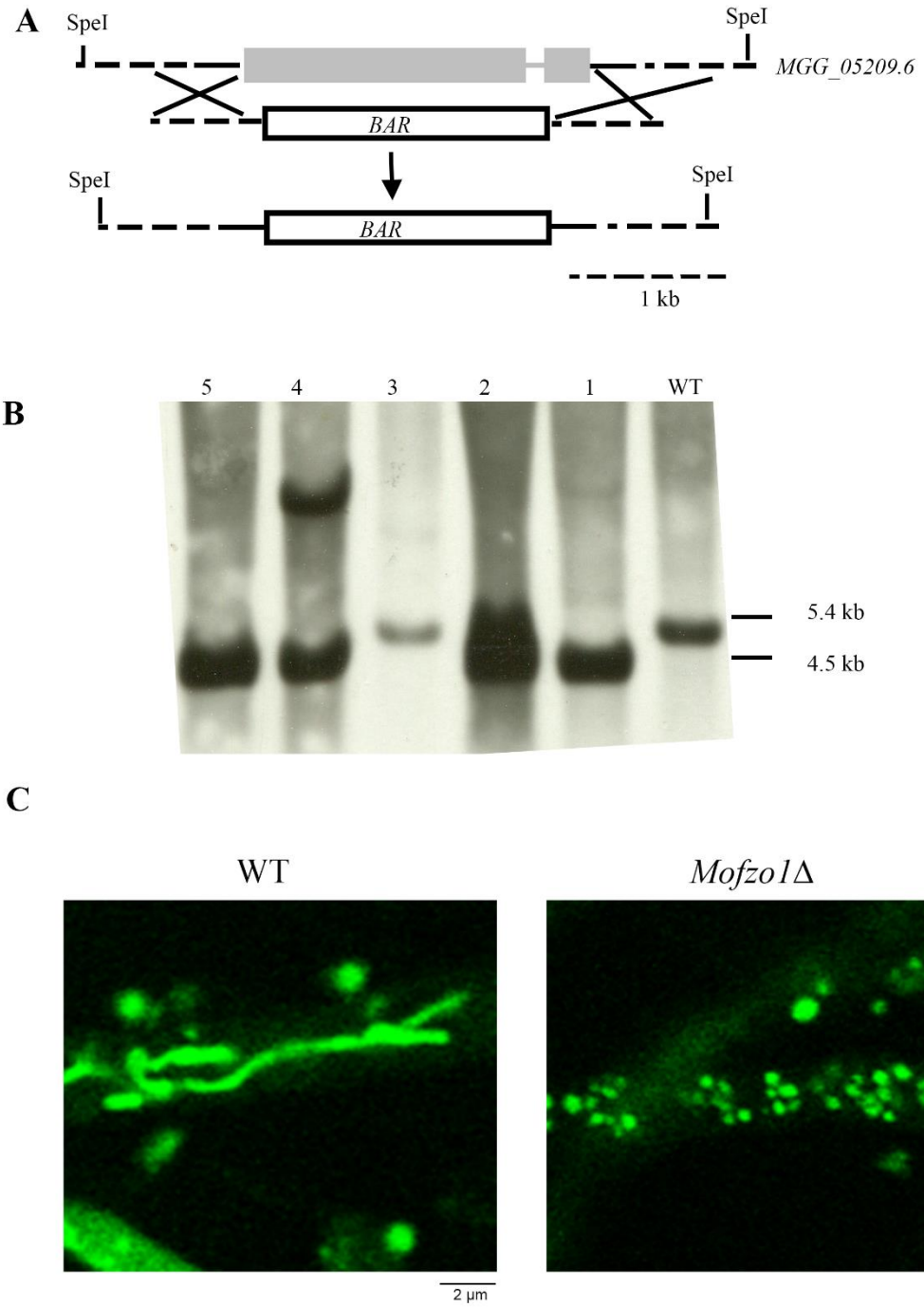
A
SpeI
SpeI
MGG_05209.6
BAR
SpeI
SpeI
BAR
1 kb
B
5
4
3
2
1
WT
5.4 kb
4.5 kb
C
WT
Mofzo1Δ
2 µm
2 µm

4.2.8 Loss of mitochondrial fusion disrupts maintenance of biotrophy.

After the role of MoFzo1 in mitochondrial fusion was confirmed, *Mofzo1*Δ was used to identify the role of mitochondrial fusion during host pathogen interactions. Pathogenicity of *Mofzo1*Δ was highly reduced (Figure 27A). In spray inoculation of conidia on 3-week old seedlings, the *MoFzo1*Δ showed highly reduced pathogenicity on leaves of CO39 at 7 days post inoculation (Figure 27A). Under the same conditions, typical lesions were observed on leaves inoculated with the WT conidia or the conidia of a complementary strain *MoFzo1*Δ-Comp (Figure 27A). However, such lesions were absent in the leaves inoculated with *Mofzo1*Δ conidia (Figure 27A). These results indicate that mitochondrial fusion is required for proper pathogenesis in *M. oryzae*.

To further understand the function of mitochondrial fusion during invasive growth, detailed time course analysis was performed on rice sheath infected by the *Mofzo1*Δ conidia. Both *Mofzo1*Δ and WT conidia could infect the rice epidermal cells. However, very strong HR could be detected in the rice cells infected by *Mofzo1*Δ at 30 hpi, compare to WT (Figure 27B). More importantly, the number of mitochondria in *Mofzo1*Δ invasive hyphae was much smaller than that in WT, which suggests that the invasive hyphae of *Mofzo1*Δ is sick. Based on these data, it is clear that mitochondrial fusion is required at the early stage of infection, and is probably required to maintain *M. oryzae* viability during biotrophic growth.

Figure 27. Mitochondrial fusion is required for proper pathogenesis in *M. oryzae*.

(A) Pathogenicity is highly reduced in *Mofzo1*Δ based on rice infection. The pathogenesis defect in *Mofzo1*Δ is restored to WT level in the complementary strain, *Mofzo1*Δ-Comp. 20 mL conidia suspension ($1x10^7$/mL) from indicated strains was inoculated on the 3-week rice seedlings. The lesions were checked at 5 dpi.

(B) Invasive growth of *Mofzo1*Δ is blocked at 30 hpi. 20 μL conidia suspension was inoculated on prepared rice sheath. The rice sheath was observed under microscope at indicated time points.

Figure 27

A

B

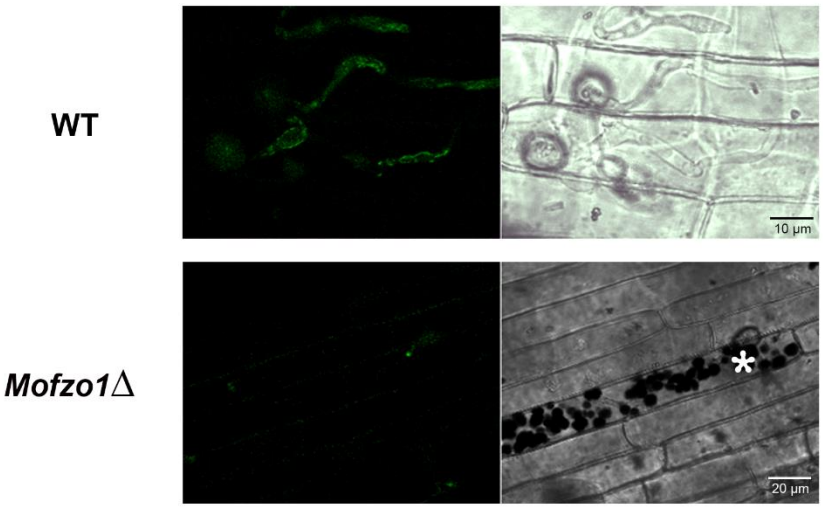

4.2.9 Effect of anti-oxidants on mitochondrial dynamics in invasive hyphae

Mitochondrial fragmentation could be triggered by various environmental factors, such as ROS (Polyakov et al 2003). To understand the molecular mechanism underlying mitochondrial fragmentation, antioxidant (NAC), was used to identify the role of ROS in mitochondrial fragmentation. Antioxidant was added to inoculated conidia droplets on the rice sheath surface at 36 hpi. Subsequently, mitochondrial morphology was examined under a confocal microscope at 48 hpi. Initially, three different concentrations (30 mM, 40 mM and 50 mM) of antioxidant (NAC) were added into inoculated conidia droplets. As the NAC concentration increasing, the invasive growth was inhibited gradually (Figure 28A). More clearly, 50 mM NAC could completely block the invasive growth, which suggests that ROS is important in invasive growth. However, antioxidant (30 mM and 40 mM) treatments could not repress the mitochondrial fragmentation, as shown in Figure 28A. In presence of 40 mM NAC, although the growth was even inhibited to some extent, the mitochondria still became punctate at 48 hpi, which is comparable to invasive growth without additional antioxidant treatment (Figure 28B and 28C). At 72 hpi, filamentous or tubular mitochondria could be observed in invasive hyphae in presence of 40 mM NAC. Taken together, these results suggest that ROS is not the factor that triggers mitochondrial fragmentation.

Figure 28. Antioxidant treatment could not delay mitochondrial dynamics during invasive growth.

(A) The effect of different concentration of NAC on mitochondrial dynamics. To test effects of different concentration NAC on invasive mitochondrial dynamics, 20 μL conidia ($1x10^3$ /mL) were inoculated on the pre-cut rice sheath. Then different concentrations of NAC were added at 36 hpi. The inoculated rice sheath was then observed under a confocal microscope at the indicated time points.

(B) The 3D reconstruction of the mitochondrial morphology at the indicated time points. All the images were captured as Z-stacks and the 3D reconstruction of Z-stacks was processed in Bitplan Imaris (Zurich, Switzerland).

(C) The number of filamentous and tubular mitochondria was counted from images in panel **(B)**.

Figure 28

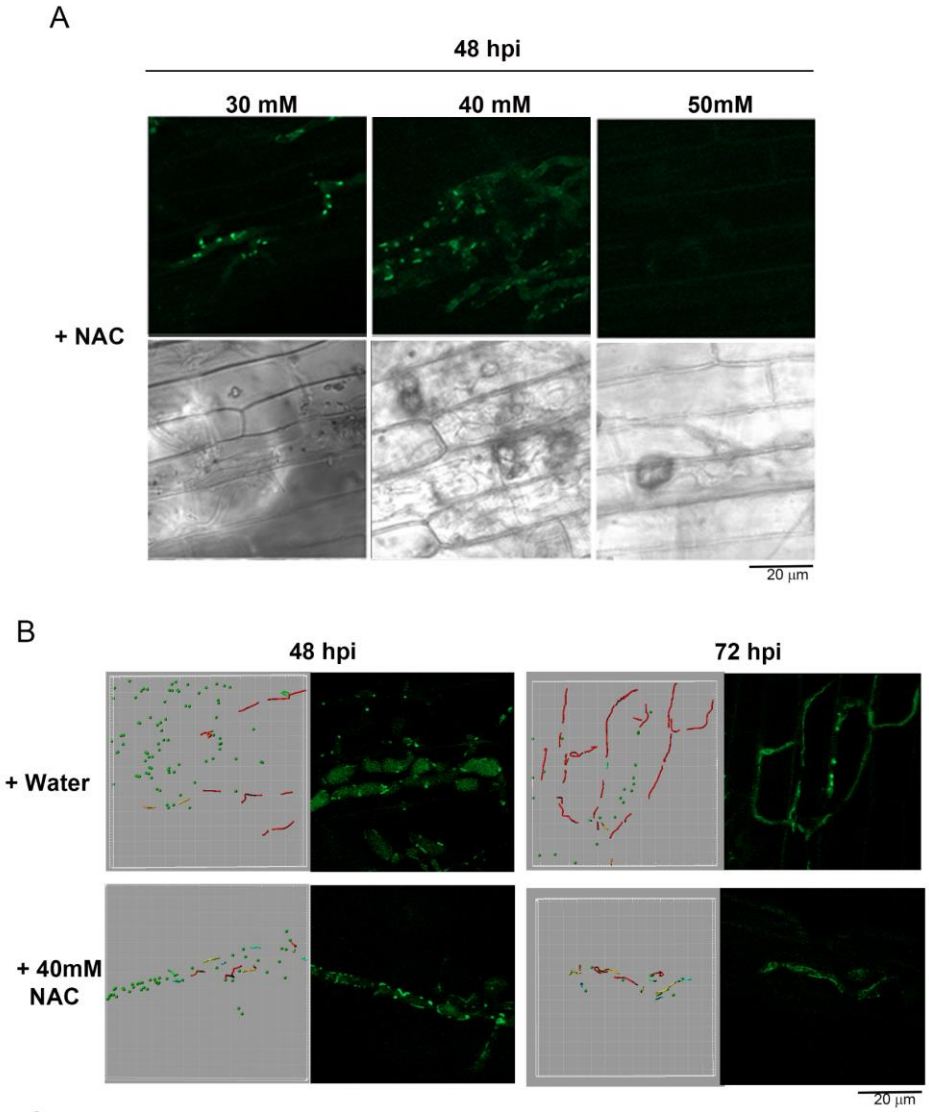
A
48 hpi
30 mM
40 mM
50mM
+ NAC
20 µm
B
48 hpi
72 hpi
+ Water
+ 40mM NAC
20 µm
C
% of total mitochondria
100
90
80
70
60
50
40
30
20
10
0
Water
40mM NAC
Punctate Mitochondria
Filamentous Mitochondria
Punctate Mitochondria
Filamentous Mitochondria
48 hpi
72 hpi

4.2.10 Effect of carbon metabolism on mitochondrial dynamics

After ruling out ROS as the trigger for mitochondrial dynamics, I examined the role of nutrients on mitochondrial dynamics. Various carbon sources (1.5 mg/L) were individually added into inoculated conidia droplets on the rice sheath surface at 36 hpi. Mitochondrial morphology was assessed under a confocal microscope at 48 hpi and 72 hpi. I found that all the carbon sources listed (Glucose, Sucrose and maltose) could delay mitochondrial fragmentation (Figure 29A), which indicates that the carbon source depletion might be a major factor triggering mitochondrial fragmentation. Briefly, in the control (no additional carbon sources), around 90% mitochondria appeared fragmented at 48 hpi (Figure 29A), while mitochondrial fragmentation occurred at 72 hpi in presence of the indicated carbon sources. At 72 hpi, 78%, 76% and 87% of mitochondria became punctate upon additional supplementary of glucose, sucrose and maltose, respectively (Figure 29B), while more than 60% mitochondria in WT appeared filamentous again. At 84 hpi, the filamentous mitochondria appeared in invasive hyphae with the additional carbon sources. Based on these data, I conclude that the presence of excessive carbon source impacts mitochondrial dynamics in invasive hyphae during rice blast development.

4.2.11 Glucose 6-phosphate delays mitochondrial fragmentation

As all the carbon sources mentioned above could delay mitochondrial fragmentation to some extent, it is possible that a downstream molecule in the carbon metabolic pathway regulates mitochondrial dynamics.

Figure 29. Carbon sources could delay mitochondrial dynamics *in planta*.

(A) The effects of different carbon sources on mitochondrial dynamics. $1x10^3$ /mL conidia were inoculated on the pre-cut rice sheath. Then indicated carbon sources were added at 36 hpi. The inoculated rice sheath was observed under a confocal microscope at the indicated time points. The 3D reconstruction of the mitochondrial morphology at the time points. All the images were documented as Z-stacks and the 3D rendering of Z-stacks carried out using Bitplan Imaris.

(B) The quantitative data corresponding to the 3D rendering in panel A. The original raw data were generated by Bitplan Imaris automatically. The data analysis and processing were done in Microsoft Excel.

Figure 29

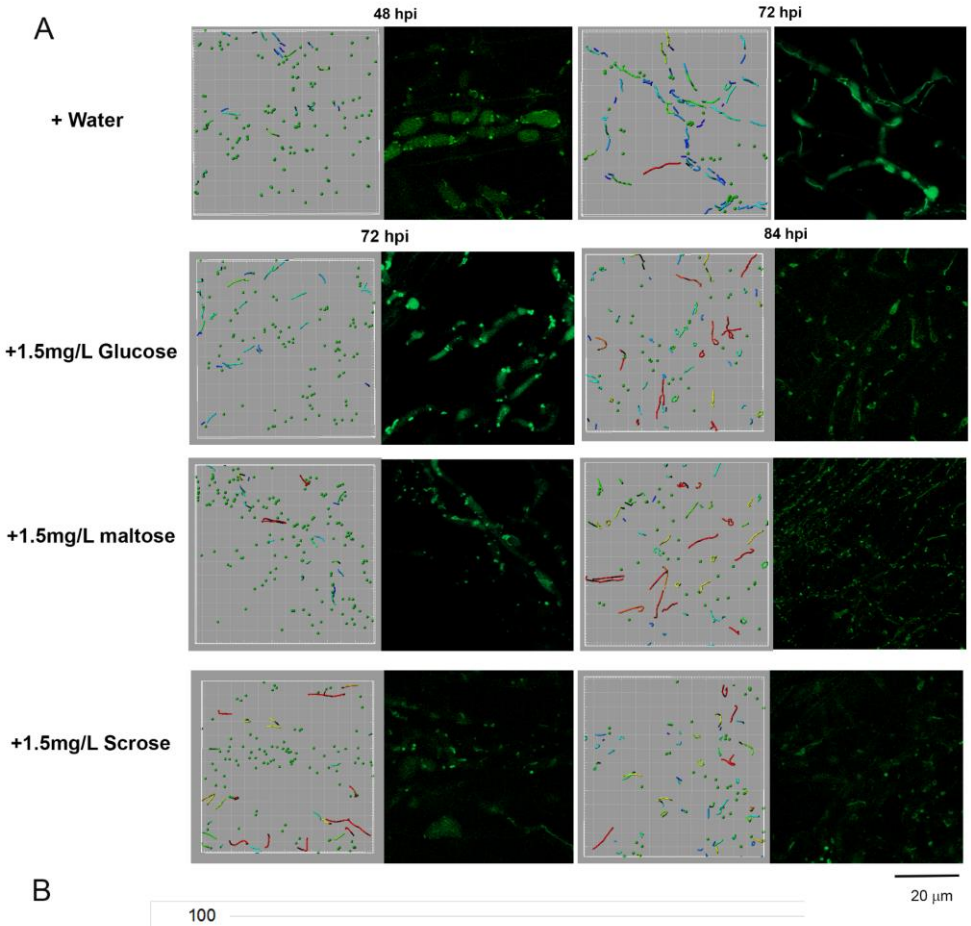
A
48 hpi
72 hpi
+ Water
72 hpi
84 hpi
+1.5mg/L Glucose
+1.5mg/L maltose
+1.5mg/L Scrose
20 μm
B
% of total mitochondria
100
90
80
70
60
50
40
30
20
10
0
Water
1.5 mg/L Maltose
1.5 mg/L Glucose
1.5 mg/L Sucrose
48 h Puncta Mitochondria
48 h Filamentous Mitochondria
72 h Puncta Mitochondria
72 h Filamentous Mitochondria
84 h Puncta Mitochondria
84 h Filamentous Mitochondria

Figure 30. G-6-P could delay mitochondrial dynamics.

(A) The effects of G-1-P and G-6-P on mitochondrial dynamics during invasive growth. To understand the effects of G-1-P and G-6-P on mitochondrial dynamics, 20 μL conidia ($1x10^3$/mL) were inoculated on rice sheath. Subsequently, indicated chemicals were added to the conidia droplets at 36 hpi. Images were taken under a confocal microscope at indicated time points.

(B) The quantitative data obtained from the images in panel **(A)**.

Figure 30

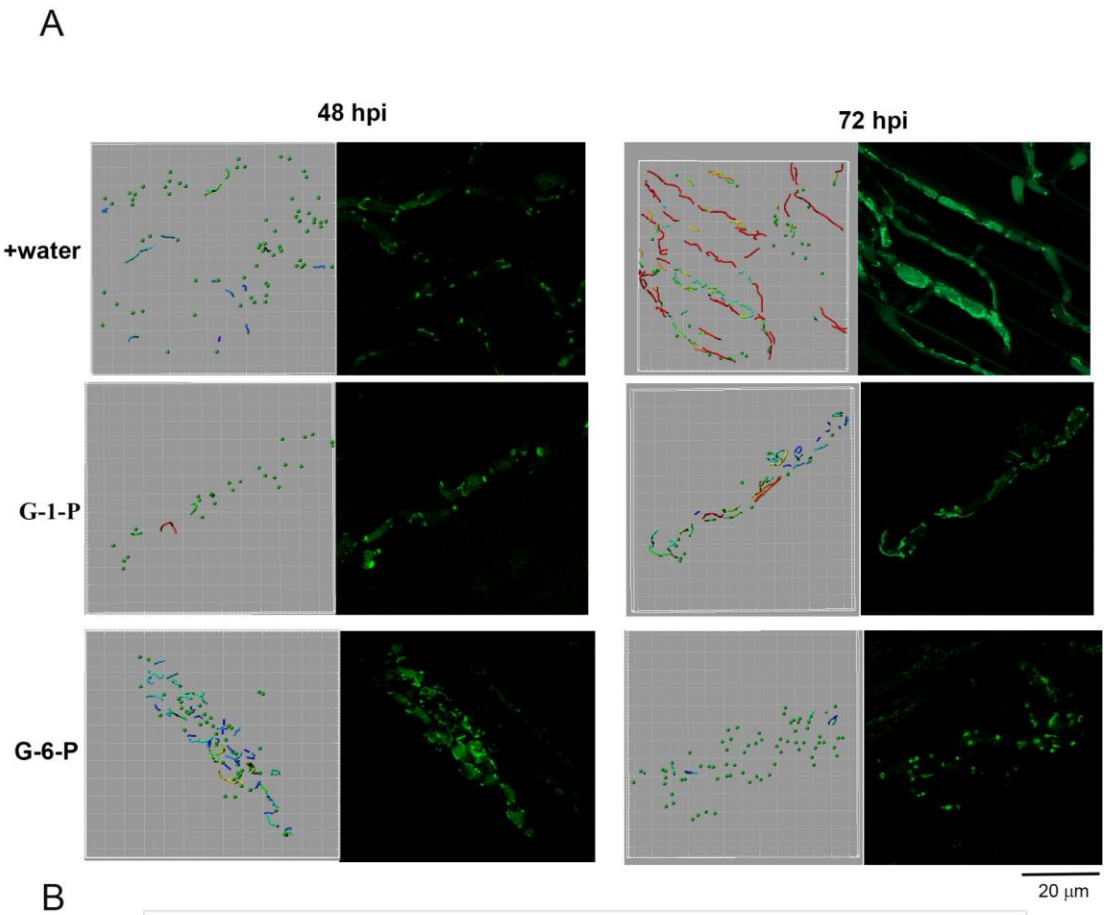
A
48 hpi
72 hpi
+water
G-1-P
G-6-P
20 µm

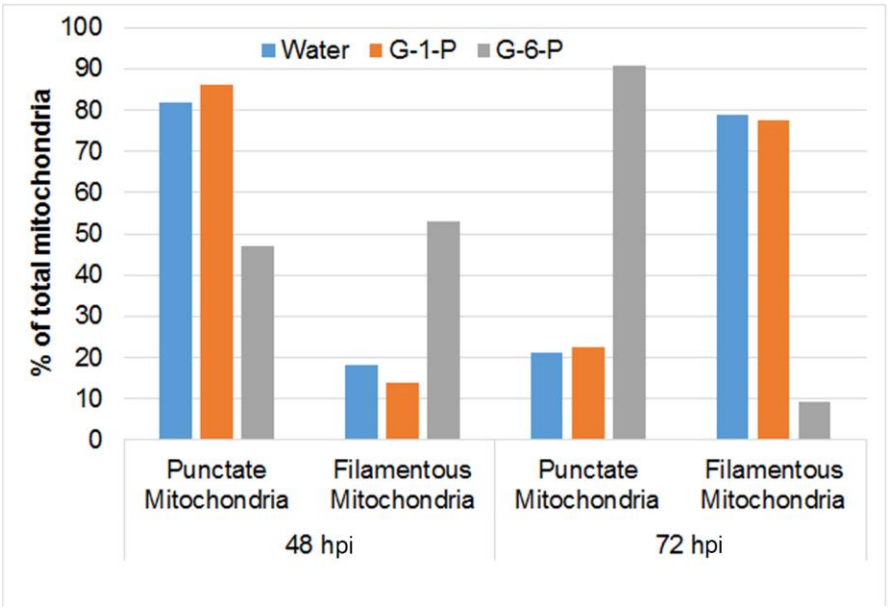
B
Water
G-1-P
G-6-P
% of total mitochondria
100
90
80
70
60
50
40
30
20
10
0
Punctate Mitochondria
Filamentous Mitochondria
Punctate Mitochondria
Filamentous Mitochondria
48 hpi
72 hpi

Based on the literature (Wilson et al 2007), the *MoTPS1* deletion mutant was blocked at the early stage of infection. As MoTps1 is a glucose-6-phophate (G-6-P) sensor, G-6-P might be involved in mitochondrial fragmentation. To test this hypothesis, G-1-P and G-6-P was added into the inoculated conidia droplets at 36 hpi individually, and mitochondrial morphology was assessed at 48 hpi and 72 hpi. As expected, nearly 53% of total mitochondria remained tubular or filamentous in presence of G-6-P at 48 hpi (Figure 30A and 30B) while in presence of G-1-P, only about 14% of total mitochondria were filamentous or tubular (Figure 30A and 30B). Moreover, at 72 hpi, more than 90% of total mitochondria appeared punctate in presence of G-6-P, while the majority mitochondria became filamentous in presence of G-1-P. Taken together, these results indicate that G-6-P could delay mitochondrial fragmentation during invasive growth in *M. oryzae*.

4.2.12 Mitochondrial dysfunction during *in planta* growth

Although the antioxidant treatment did not alter mitochondrial fragmentation, it did change the number and the size of punctate mitochondria (Figure 28A and 28B). These results indicate that there might be another mitochondrial event besides fragmentation upon disruption of redox homeostasis. Based on the size and shape of mitochondria, it is possible that mitochondria dysfunction occurs after/during fragmentation. To verify this, I first checked the ROS levels in the punctate mitochondria at 48 hpi using the reduction-oxidation sensitive green fluorescent protein (roGFP). roGFP was created by substitution of surface-exposed residues on the *Aequorea victoria* green fluorescent protein (GFP) with cysteines in appropriate positions to form

disulfide bonds. The roGFP has two fluorescence excitation maximum at about 400 and 490 nm and display rapid and reversible ratiometric changes in fluorescence in response to changes in ambient redox potential *in vitro* and *in vivo* (Rhee et al 2010). Previous research has utilized roGFP to quantify the ROS levels in mitochondria (Hanson et al 2004). Therefore, mito-roGFP here was used to measure the mitochondrial ROS during invasive growth. The ROS levels in the punctate mitochondria found at 48 hpi (Figure 31A) was much higher than those of the filamentous mitochondria found at 30 hpi (Figure 31A).

To further verify whether the punctate mitochondria reached to a damaged status, MoYbh3 was tagged with mCherry in a mito-GFP strain. Ybh3 contains a BCL-2 homology (BH3) domain or as a member of the BAX inhibitor family, and it translocates to mitochondria under apoptosis-inducing conditions in a process involving Mir1p and Cor1p (Buttner et al 2011). To test whether mCherry-MoYbh3 plays a similar role as ScYbh3 in response to mitochondrial damage, mCherry-MoYbh3 location was first observed at later stages of appressorium formation, when autophagic cell death occurs. As expected, mCherry-MoYbh3 would colocalize with mitochondria during autophagic cell death (Figure 31B), which suggests that MoYbh3 could be used as a marker for damaged mitochondria. During invasive growth, mCherry-MoYbh3 could be found in the punctate mitochondria at 48 hpi but not at 30 hpi (Figure 31B). These results suggest that mitochondria are highly damaged at the 48 hpi during initiation of rice blast.

Figure 31. mCherry-MoYbh3 translocates into mitochondria during mitochondrial dynamics.

(A) roGFP expressed in invasive hyphae. The images were taken on the infected rice sheath by Magnaporthe strains expressing roGFP. For reduced roGFP, the excitation wavelength was set at 488 nm, while 405 nm was used to excite oxidized roGFP (pseudocolored as red). For full oxidation of roGFP, rice sheath was incubated in 10 mM H_2O_2 for 30 min prior to observation. Some of the mitochondria in oxidative state in the middle panels are denoted by arrowheads. Mitochondria in reductive state in the lower panels are denoted by arrowheads.

(B) mCherry-MoYbh3 colocalizes with mitochondria during autophagic cell death and invasive growth. The location of MoYbh3-mCherry in appressoria approaching cell death (16 hpi) was observed using a confocal microscope.

Figure 31

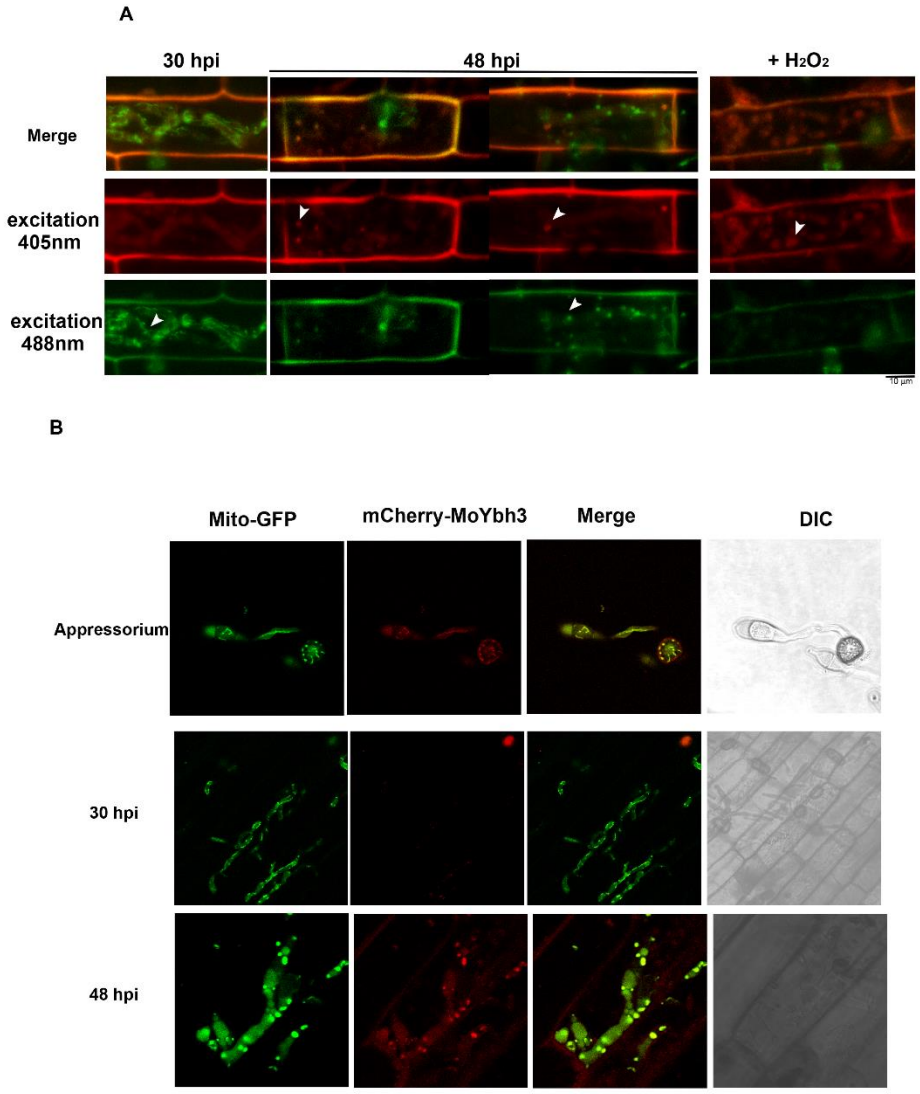
A
30 hpi
48 hpi
+ H2O2
Merge
excitation 405nm
excitation 488nm
B
Mito-GFP
mCherry-MoYbh3
Merge
DIC
Appressorium
30 hpi
48 hpi

4.2.13 Mitochondrial dysfunction activates MoRtg2 expression

During mitochondrial dysfunction, one of the important pathways in yeast to rescue the cells from programed cell death is the retrograde pathway (RTG pathway) (Butow & Avadhani 2004, Liu & Butow 2006). Upon mitochondrial dysfunction, Rtg2 expression is highly upregulated. And thereby, the enzyme activity of Mks1 is inhibited and herein Rtg1/Rtg3 translocates into the nucleus to upregulate target genes (Liu et al 2003, Sekito et al 2002). Rtg1 and Rtg3 are both transcription factors, which activate transcription of genes with R boxes. And herein, the retrograde pathway could operate some other cellular processes to rescue the cells from mitochondrial dysfunction. To test whether the retrograde pathway is activated at 48 hpi, the expression level of Rtg2 was measured first at 30 hpi and 48 hpi. Initially, the full-length *M. oryzae RTG2* was identified though BLAST. Based on the BLASTP analysis, *MGG_04524.6* was considered as the ortholog of *ScRTG2* (Figure 32A). As expected, transcription of Rtg2 was highly upregulated at 48 hpi (Figure 32B), which suggests that the retrograde pathway may be activated at 48 hpi.

4.2.14 MoRtg2 expression triggers mCherry-MoRtg3 translocation

To further confirm that the retrograde pathway is conserved and plays an important role in invasive growth, a mCherry-MoRtg3 strain was made. Initially, *MGG_05709* was identified through BLAST as a *MoRTG3* candidate. Then through protein sequence comparison, the core sequence for nuclear localization is conserved in *MGG_05709* (Figure 33A).

Figure 32. MoRtg2 is upregulated at 48 hpi

(A) Protein sequence alignment of *M. oryzae* Rtg2. Protein sequences of Rtg2 from *M. oryzae* and *S. cerevisiae* were aligned with Clustal W based on the aminoacide sequence alignment method. The level of similarity of each amino acid was labeled in different colors. ‘ * ’ represents identical amino acid. ‘ . ’ and ‘ : ’ represent low and highly similar amino acid respectively.

(B) *MoRTG2* transcription level is highly upgraded in rice sheath infected by *M. oryzae* at 48 hpi. qRT-PCR was performed by utilizing the RNA extracted from the infected rice sheath at indicated time points.

Figure 32

Figure 32

```
ScRtg2          -----MSTLSDSDTETEVVSRNLCGIVDIGS-NGIRFSISSKAAHHARIMPCVFKDRVGL 54
MoRtg2          MAQHGFNQIAGAHGGDSINPNDLNMVGNYGSSYQNAFSGNNNQQNSYANGSALFGDDELL 60
                     :. ::.:.   .: ..:*  : : **     ** ..:  :     ..:* *   *

ScRtg2          SLYEVQYNTHTNAKCPIPRDIIKEVCSAMKRFKLICDDFGVPETSVRVIATEATRDAINA 114
MoRtg2          EGLASPTDTSPNMHSNGPDFGNMNEMTMGGYSNSIYTTHGMPMDQNRISGYSNTPEGDPI 120
                .      :* .* :.  *     :  :     : *   .*:*  . *: . . * :.

ScRtg2          DEFVNAVYGSTGWKVEILGQEDETRVGIYGVVSSFNTVRGLYLDVAGGSTQLSWVISSHG 174
MoRtg2          QSPFAHNFNQYRQMQHPQSFGNSLQSPIYGASPLPGSEINHEADPNYMSSKVRPRIPTAM 180
                :. .   :..     .  .  :. :  ***. .  .:  .   *    *:::   *.:

ScRtg2          EVKQSSKPVSLPYGAGTLLRRMRTDDNRALFYEIKEAYKDAIEKIGIPQEMIDDAKKEGG 234
MoRtg2          ARKSSGGRTPMTPKASAAMASLTIG-SADSFNPQPIRTNGANHEKAHSGQWLNTPNSIGS 239
                  *.*.  ...:  *.: :  :  . .   *       :.* .: . . : :: .:. *.

ScRtg2          FDLWTRGGGLRGMGHLLLYQSEGYPIQTIINGYACTYEEFSSMSDYLFLKQKIPGSSKEH 294
MoRtg2          YP----GSGFSSPIQPGLHSAQINDILLKG-GTSMPAKLNSPLTSTQEAKRKRRRES--H 292
                :    *.*: .  :  *:.::   *     * : . :  *.::.    *:*   .*  *

ScRtg2          KIFKVSDRRALQLPAVGLFMSAVFEAIPQIKAVHFSEGGVREGSLYSLLPKEIRAQDPLL 354
MoRtg2          NLVERRRRDNINERIQDLSKLVPQHRLEDEKIKKLIQNGTPLSPTLAGISSPSQATSGLA 352
                ::.:   *  ::    .*   .  . : : *  :: :.*.  ..  : :..  :* . *

ScRtg2          IASRPYAPLLTEKYLYLLRTSIPQEDIPEIVNERIAPALCNLAFVHASYPKELQPTAALH 414
MoRtg2          GPG---ARRAAGGSTGNITTGLP------IDDKDKGPNKGDILNGAVSWTRDLMWMLQLK 403
                 ..   *   :      : *.:*      * ::  .*   ::    .*:.::*     *:

ScRtg2          VATRGIIAGCHGLSHRARALIGIALCSRWGGNIPESEEKYSQELEQVVLREGDKAEALRI 474
MoRtg2          LQQQ---------EEMANYIIEIGGQVPFEP--TDDEKRMQSELAEAMQR-CEMVEEGKN 451
                :  :         .. *. :* *.    :    .:.*:: ..** :.: *  : .*  :

ScRtg2          VWWTKYIGTIMYVICGVHPGGNIRDNVFDFHVSKRSEVETSLKELIIDDANTITKVKEEST 534
MoRtg2          FTYSRRAGSGLRVPHHTDYKGEP------LDGTNRNTVDG-VSSLSPGGTMTNDVGLGSD 504
                . :::  *: : *   ..  *:       :. ::*. *:  :..*  ..: *..*   *

ScRtg2          RKNRGYEVVVRISKDDLKTSASVRSRIITLQKKVRKLSRGSVERVKIGVQFYEE 588
MoRtg2          LGNHGQGPFWNEDDD--------GSGELDFKEEDEYMDLN-------------- 536
                  *:*   . . ..*         *  : :::: . :. .
```

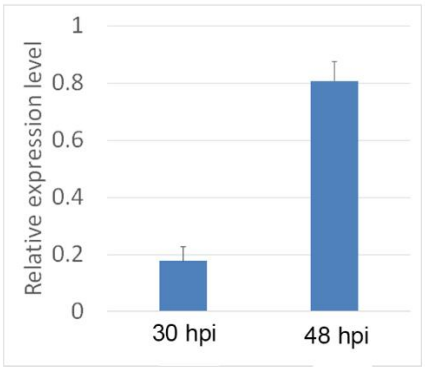

Figure 33. MoRtg3 translocates into the nucleus at 48 hpi during invasive growth

(A) Alignment of MoRtg3 and ScRtg3 by Clustal W. The conserved nuclear localization sequence is labeled gray. The level of similarity of each amino acid was labeled in different colors.

(B) The localization of mCherry-Rtg3 in presence of Paraquat. Paraquat was added into CM for 1 h prior to microscopy observation. The Fungal nucleus was stained by DAPI (pseudocolored as green).

(C) The localization of mCherry-MoRtg3 in invasive hyphae. The invasive hyphae were observed under a confocal microscope at the indicated time points. The aggregates of mCherry-MoRtg3 are denoted by the arrowhead.

Figure 33

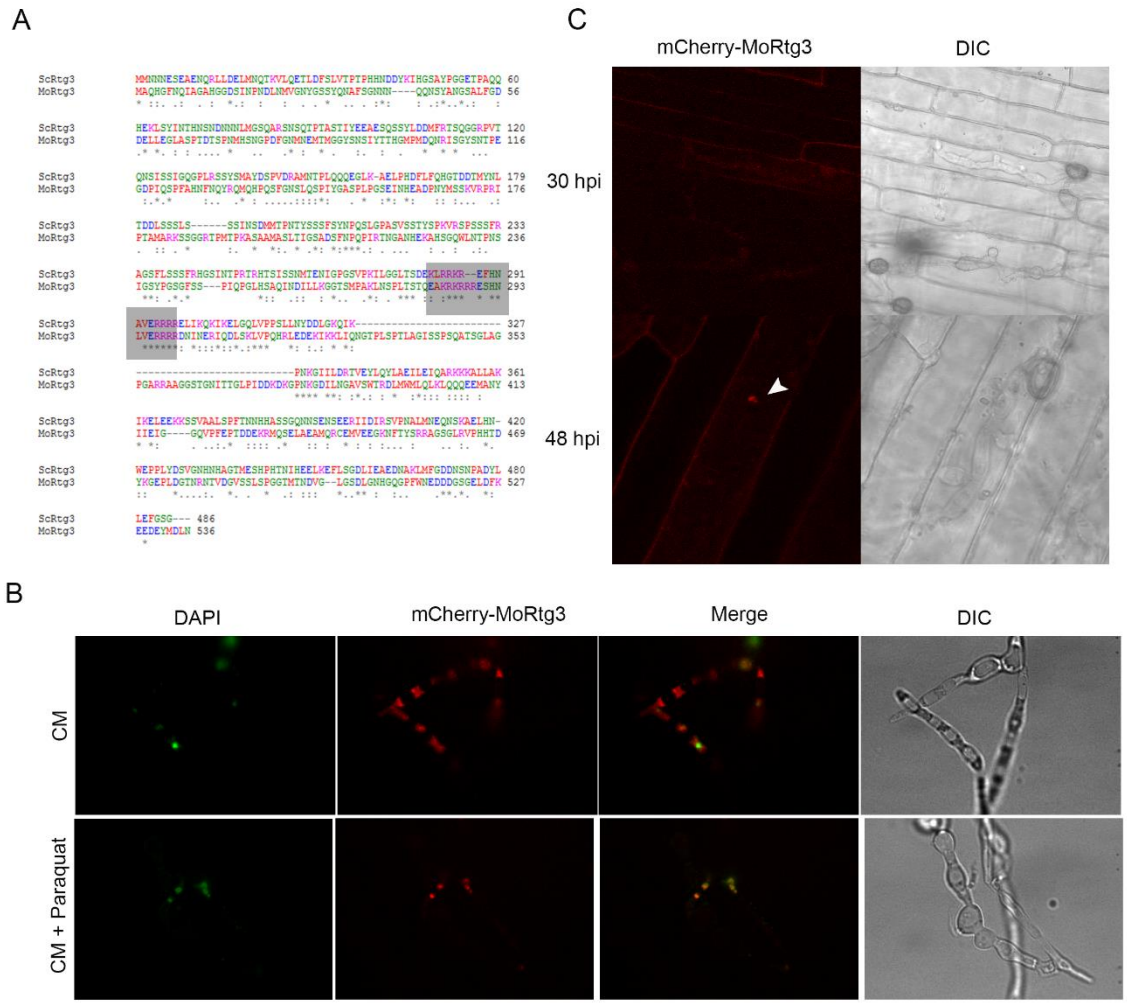
A
ScRtg3
MoRtg3
C
mCherry-MoRtg3
DIC
30 hpi
48 hpi
B
DAPI
mCherry-MoRtg3
Merge
DIC
CM
CM + Paraquat

Thus, it is highly possible that MGG_05709 is the *MoRTG3*. To further verify whether MoRtg3 would be translocate into nucleus in response to mitochondrial damage, mCherry-MoRtg3 was tagged in a mito-GFP strain. To test whether mCherry-MoRtg3 plays a similar role as ScRtg3 in response to mitochondrial damage, mycelia of mCherry-MoRtg3 was first grown in CM, and then a mitochondrial damage drug (10 μM, paraquat) was added. As expected, mCherry-MoRtg3 was mainly in cytosol when grown in CM and could rarely be found to co-localize with the nucleus (stained by hoechst) (Figure 33B). In presence of paraquat, mCherry-MoRtg3 could be clearly found to co-localize with the nucleus (Figure 34B), Based on this information, MoRtg3 has similar translocation as ScRtg3 in response to mitochondrial damage. Next, mCherry-MoRtg3 location was observed in later stages of invasive growth. As expected, mCherry-MoRtg3 could be found in the nucleus at 48 hpi (Figure 33C), but not at 30 hpi (Figure 33C). These results suggest that mitochondrial retrograde pathway was activate at 48 hpi.

4.2.15 MoRtg2 is required for the biotrophy to necrotrophy switch

As mitochondrial retrograde pathway activation could be clearly observed at 48 hpi during invasive growth, the mitochondrial retrograde pathway might be an important pathway regulating the pathogenicity of *M. oryzae*. To further address this question, a mitochondrial retrograde pathway defective mutant (*Mortg2*Δ) was generated and characterized. The *Mortg2*Δ mutants were then generated by replacing the entire ORF with the Sulfonylurea--resistance maker cassette (*ILV2,* Figure 34A) in the Mito-GFP strain.

Figure 34. Generation of *Mortg2*Δ

The strategy used to generate *Mortg2*Δ is depicted in panel **(A)**, where the gray boxes and the white boxes represent the coding regions of *MoRTG2* and *ILV2* respectively. The restriction enzyme used to digest the whole genomic was labeled. The southern blot of wild type and *Mortg2*Δ genomic DNA was shown in panel **(B)**.

Figure 34

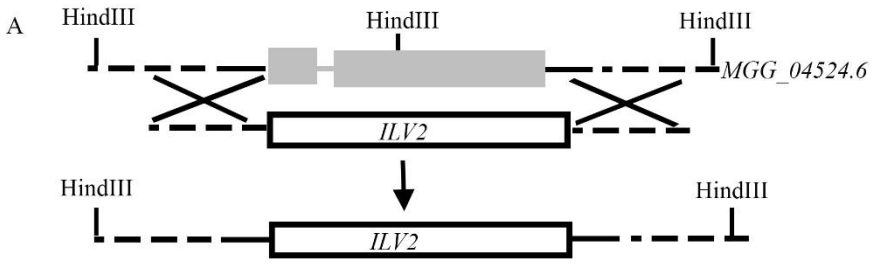
A
HindIII
HindIII
HindIII
MGG_04524.6
ILV2
HindIII
HindIII
ILV2

B

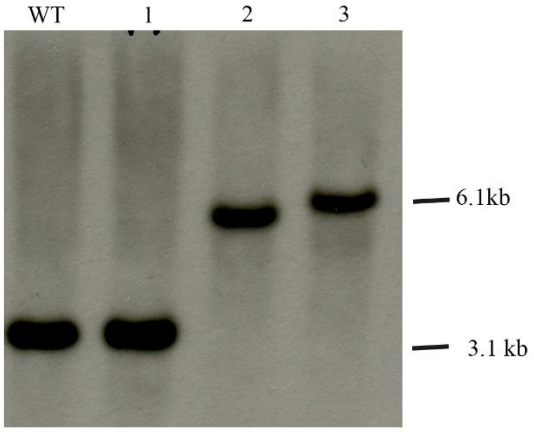
WT
1
2
3
6.1kb
3.1 kb

Figure 35. MoRtg2 is required for proper pathogenesis of *M. oryzae*.

(A) Pathogenesis of the retrograde pathway defective mutant, *Mortg2*Δ, is highly reduced based on the rice infection assay. The rice seedling infection assays were carried out as described in the Materials and Methods section. The blast lesions were examined at 7 dpi.

(B) Invasive growth of *Mortg2*Δ is slowed at 72 hpi. The rice sheath infection assays were performed as described in the Materials and Methods section . The images were taken at the indicated time points under a confocal microscope. The GFP signals are mito-GFP. The increased HR is denoted by an asterisk.

Figure 35

A

B

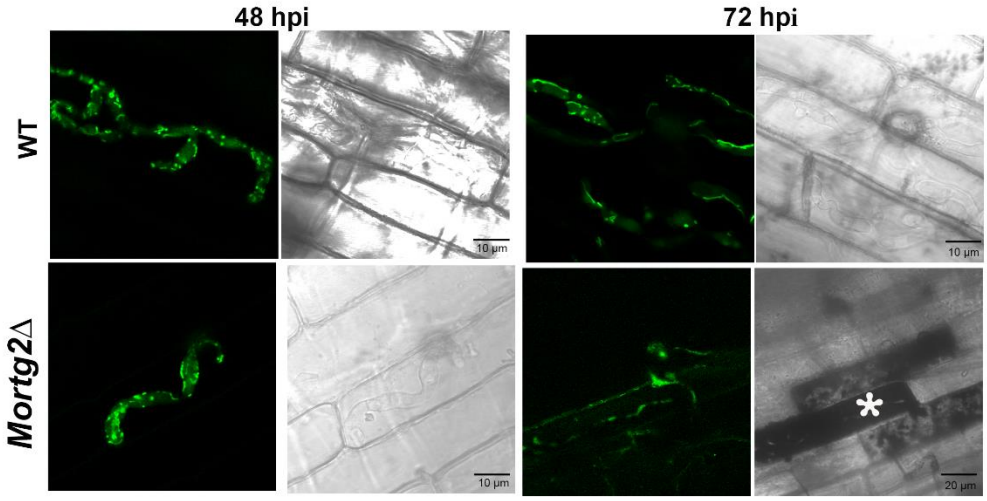

The deletion strains were confirmed by Southern blotting (Figure 34B). Two independent strains were then characterized for pathogenesis. Pathogenicity of the *Mortg2*Δ mutant is highly reduced. In spray inoculation of WT conidia on 3-week old seedlings, typical disease lesions could be found on leaves of CO39 at 7 dpi (Figure 35A). Only small black puncta or dots could be found on leaves of CO39 inoculated *Mortg2*Δ conidia at 7 dpi (Figure 35A). Based on these data, I conclude that MoRtg2 indeed plays a crucial role in *M. oryzae* pathogenesis.

To further understand the reason of reduced pathogenicity in *Mortg2*Δ mutants, time course detailed analysis was performed on the rice sheath infection assay. The infection of *Mortg2*Δ at 48 hpi was as good as the WT strain and both of them grew well in the primary infected plant cells (Figure 35B). The HR responses were similar in the rice sheathe infected by *Mortg2*Δ and WT. However, the invasive growth differed around 72 hpi. The spreading of invasive hyphae was similar to what we observed in 48 hpi (2-3 plant cells) in *Mortg2*Δ, while the WT invasive hyphae spread into 5-7 plant cells in 72 hpi (Figure 35B). As biotrophic to necrotrophic growth switch occurs between 48 hpi and 72 hpi, which clearly suggests that disruption of mitochondrial fission stops the biotrophic to necrotrophic switch. Based on these data, I conclude that the retrograde pathway is important during host pathogen interactions.

4.3 Discussion

Although numerous deletion mutants of *M. oryzae* have been shown to be defective in controlling plant ROS levels when grown invasively in rice cells, no report has carefully studied the function of fungal mitochondria during host pathogen interactions (Li et al 2011, Patkar et al 2012, Zhou et al 2012). Here, we found very interesting mitochondrial morphological changes during invasive growth of *M. oryzae*. And such mitochondrial morphological changes play very important roles in *M. oryzae* pathogenesis.

Based on the detailed analysis of invasive growth in *Mofzo1*Δ, mitochondrial fusion is likely required for early stages of invasive growth. In other words, filamentous mitochondria are necessary for proper growth and development of primary and secondary invasive hyphae. These results are very interesting, as fragmented mitochondria are always associated with lower metabolic capacity and higher cellular ROS. Meanwhile, the rice ROS spikes around 28 hpi at early stages of invasive growth. In other words, at the initiation stage of invasive growth, *M. oryzae* tries to maintain lower intracellular ROS as the ROS level in rice environment is already extremely high.

To my surprise, ROS is not a factor that triggers mitochondrial fragmentation. By contrast, nutrition is a key trigger for mitochondrial fragmentation. Furthermore, G-6-P regulates mitochondrial dynamics, which is consistent with the previous reports in yeast that metabolic pathways regulate mitochondrial dynamics and mitochondrial dynamics is a result of metabolic

reprograming (Guido et al 2012). In *M. oryzae*, the importance of G-6-P was also suggested based on the observation that the G-6-P sensor (MoTps1) defective mutant shows highly reduced pathogenicity and the invasive growth of this mutant is blocked at an early stage (Wilson et al 2007).

These results make a controversial scenario on the relationship between ROS and mitochondrial dynamics. One explanation of such conflict is that mitochondrial fragmentation would activate a downstream pathway of carbon depletion to rescue the cells from carbon starvation. Here, I showed that the RTG pathway is a possible downstream pathway of carbon depletion. Disruption of the RTG pathway by deletion of Rtg2 leads to highly reduced pathogenicity. The invasive growth defects in Rtg2 deletion mutant are similar to that in *Modnm1*Δ, which again supports the idea that the mitochondrial dynamics triggers the mitochondrial retrograde pathway during *M. oryzae* and rice interactions.

To summarize, mitochondrial fragmentation occurs during the biotrophy to necrotrophy switch. A key regulator of such mitochondrial dynamics is carbon source depletion. The mitochondrial fragmentation would herein activate the RTG pathway to assist fungal adaptation into host during establishment of rice blast.

CHAPTER V GENERAL DISCUSSIONS AND CONCLUSIONS

In recent years, our understanding of rice blast has increased dramatically (Lee & Dean 1993, Liu et al 2007, Ramanujam & Naqvi 2010). However, the pathways involved in invasive growth are still largely unknown. Considering that invasive growth is an important aspect of the pathogenesis process, it is valuable to identify the pathways involved in regulation of invasive growth in the host.

In this study, I attempted to identify one of the pathways involved in metabolic reprogramming during invasive growth. Mitochondrial dynamics was first examined during the early 72 hpi. A very interesting filamentous-puncta-filamentous cycle was observed in mitochondrial morphology. To uncover the role of mitochondrial dynamics observed during invasive growth. Mitochondrial fusion or fission mutants were generated by deleting *MoFZO1* or *MoDNM1* respectively. The function of *MoFZO1* and *MoDNM1* is well conserved based on our observation in vegetative growth. Disruption of mitochondrial fusion led to enhanced plant response at 30 hpi. At 30 hpi, the majority of mitochondria were filamentous in WT. This suggests that mitochondrial fusion is required during the early stage of infection. However, disruption of mitochondrial fission led to enhanced plant response at 72 hpi, which suggests that mitochondrial fission might be required for biotrophy to necrotrophy transition. In future, the requirement of mitochondrial fragmentation in biotrophy to necrotrophy transition needs to be studied

systematically. To understand whether mitochondrial fission is required for biotrophy to necrotrophy transition, a marker of biotrophy to necrotrophy transition should be established first. Later on, the observation of such marker during invasive growth of WT and *Modnm1*Δ could be used to elucidate the exact role of mitochondrial fragmentation.

To understand the function of mitochondrial dynamics, the retrograde pathway in mitochondria was examined. The mitochondria-to-nucleus retrograde pathway seems well conserved in *M. oryzae*. A key factor involved in the mitochondria-to-nuclear retrograde pathway is mitochondrial dysfunction, followed by Rtg1/3 translocation and upregulation of Rtg2 expression. These three elements of retrograde pathway were examined in detail.

MoYbh3 was found to translocate into mitochondria during invasive growth thus supporting the importance of metabolic status of mitochondria therein. Secondly, mito-roGFP was used to examine the ROS levels in mitochondria. Similar to MoYbh3, the ROS levels were much higher in fragmented mitochondria observed at 48 hpi than those in filamentous mitochondria observed at 30 hpi.

I first confirmed that Rtg3 indeed translocated into the nucleus during mitochondrial damage, indicating that such function of Rtg3 is conserved in *M. oryzae*. Then the translocation of Rtg3 was examined in invasive growth.

As expected, mCherry-Rtg3 could be found in the nucleus at the stage where mitochondrial fragment, while mCherry-Rtg3 was mainly in cytosol in 30 hpi. These results suggest that the retrograde pathway is activated in invasive growth when mitochondrial fragmentation occurs. Gene-deletion analysis of *MoRTG2* was carried out to further understand the function of retrograde pathway. *Mortg2*Δ showed highly reduced pathogenicity and the invasive growth was inhibited at 48 hpi. Based on these data, the retrograde pathway is deemed to be activated during invasive growth in *M. oryzae*. In future, it would be important to elucidate the role of mitochondria-to-nucleus retrograde pathway during biotrophy to necrotrophy switch in *M. oryzae*.

During the studies on mitochondrial dynamics, I found that mito-GFP signal could be found in vacuoles, which suggests a specific pathway to deliver mitochondria to vacuoles. A well-studied pathway to deliver mitochondria to vacuoles is mitophagy (Ashrafi & Schwarz 2013, Novak 2012, Pallanck 2013, Youle & Narendra 2011). Mitophagy is a pathway to deliver damaged or excess mitochondria to vacuoles to control the mitochondrial quality and/or quantity. Although the main macroautophagy machineries are conserved in *M. oryzae,* The mitophagy specific mediator ScAtg32 is not conserved, which raises a big problem to study mitophagy in *M. oryzae* (Meijer et al 2007). To understand the mitophagy in *M. oryzae*, I first established the mitophagy assays modified from the mitophagy assays used in Yeast (Kanki et al 2009). Then I found that MoAtg24 might be a mitophagy specific protein in *M. oryzae*. In yeast, ScAtg24 is not a mitophagy specific protein, as it is partially required in mitophagy and pexophagy (Kanki et al 2009). MoAtg24 is similar

to ScAtg24, containing PX and BAR domain. However, MoAtg24 is induced by oxidative stress and starvation, which is not the case in ScAtg24 (Klionsky et al 2003). More importantly, MoAtg24 is not required for pexophagy in *M. oryzae*, which is in total contrast to its function in yeast (Ano et al 2005). Another important finding is that MoAtg24 is required for mitophagy, which provides a tool to research the function of mitophagy in filamentous fungi.

The mitophagy could be observed at foot cells during conidiation. To further confirm the role of mitophagy in conidiation, ScAtg32 was expressed in *Moatg24*Δ. The *Moatg24*Δ with ScAtg32 showed increased conidiation after two days upon light induction. However, the amount of conidia collected after 5 days upon light induction was highly decrease, because of the collapse of conidiation. These data suggest that the regulation of mitophagy is important for conidia maturation.

In this study, although mitochondrial rebuild or biogenesis at 72 hpi was clearly observed, its role is not studied. In future, more experiments need to be designed to answer whether mitochondrial rebuild or biogenesis also plays a very important role in pathogenesis of *M. oryzae*. To address this question, a mitochondrial biogenesis defective mutant, *Mopuf3*Δ could be generated. Later on, detailed characterization could be carried out.

In summary, the observation of mitochondrial dynamics during invasive growth raised several important questions. I tried to understand the function of mitochondrial dynamics through altering the mitochondrial fusion and fission machineries. The mitochondrial fusion is required for biotrophic maintenance and mitochondrial fission is necessary for biotrophy-to-necrotrophy transition. Such mitochondrial dynamics could be delayed by additional carbon source instead of antioxidants. The possible role of this mitochondrial dynamics is to activate mitochondria-to-nucleus retrograde pathway. This retrograde pathway could activate gene expression, which might be needed to upregulate the necessary genes for metabolic re-programing. Mitophagy is also part of such mitochondrial dynamics and also is required for proper pathogenesis in *M. oryzae*. Taken together, mitochondrial dynamics and mitochondrial turnover are required for rice blast development.

REFERENCES

Adams TH, Wieser JK, Yu JH. 1998. Asexual sporulation in Aspergillus nidulans. *Microbiology and molecular biology reviews : MMBR* 62: 35-54

Amuthan G, Biswas G, Zhang SY, Klein-Szanto A, Vijayasarathy C, Avadhani NG. 2001. Mitochondria-to-nucleus stress signaling induces phenotypic changes, tumor progression and cell invasion. *The EMBO journal* 20: 1910-20

Ano Y, Hattori T, Oku M, Mukaiyama H, Baba M, et al. 2005. A sorting nexin PpAtg24 regulates vacuolar membrane dynamics during pexophagy via binding to phosphatidylinositol-3-phosphate. *Molecular biology of the cell* 16: 446-57

Asakura M, Ninomiya S, Sugimoto M, Oku M, Yamashita S, et al. 2009. Atg26-mediated pexophagy is required for host invasion by the plant pathogenic fungus *Colletotrichum orbiculare*. *The Plant cell* 21: 1291-304

Ashrafi G, Schwarz TL. 2013. The pathways of mitophagy for quality control and clearance of mitochondria. *Cell death and differentiation* 20: 31-42

Azzi A, Chance B. 1969. The "energized state" of mitochondria: lifetime and ATP equivalence. *Biochimica et biophysica acta* 189: 141-51

Balhadere PV, Talbot NJ. 2001. PDE1 encodes a P-type ATPase involved in appressorium-mediated plant infection by the rice blast fungus *Magnaporthe grisea*. *The Plant cell* 13: 1987-2004

Bao L, Avshalumov MV, Patel JC, Lee CR, Miller EW, et al. 2009. Mitochondria are the source of hydrogen peroxide for dynamic brain-cell signaling. *The Journal of neuroscience : the official journal of the Society for Neuroscience* 29: 9002-10

Battersby BJ, Richter U. 2013. Why translation counts for mitochondria - retrograde signalling links mitochondrial protein synthesis to mitochondrial biogenesis and cell proliferation. *Journal of cell science* 126: 4331-8

Benard G, Karbowski M. 2009. Mitochondrial fusion and division: Regulation and role in cell viability. *Seminars in cell & developmental biology* 20: 365-74

Bleazard W, McCaffery JM, King EJ, Bale S, Mozdy A, et al. 1999. The dynamin-related GTPase Dnm1 regulates mitochondrial fission in yeast. *Nature cell biology* 1: 298-304

Bodemer C, Rotig A, Rustin P, Cormier V, Niaudet P, et al. 1999. Hair and skin disorders as signs of mitochondrial disease. *Pediatrics* 103: 428-33

Butow RA, Avadhani NG. 2004. Mitochondrial signaling: the retrograde response. *Molecular cell* 14: 1-15

Buttner S, Eisenberg T, Carmona-Gutierrez D, Ruli D, Knauer H, et al. 2007. Endonuclease G regulates budding yeast life and death. *Molecular cell* 25: 233-46

Buttner S, Ruli D, Vogtle FN, Galluzzi L, Moitzi B, et al. 2011. A yeast BH3-only protein mediates the mitochondrial pathway of apoptosis. *The EMBO journal* 30: 2779-92

Chattopadhyay S, Marques JT, Yamashita M, Peters KL, Smith K, et al. 2010. Viral apoptosis is induced by IRF-3-mediated activation of Bax. *The EMBO journal* 29: 1762-73

Chen H, Chan DC. 2010. Physiological functions of mitochondrial fusion. *Annals of the New York Academy of Sciences* 1201: 21-5

Chen J, Young SM, Allen C, Waller A, Ursu O, et al. 2010. Profiling a Selective Probe for RTG Branch of Yeast TORC1 Signaling Pathway In *Probe Reports from the NIH Molecular Libraries Program*. Bethesda (MD)

Cocheme HM, Murphy MP. 2008. Complex I is the major site of mitochondrial superoxide production by paraquat. *The Journal of biological chemistry* 283: 1786-98

Cockrell RS, Harris EJ, Pressman BC. 1967. Synthesis of ATP driven by a potassium gradient in mitochondria. *Nature* 215: 1487-8

Cottrell SF. 1982. Formation of mitochondria during the yeast cell cycle. *Cell biology international reports* 6: 125-30

Criddle DN, Gillies S, Baumgartner-Wilson HK, Jaffar M, Chinje EC, et al. 2006. Menadione-induced reactive oxygen species generation via redox cycling promotes apoptosis of murine pancreatic acinar cells. *The Journal of biological chemistry* 281: 40485-92

Dagdas YF, Yoshino K, Dagdas G, Ryder LS, Bielska E, et al. 2012. Septin-mediated plant cell invasion by the rice blast fungus, *Magnaporthe oryzae*. *Science* 336: 1590-5

Damsky CH. 1976. Environmentally induced changes in mitochondria and endoplasmic reticulum of Saccharomyces carlsbergensis yeast. *The Journal of cell biology* 71: 123-35

Dangl JL, Dietrich RA, Richberg MH. 1996. Death Don't Have No Mercy: Cell Death Programs in Plant-Microbe Interactions. *The Plant cell* 8: 1793-807

Deng YZ, Qu Z, He Y, Naqvi NI. 2012. Sorting nexin Snx41 is essential for conidiation and mediates glutathione-based antioxidant defense during invasive growth in *Magnaporthe oryzae*. *Autophagy* 8: 1058-70

Deng YZ, Ramos-Pamplona M, Naqvi NI. 2009a. Autophagy-assisted glycogen catabolism regulates asexual differentiation in *Magnaporthe oryzae*. *Autophagy* 5

Deng YZ, Ramos-Pamplona M, Naqvi NI. 2009b. Autophagy-assisted glycogen catabolism regulates asexual differentiation in *Magnaporthe oryzae*. *Autophagy* 5: 33-43

Dickman MB, Park YK, Oltersdorf T, Li W, Clemente T, French R. 2001. Abrogation of disease development in plants expressing animal antiapoptotic genes. *Proceedings of the National Academy of Sciences of the United States of America* 98: 6957-62

Ding SL, Liu W, Iliuk A, Ribot C, Vallet J, et al. 2010a. The tig1 histone deacetylase complex regulates infectious growth in the rice blast fungus *Magnaporthe oryzae*. *The Plant cell* 22: 2495-508

Ding WX, Ni HM, Li M, Liao Y, Chen X, et al. 2010b. Nix is critical to two distinct phases of mitophagy, reactive oxygen species-mediated autophagy induction and Parkin-ubiquitin-p62-mediated mitochondrial priming. *The Journal of biological chemistry* 285: 27879-90

Ding WX, Yin XM. 2012. Mitophagy: mechanisms, pathophysiological roles, and analysis. *Biological chemistry* 393: 547-64

Edlich F, Banerjee S, Suzuki M, Cleland MM, Arnoult D, et al. 2011. Bcl-x(L) retrotranslocates Bax from the mitochondria into the cytosol. *Cell* 145: 104-16

Ellson CD, Andrews S, Stephens LR, Hawkins PT. 2002. The PX domain: a new phosphoinositide-binding module. *Journal of cell science* 115: 1099-105

Evtodienko YV, Azarashvili TS, Teplova VV, Odinokova IV, Saris N. 2000. Regulation of oxidative phosphorylation in the inner membrane of rat liver mitochondria by calcium ions. *Biochemistry. Biokhimiia* 65: 1023-6

Fendt SM, Sauer U. 2010. Transcriptional regulation of respiration in yeast metabolizing differently repressive carbon substrates. *BMC systems biology* 4: 12

Finkel T, Hwang PM. 2009. The Krebs cycle meets the cell cycle: mitochondria and the G1-S transition. *Proceedings of the National Academy of Sciences of the United States of America* 106: 11825-6

Fritz S, Rapaport D, Klanner E, Neupert W, Westermann B. 2001. Connection of the mitochondrial outer and inner membranes by Fzo1 is critical for organellar fusion. *The Journal of cell biology* 152: 683-92

Giege P, Grienenberger JM, Bonnard G. 2008. Cytochrome c biogenesis in mitochondria. *Mitochondrion* 8: 61-73

Giorgi C, Romagnoli A, Pinton P, Rizzuto R. 2008. Ca2+ signaling, mitochondria and cell death. *Current molecular medicine* 8: 119-30

Giraldo MC, Dagdas YF, Gupta YK, Mentlak TA, Yi M, et al. 2013. Two distinct secretion systems facilitate tissue invasion by the rice blast fungus Magnaporthe oryzae. *Nature communications* 4: 1996

Green DE. 1983. Mitochondria--structure, function, and replication. *The New England journal of medicine* 309: 182-3

Greenberg JT. 1997. Programmed Cell Death in Plant-Pathogen Interactions. *Annual review of plant physiology and plant molecular biology* 48: 525-45

Guaragnella N, Pereira C, Sousa MJ, Antonacci L, Passarella S, et al. 2006. YCA1 participates in the acetic acid induced yeast programmed cell death also in a manner unrelated to its caspase-like activity. *FEBS letters* 580: 6880-4

Guha M, Avadhani NG. 2013. Mitochondrial retrograde signaling at the crossroads of tumor bioenergetics, genetics and epigenetics. *Mitochondrion* 13: 577-91

Guido C, Whitaker-Menezes D, Lin Z, Pestell RG, Howell A, et al. 2012. Mitochondrial fission induces glycolytic reprogramming in cancer-associated myofibroblasts, driving stromal lactate production, and early tumor growth. *Oncotarget* 3: 798-810

Hailey DW, Rambold AS, Satpute-Krishnan P, Mitra K, Sougrat R, et al. 2010. Mitochondria supply membranes for autophagosome biogenesis during starvation. *Cell* 141: 656-67

Hanson GT, Aggeler R, Oglesbee D, Cannon M, Capaldi RA, et al. 2004. Investigating mitochondrial redox potential with redox-sensitive green fluorescent protein indicators. *The Journal of biological chemistry* 279: 13044-53

He M, Kershaw MJ, Soanes DM, Xia Y, Talbot NJ. 2012. Infection-associated nuclear degeneration in the rice blast fungus *Magnaporthe oryzae* requires non-selective macro-autophagy. *PloS one* 7: e33270

He Y, Deng YZ, Naqvi NI. 2013. Atg24-assisted mitophagy in the foot cells is necessary for proper asexual differentiation in *Magnaporthe oryzae*. *Autophagy* 9: 1818-27

Hermann GJ, Thatcher JW, Mills JP, Hales KG, Fuller MT, et al. 1998. Mitochondrial fusion in yeast requires the transmembrane GTPase Fzo1p. *The Journal of cell biology* 143: 359-73

Ibrahim NG, Stuchell RN, Beattie DS. 1973. Formation of the yeast mitochondrial membrane. 2. Effects of glucose repression on mitochondrial protein synthesis. *European journal of biochemistry / FEBS* 36: 519-27

Ingerman E, Perkins EM, Marino M, Mears JA, McCaffery JM, et al. 2005. Dnm1 forms spirals that are structurally tailored to fit mitochondria. *The Journal of cell biology* 170: 1021-7

Inoue M, Sato EF, Nishikawa M, Park AM, Kira Y, et al. 2003. Mitochondrial generation of reactive oxygen species and its role in aerobic life. *Current medicinal chemistry* 10: 2495-505

Jakobs S, Martini N, Schauss AC, Egner A, Westermann B, Hell SW. 2003. Spatial and temporal dynamics of budding yeast mitochondria lacking the division component Fis1p. *Journal of cell science* 116: 2005-14

Jazwinski SM. 2004. Yeast replicative life span--the mitochondrial connection. *FEMS yeast research* 5: 119-25

Jin SM, Youle RJ. 2012. PINK1- and Parkin-mediated mitophagy at a glance. *Journal of cell science* 125: 795-9

Kankanala P, Czymmek K, Valent B. 2007. Roles for rice membrane dynamics and plasmodesmata during biotrophic invasion by the blast fungus. *The Plant cell* 19: 706-24

Kanki T, Klionsky DJ. 2010. The molecular mechanism of mitochondria autophagy in yeast. *Molecular microbiology* 75: 795-800

Kanki T, Wang K, Cao Y, Baba M, Klionsky DJ. 2009. Atg32 is a mitochondrial protein that confers selectivity during mitophagy. *Developmental cell* 17: 98-109

Khang CH, Berruyer R, Giraldo MC, Kankanala P, Park SY, et al. 2010. Translocation of *Magnaporthe oryzae* effectors into rice cells and their subsequent cell-to-cell movement. *The Plant cell* 22: 1388-403

Kim KS, Rosenkrantz MS, Guarente L. 1986. Saccharomyces cerevisiae contains two functional citrate synthase genes. *Molecular and cellular biology* 6: 1936-42

Kim S, Park SY, Kim KS, Rho HS, Chi MH, et al. 2009. Homeobox transcription factors are required for conidiation and appressorium development in the rice blast fungus *Magnaporthe oryzae*. *PLoS genetics* 5: e1000757

Kim S, Singh P, Park J, Park S, Friedman A, et al. 2011. Genetic and molecular characterization of a blue light photoreceptor MGWC-1 in *Magnaporth oryzae*. *Fungal genetics and biology : FG & B* 48: 400-7

Klionsky DJ, Abdalla FC, Abeliovich H, Abraham RT, Acevedo-Arozena A, et al. 2012. Guidelines for the use and interpretation of assays for monitoring autophagy. *Autophagy* 8: 445-544

Klionsky DJ, Cregg JM, Dunn WA, Jr., Emr SD, Sakai Y, et al. 2003. A unified nomenclature for yeast autophagy-related genes. *Developmental cell* 5: 539-45

Kurihara Y, Kanki T, Aoki Y, Hirota Y, Saigusa T, et al. 2012. Mitophagy plays an essential role in reducing mitochondrial production of reactive oxygen species and mutation of mitochondrial DNA by maintaining mitochondrial quantity and quality in yeast. *The Journal of biological chemistry* 287: 3265-72

Laluk K, Mengiste T. 2010. Necrotroph attacks on plants: wanton destruction or covert extortion? *The Arabidopsis book / American Society of Plant Biologists* 8: e0136

Lee K, Singh P, Chung WC, Ash J, Kim TS, et al. 2006. Light regulation of asexual development in the rice blast fungus, *Magnaporthe oryzae*. *Fungal genetics and biology : FG & B* 43: 694-706

Lee WS, Sokol RJ. 2007. Liver disease in mitochondrial disorders. *Seminars in liver disease* 27: 259-73

Lee YH, Dean RA. 1993. cAMP Regulates Infection Structure Formation in the Plant Pathogenic Fungus *Magnaporthe grisea*. *The Plant cell* 5: 693-700

Levonen AL, Patel RP, Brookes P, Go YM, Jo H, et al. 2001. Mechanisms of cell signaling by nitric oxide and peroxynitrite: from mitochondria to MAP kinases. *Antioxidants & redox signaling* 3: 215-29

Li G, Zhou X, Kong L, Wang Y, Zhang H, et al. 2011. MoSfl1 is important for virulence and heat tolerance in *Magnaporthe oryzae*. *PloS one* 6: e19951

Liao X, Butow RA. 1993. RTG1 and RTG2: two yeast genes required for a novel path of communication from mitochondria to the nucleus. *Cell* 72: 61-71

Liao XS, Small WC, Srere PA, Butow RA. 1991. Intramitochondrial functions regulate nonmitochondrial citrate synthase (CIT2) expression in Saccharomyces cerevisiae. *Molecular and cellular biology* 11: 38-46

Liu H, Suresh A, Willard FS, Siderovski DP, Lu S, Naqvi NI. 2007. Rgs1 regulates multiple Galpha subunits in Magnaporthe pathogenesis, asexual growth and thigmotropism. *The EMBO journal* 26: 690-700

Liu W, Liu J, Triplett L, Leach JE, Wang GL. 2013. Novel Insights into Rice Innate Immunity against Bacterial and Fungal Pathogens. *Annual review of phytopathology*

Liu Z, Butow RA. 1999. A transcriptional switch in the expression of yeast tricarboxylic acid cycle genes in response to a reduction or loss of respiratory function. *Molecular and cellular biology* 19: 6720-8

Liu Z, Butow RA. 2006. Mitochondrial retrograde signaling. *Annual review of genetics* 40: 159-85

Liu Z, Sekito T, Spirek M, Thornton J, Butow RA. 2003. Retrograde signaling is regulated by the dynamic interaction between Rtg2p and Mks1p. *Molecular cell* 12: 401-11

Ludovico P, Rodrigues F, Almeida A, Silva MT, Barrientos A, Corte-Real M. 2002. Cytochrome c release and mitochondria involvement in programmed cell death induced by acetic acid in Saccharomyces cerevisiae. *Molecular biology of the cell* 13: 2598-606

Malpass K. 2013. Neurodegenerative disease: defective mitochondrial dynamics in the hot seat-a therapeutic target common to many neurological disorders? *Nature reviews. Neurology* 9: 417

Mao K, Klionsky DJ. 2013. Participation of mitochondrial fission during mitophagy. *Cell cycle* 12: 3131-2

Marcel S, Sawers R, Oakeley E, Angliker H, Paszkowski U. 2010. Tissue-adapted invasion strategies of the rice blast fungus *Magnaporthe oryzae*. *The Plant cell* 22: 3177-87

Matsunaga K, Morita E, Saitoh T, Akira S, Ktistakis NT, et al. 2010. Autophagy requires endoplasmic reticulum targeting of the PI3-kinase complex via Atg14L. *The Journal of cell biology* 190: 511-21

Mayer AM, Staples RC, Gil-ad NL. 2001. Mechanisms of survival of necrotrophic fungal plant pathogens in hosts expressing the hypersensitive response. *Phytochemistry* 58: 33-41

Meijer WH, van der Klei IJ, Veenhuis M, Kiel JA. 2007. ATG genes involved in non-selective autophagy are conserved from yeast to man, but the selective Cvt and pexophagy pathways also require organism-specific genes. *Autophagy* 3: 106-16

Moustris A, Edwards MJ, Bhatia KP. 2011. Movement disorders and mitochondrial disease. *Handbook of clinical neurology* 100: 173-92

Murphy MP. 2009. How mitochondria produce reactive oxygen species. *The Biochemical journal* 417: 1-13

Nicholls DG. 2005. Mitochondria and calcium signaling. *Cell calcium* 38: 311-7

Novak I. 2012. Mitophagy: a complex mechanism of mitochondrial removal. *Antioxidants & redox signaling* 17: 794-802

Odinokova IV, Sung KF, Mareninova OA, Hermann K, Evtodienko Y, et al. 2009. Mechanisms regulating cytochrome c release in pancreatic mitochondria. *Gut* 58: 431-42

Okamoto K, Kondo-Okamoto N, Ohsumi Y. 2009. Mitochondria-anchored receptor Atg32 mediates degradation of mitochondria via selective autophagy. *Developmental cell* 17: 87-97

Oliver RP, Solomon PS. 2010. New developments in pathogenicity and virulence of necrotrophs. *Current opinion in plant biology*

Pallanck L. 2013. Mitophagy: mitofusin recruits a mitochondrial killer. *Current biology : CB* 23: R570-2

Pan R, Hu J. 2011. The conserved fission complex on peroxisomes and mitochondria. *Plant signaling & behavior* 6: 870-2

Patkar RN, Ramos-Pamplona M, Gupta AP, Fan Y, Naqvi NI. 2012. Mitochondrial beta-oxidation regulates organellar integrity and is necessary for conidial germination and invasive growth in *Magnaporthe oryzae*. *Molecular microbiology* 86: 1345-63

Peter BJ, Kent HM, Mills IG, Vallis Y, Butler PJ, et al. 2004. BAR domains as sensors of membrane curvature: the amphiphysin BAR structure. *Science* 303: 495-9

Polyakov VY, Soukhomlinova MY, Fais D. 2003. Fusion, fragmentation, and fission of mitochondria. *Biochemistry. Biokhimiia* 68: 838-49

Ramanujam R, Naqvi NI. 2010. PdeH, a high-affinity cAMP phosphodiesterase, is a key regulator of asexual and pathogenic differentiation in *Magnaporthe oryzae*. *PLoS pathogens* 6: e1000897

Redpath CJ, Bou Khalil M, Drozdzal G, Radisic M, McBride HM. 2013. Mitochondrial hyperfusion during oxidative stress is coupled to a dysregulation in calcium handling within a C2C12 cell model. *PloS one* 8: e69165

Rhee SG, Chang TS, Jeong W, Kang D. 2010. Methods for detection and measurement of hydrogen peroxide inside and outside of cells. *Molecules and cells* 29: 539-49

Ryder LS, Dagdas YF, Mentlak TA, Kershaw MJ, Thornton CR, et al. 2013. NADPH oxidases regulate septin-mediated cytoskeletal remodeling during plant infection by the rice blast fungus. *Proceedings of the National Academy of Sciences of the United States of America* 110: 3179-84

Sack MN, Finkel T. 2012. Mitochondrial metabolism, sirtuins, and aging. *Cold Spring Harbor perspectives in biology* 4

Samalova M, Meyer AJ, Gurr SJ, Fricker MD. 2013. Robust anti-oxidant defences in the rice blast fungus *Magnaporthe oryzae* confer tolerance to the host oxidative burst. *The New phytologist*

Santel A, Fuller MT. 2001. Control of mitochondrial morphology by a human mitofusin. *Journal of cell science* 114: 867-74

Scherz-Shouval R, Elazar Z. 2007. ROS, mitochondria and the regulation of autophagy. *Trends in cell biology* 17: 422-7

Sekito T, Liu Z, Thornton J, Butow RA. 2002. RTG-dependent mitochondria-to-nucleus signaling is regulated by MKS1 and is linked to formation of yeast prion [URE3]. *Molecular biology of the cell* 13: 795-804

Sesaki H, Jensen RE. 2004. Ugo1p links the Fzo1p and Mgm1p GTPases for mitochondrial fusion. *The Journal of biological chemistry* 279: 28298-303

Sesaki H, Southard SM, Yaffe MP, Jensen RE. 2003. Mgm1p, a dynamin-related GTPase, is essential for fusion of the mitochondrial outer membrane. *Molecular biology of the cell* 14: 2342-56

Smaili SS, Hsu YT, Carvalho AC, Rosenstock TR, Sharpe JC, Youle RJ. 2003. Mitochondria, calcium and pro-apoptotic proteins as mediators in cell death signaling. *Brazilian journal of medical and biological research = Revista brasileira de pesquisas medicas e biologicas / Sociedade Brasileira de Biofisica ... [et al.]* 36: 183-90

Song Y, Xiao Y, Wang JM, Chen Q. 2014. The different molecular mechanisms of mitophagy between yeast and mammals. *Critical reviews in eukaryotic gene expression* 24: 29-38

Springer ML, Yanofsky C. 1989. A morphological and genetic analysis of conidiophore development in *Neurospora crassa*. *Genes & development* 3: 559-71

Stromhaug PE, Klionsky DJ. 2001. Approaching the molecular mechanism of autophagy. *Traffic* 2: 524-31

Tieu Q, Okreglak V, Naylor K, Nunnari J. 2002. The WD repeat protein, Mdv1p, functions as a molecular adaptor by interacting with Dnm1p and Fis1p during mitochondrial fission. *The Journal of cell biology* 158: 445-52

Tondera D, Grandemange S, Jourdain A, Karbowski M, Mattenberger Y, et al. 2009. SLP-2 is required for stress-induced mitochondrial hyperfusion. *The EMBO journal* 28: 1589-600

Torres MA. 2010. ROS in biotic interactions. *Physiologia plantarum* 138: 414-29

Tosa Y, Tamba H, Tanaka K, Mayama S. 2006. Genetic Analysis of Host Species Specificity of *Magnaporthe oryzae* Isolates from Rice and Wheat. *Phytopathology* 96: 480-4

Tufan HA, McGrann GR, MacCormack R, Boyd LA. 2012. TaWIR1 contributes to post-penetration resistance to *Magnaporthe oryzae*, but not Blumeria graminis f. sp. tritici, in wheat. *Molecular plant pathology* 13: 653-65

Upton JP, Valentijn AJ, Zhang L, Gilmore AP. 2007. The N-terminal conformation of Bax regulates cell commitment to apoptosis. *Cell death and differentiation* 14: 932-42

van Wees S. 2008. Phenotypic analysis of Arabidopsis mutants: trypan blue stain for fungi, oomycetes, and dead plant cells. *CSH protocols* 2008: pdb prot4982

Vellosillo T, Vicente J, Kulasekaran S, Hamberg M, Castresana C. 2010. Emerging complexity in reactive oxygen species production and signaling during the response of plants to pathogens. *Plant physiology* 154: 444-8

Volkmann N, Marassi FM, Newmeyer DD, Hanein D. 2014. The rheostat in the membrane: BCL-2 family proteins and apoptosis. *Cell death and differentiation* 21: 206-15

Wang CW, Klionsky DJ. 2003. The molecular mechanism of autophagy. *Molecular medicine* 9: 65-76

Wang ZY, Jenkinson JM, Holcombe LJ, Soanes DM, Veneault-Fourrey C, et al. 2005. The molecular biology of appressorium turgor generation by the rice blast fungus *Magnaporthe grisea*. *Biochemical Society transactions* 33: 384-8

Westermann B. 2010. Mitochondrial fusion and fission in cell life and death. *Nature reviews. Molecular cell biology* 11: 872-84

Wilson RA, Gibson RP, Quispe CF, Littlechild JA, Talbot NJ. 2010. An NADPH-dependent genetic switch regulates plant infection by the rice blast fungus. *Proceedings of the National Academy of Sciences of the United States of America* 107: 21902-7

Wilson RA, Jenkinson JM, Gibson RP, Littlechild JA, Wang ZY, Talbot NJ. 2007. Tps1 regulates the pentose phosphate pathway, nitrogen metabolism and fungal virulence. *The EMBO journal* 26: 3673-85

Wilson RA, Talbot NJ. 2009. Under pressure: investigating the biology of plant infection by *Magnaporthe oryzae*. *Nature reviews. Microbiology* 7: 185-95

Wissing S, Ludovico P, Herker E, Buttner S, Engelhardt SM, et al. 2004. An AIF orthologue regulates apoptosis in yeast. *The Journal of cell biology* 166: 969-74

Witter RF, Watson ML, Cottone MA. 1955. Morphology and ATP-ase of isolated mitochondria. *The Journal of biophysical and biochemical cytology* 1: 127-38

Yang Z, Klionsky DJ. 2009. An overview of the molecular mechanism of autophagy. *Current topics in microbiology and immunology* 335: 1-32

Yi M, Chi MH, Khang CH, Park SY, Kang S, et al. 2009. The ER chaperone LHS1 is involved in asexual development and rice infection by the blast fungus *Magnaporthe oryzae*. *The Plant cell* 21: 681-95

Yin F, Boveris A, Cadenas E. 2014. Mitochondrial energy metabolism and redox signaling in brain aging and neurodegeneration. *Antioxidants & redox signaling* 20: 353-71

Youle RJ, Narendra DP. 2011. Mechanisms of mitophagy. *Nature reviews. Molecular cell biology* 12: 9-14

Zhang H, Kong X, Kang J, Su J, Li Y, et al. 2009. Oxidative stress induces parallel autophagy and mitochondria dysfunction in human glioma U251 cells. *Toxicological sciences : an official journal of the Society of Toxicology* 110: 376-88

Zhang S, Xu JR. 2014. Effectors and effector delivery in *Magnaporthe oryzae*. *PLoS pathogens* 10: e1003826

Zhang Y, Chan NC, Ngo HB, Gristick H, Chan DC. 2012. Crystal structure of mitochondrial fission complex reveals scaffolding function for mitochondrial division 1 (Mdv1) coiled coil. *The Journal of biological chemistry* 287: 9855-61

Zhou X, Zhang H, Li G, Shaw B, Xu JR. 2012. The Cyclase-associated protein Cap1 is important for proper regulation of infection-related morphogenesis in *Magnaporthe oryzae*. *PLoS pathogens* 8: e1002911

Zorzano A, Bach D, Pich S, Palacin M. 2004. [Role of novel mitochondrial proteins in energy balance]. *Revista de medicina de la Universidad de Navarra* 48: 30-5

Zurbriggen MD, Carrillo N, Hajirezaei MR. 2010. ROS signaling in the hypersensitive response: when, where and what for? *Plant signaling & behavior* 5: 393-6

APPENDIX

First author publication as listed on page xiv.

Autophagy 9:11, 1–10; November 2013; © 2013 Landes Bioscience

Atg24-assisted mitophagy in the foot cells is necessary for proper asexual differentiation in *Magnaporthe oryzae*

Yunlong He,[1] Yi Zhen Deng[1] and Naweed I Naqvi[1,2,*]

[1]Temasek Life Sciences Laboratory and Department of Biological Sciences; National University of Singapore; Singapore; [2]School of Biological Sciences; Nanyang Technological University; Singapore

Keywords: MoAtg24, conidiation, foot cell, mitophagy, *Magnaporthe oryzae*, reactive oxygen species, redox, sorting nexin

Abbreviations: Atg, autophagy related; BAR, Bin–Amphiphysin–Rvs; CMAC, 7-amino-4-chloromethylcoumarin; GFP, green fluorescent protein; GSH, glutathione; Kb, kilobase pair; NAC, N-acetylcysteine; ORF, open reading frame; PtdIns3P, phosphatidylinositol-3-phosphate; PMSF, phenylmethylsulfonyl fluoride; PX, Phox homology; RFP, red fluorescent protein; ROS, reactive oxygen species; WT, wild type

Macroautophagy-mediated glycogen catabolism is required for asexual differentiation in the blast fungus, *Magnaporthe oryzae*. However, the function(s) of selective subtypes of autophagy has not been studied therein. Here, we report that mitophagy, selective autophagic delivery of mitochondria to the vacuoles for degradation, occurs during early stages of Magnaporthe conidiation. Specifically, mitophagy was evident in the foot cells while being undetectable in aerial hyphae and/or conidiophores. We show that loss of MoAtg24, a sorting nexin related to yeast Snx4, disrupts mitophagy and consequently leads to highly reduced conidiation, suggesting that mitophagy in the foot cells plays an important role during asexual development in Magnaporthe. Ectopic expression of yeast *ScATG32* partially suppressed the conidiation initiation defects associated with *MoATG24* deletion. MoAtg24 was neither required for pexophagy nor for macroautophagy, or for MoAtg8 localization per se, but directly associated with and likely recruited mitochondria to the autophagic structures during mitophagy. Lastly, MoAtg24 was also required for oxidative stress response in Magnaporthe.

Introduction

M. oryzae is a filamentous fungus, which causes the rice blast disease worldwide.[1] The pathogenic life cycle in *M. oryzae* consists of conidiation, appressorium formation and maturation, and infection, in which conidiation is an essential step.[2,3] Without conidiation, the specialized infection structures, functional appressoria, would not be formed and consequentially infection would not occur.[3,4] Although, there are some reports on appressoria formation during the mycelial phase, the pathogenic function of such precocious mutant appressoria was found to be compromised.[5] As a common developmental process in filamentous fungi, conidiation has been extensively studied in detail.[6,7] In darkness, aerial hyphae emerge from the vegetative mycelia, with the help of hydrophobin proteins.[8,9] The conidiation process begins with the growth of a conidiophore stalk by apical extension from a thick-walled vegetative cell termed a foot cell. The foot cell connects aerial hyphae to the vegetative mycelia and ensures supply of energy and other necessary nutrients to the aerial hyphae during conidiation.[10] After photo-induction, the tip of aerial hypha is remodeled by light-regulated pathways to form a swollen structure, called the conidiophore.[5-9] About 3 to 5 conidia are then formed at the tip of a conidiophore in a sympodial pattern.[2-4] Currently, conidiophores are used to differentiate aerial hyphae from vegetative mycelia using light microscopes.[10]

Conidiation is regulated by circadian rhythm, physical stimuli, such as light exposure and mycelial injury, and the metabolic state.[5-10] Previously, we have shown that glycogen autophagy is required for conidiation.[11] However, whether selective autophagy such as mitophagy or pexophagy is required during conidiation is unknown. In general, selective autophagy has not been well studied in filamentous fungi.[12] Until now, pexophagy has been reported to be essential for Colletotrichum pathogenesis; and infection-associated nuclear degradation in Magnaporthe is through nonselective macroautophagy.[13,14]

Mitophagy is a cellular process to selectively remove mitochondria through autophagy.[15] The molecular mechanism

*Correspondence to: Naweed I Naqvi; Email: naweed@tll.org.sg
Submitted: 12/19/12; Revised: 07/30/13; Accepted: 08/05/13
http://dx.doi.org/10.4161/auto.26057

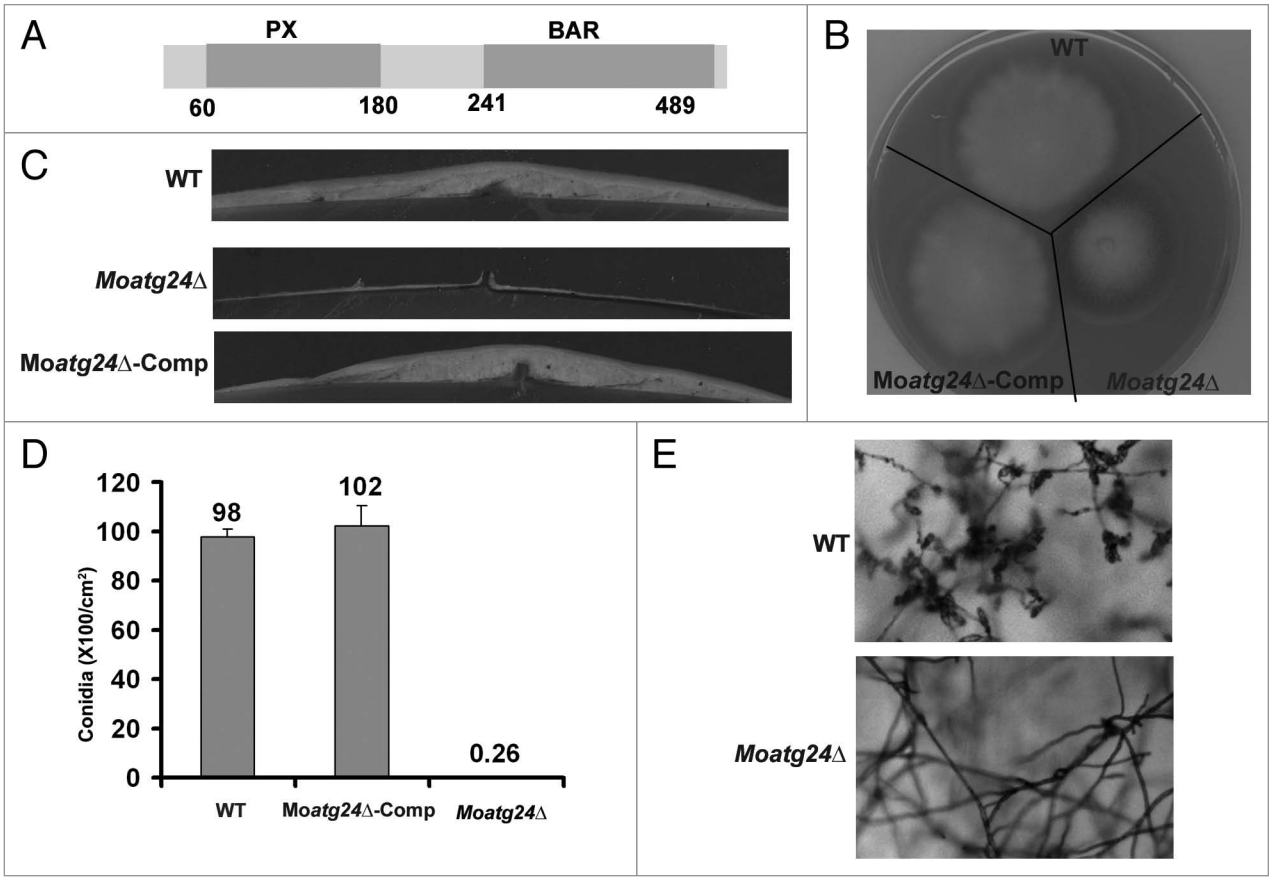

Figure 1. Characterization of the *Moatg24*Δ mutant. (**A**) Domain organization of the MoAtg24 protein. Numbers below the scheme depict amino acid residues. (**B**) Aerial hyphal growth is significantly reduced in *Moatg24*Δ. Seven-day old colony (dark grown) of the WT, *Moatg24*Δ or *Moatg24*Δ-Comp (complemented strain) was cross-sectioned at the near median region and photographed. (**C**) Radial growth is reduced in *Moatg24*Δ. Colonies of WT, *Moatg24*Δ and *Moatg24*Δ-Comp strains were grown on PA solid medium in the dark for 4 d and imaged. (**D**) Conidiation is significantly reduced in *Moatg24*Δ. Conidia of WT, *Moatg24*Δ and *Moatg24*Δ-Comp strains were quantified after being cultured on PA plates for 2 d in darkness and following 5 d under light. Mean values (± SE) presented as percentage points were derived from three independent experiments (3 colonies for each sample). (**E**) Microscope image of conidiation of WT and *Moatg24*Δ after being cultured in PA medium for 2 d in the dark followed by 3 d under constant illumination.

underlying mitophagy has been well studied in yeast.[15-17] Upon mitophagic induction, ScAtg32 is translocated to mitochondria through its membrane anchoring domain.[15-17] Consequentially, Atg32 interacts with Atg11, and the N-terminal WXXL motif of Atg32 binds and recruits Atg8 to the surface of mitochondria.[10,11] The macroautophagy machinery then follows up to form a mitophagosome, which eventually fuses with the vacuole, leading to mitochondrial degradation therein. However, the role of mitophagy has not been explored in filamentous fungi, partly due to the lack of proper Atg32 orthologs. It remains to be seen whether mitophagy operates in filamentous fungi, and if so, which protein(s) or protein complex serves an Atg32-like adaptor function in mitophagy.

In this study, we provide data to support the hypothesis that Magnaporthe MoAtg24 is directly involved in mitophagy in a manner similar to the yeast Atg32 function. Furthermore, we observed that mitophagy occurs specifically in the foot cells during conidiation. More importantly, we demonstrate that genetic disruption of mitophagy, via loss of *MoATG24* function, results in highly reduced conidiation, thus suggesting that mitophagy is critical for asexual development in Magnaporthe. Finally, we show the involvement of MoAtg24 in redox homeostasis during growth and development in the blast fungus.

Results

Disruption of *MoATG24* results in decreased aerial hyphae and conidiation

The *MoATG24* locus (MGG_03638; previously identified in a genomics study by Kershaw et al.[18]) is predicted to encode a sorting nexin containing the PX and BAR domains (**Fig. 1A**). The *MoATG24* gene was deleted by locus-specific replacement using *Agrobacterium* TDNA-mediated transformation (**Fig. S1A**). The deletion strains were confirmed by Southern blotting (**Fig. S1B**). The resultant *Moatg24*Δ strain exhibited a reduced growth rate and decreased aerial hyphae formation (**Fig. 1B and C**). The mutant produced a significantly lower number of conidia, compared with the wild type (WT; 0.26% of the WT, $p < 0.05$)

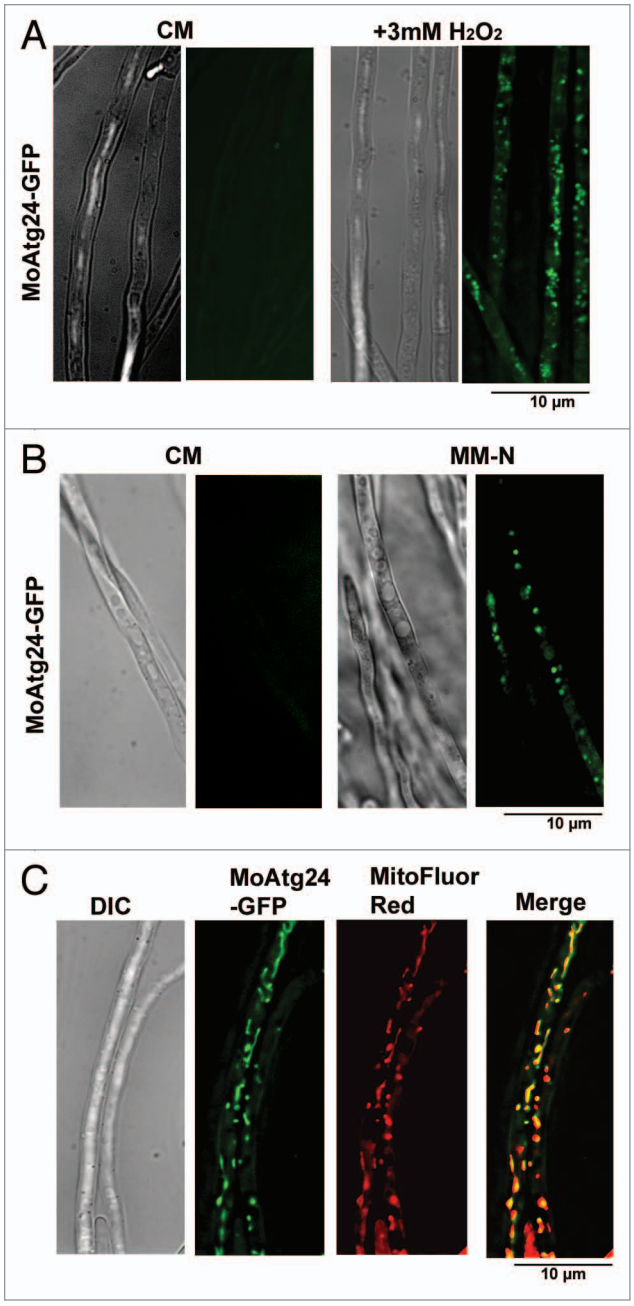

Figure 2. Subcellular localization of MoAtg24-GFP. (**A**) MoAtg24-GFP is induced by oxidative stress and localizes to cytoplasmic punctate structures. A strain expressing MoAtg24-GFP was grown in liquid CM for 48 h and shifted to CM with 3 mM H_2O_2. Images were taken with a Zeiss Widefield Fluorescence inverted microscope after growth in the presence of H_2O_2 for 1 h. (**B**) MoAtg24-GFP is induced by glycerol/MM-N starvation and localizes to cytoplasmic punctate structures. CM-cultured mycelia were shifted to BM-G and allowed to grow for 30 h and then shifted to MM-N for another 6 h before microscopy. (**C**) MoAtg24-GFP associates with mitochondria. The mycelia were grown in CM for 48 h and shifted to CM with 3 mM H_2O_2 to induce MoAtg24-GFP, and co-stained with MitoFluor Red.

(**Fig. 1D**). Aerial hyphae were initially examined to determine which stage of conidiation was affected in *Moatg24*Δ. Upon growth in the dark, aerial hyphae of *Moatg24*Δ were significantly shorter than those of the WT. After a 24 h exposure to light, three or more conidia were formed per conidiophore in the WT, while conidia were rarely seen in *Moatg24*Δ at the same time point (**Fig. 1E**). These results suggest that the loss of conidiation in *Moatg24*Δ is mainly due to a decreased rate of conidiophore formation and reduced aerial hyphal growth. In contrast, growth rate, aerial hyphae formation and conidiation were fully restored in the complemented strain *Moatg24*Δ-Comp (**Fig. 1B–D**). We conclude that Atg24 function is essential for proper initiation of asexual spores in Magnaporthe.

Subcellular localization of MoAtg24-GFP under starvation or oxidative stress conditions

To examine subcellular localization, a strain expressing MoAtg24-GFP under native regulation was generated in Magnaporthe. MoAtg24-GFP was undetectable in mycelia cultured in liquid Complete Medium (CM) (**Fig. 2A and B**). Upon induction by oxidative stress or nitrogen starvation, the MoAtg24-GFP signal intensified and appeared aggregated as punctate structures (**Fig. 2A and B**). Since cellular ROS is significantly linked to the function of peroxisomes and mitochondria,[19,20] we speculated that the MoAtg24-GFP puncta might be of peroxisomal and/or mitochondrial origin. To verify this, the spatial relationship between MoAtg24-GFP and peroxisomes or mitochondria was examined. Under ROS stress, MoAtg24-GFP nicely colocalized with mitochondria stained with MitoFluor Red (**Fig. 2C**). Under starvation conditions, MoAtg24-GFP was also localized to mitochondria (**Fig. S2B**). MoAtg24-GFP did not colocalize with peroxisomes under ROS or starvation conditions (**Fig. S2C**). Based on these results, we conclude that MoAtg24-GFP associates with mitochondria under starvation or oxidative stress conditions.

MoATG24 is essential for mitophagy

In yeast, mitophagy could be observed during the post-logarithmic growth phase in lactate or glycerol medium or during the growth transition from utilizing acetate or glycerol to nitrogen starvation.[16,17] A Magnaporthe strain carrying Mito-GFP was created and used for monitoring mitophagy. The Mito-GFP strain was grown in glycerol medium (to induce mitochondrial biogenesis) and shifted to nitrogen-starvation medium (to induce mitophagy) for growth for another 6 h. A vacuolar GFP signal was evident in starved mycelia, indicating that mitochondria were delivered into vacuoles (**Fig. 3A**). *Moatg8*Δ mutant was used as a negative control, because *MoATG8* is essential for all types of autophagy including mitophagy.[21,22] As expected, the Mito-GFP signal could not be observed in vacuoles of *Moatg8*Δ (**Fig. 3A**), suggesting that the vacuolar Mito-GFP signal was due to mitophagy and that such delivery of Mito-GFP/mitochondria to the vacuole requires Atg8 in Magnaporthe. Similarly, no vacuolar GFP signal was observed in the *Moatg24*Δ strain (**Fig. 3A**), indicating that mitophagy was likely blocked upon loss of *MoATG24*. In addition to the cell biology data, the level of mitophagy was semi-quantitatively monitored by assessing the total amounts of porin (a mitochondrial marker protein) under conditions that promote mitophagy. In WT cells, total porin amounts showed a time course-dependent decrease/degradation,

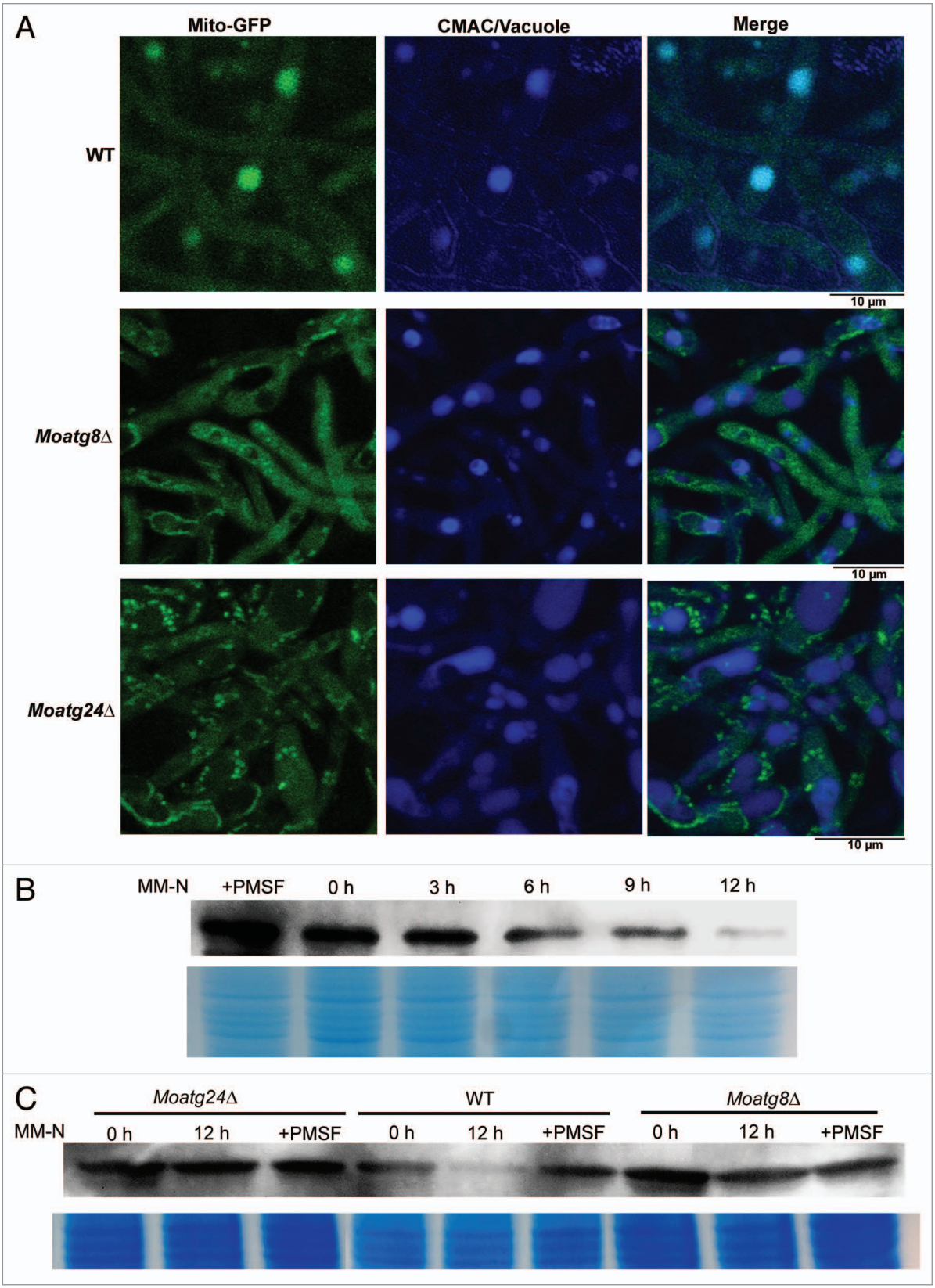

Figure 3. For figure legend, see page 5.

Figure 3 (See opposite page). MoAtg24 is required for mitophagy. (**A**) Glycerol/MM-N starvation (described previously) mycelia from WT, *Moatg8*Δ and *Moatg24*Δ strains were co-stained with 10 μM CMAC. Confocal microscopy with Mito-GFP and CMAC-stained vacuoles was performed as described in Materials and Methods, to detect mitophagy in the aforementioned strains. (**B**) Time course of vacuolar degradation of porin in WT Magnaporthe. Cells were collected at the indicated time points and cell lysates were subjected to immunoblot analysis with anti-porin antibody. (**C**) WT, *Moatg24*Δ and *Moatg8Δ* strains were cultured in CM for 2 d, then shifted to BM-G for 30 h and starved in MM-N for 12 h. Mycelia were harvested and cell lysates were subjected to immunoblot analysis with anti-porin antibody.

and the differences in levels were evident between time 0 h and 12 h (**Fig. 3B**). Such mitophagy-dependent reduction was negated in WT cells treated with PMSF. Consistent with the microscopy observation, the *Moatg24*Δ mutation blocked mitophagy and led to more stabilized levels of porin at comparable time points, similar to the results observed in *Moatg8*Δ, which is defective for selective and nonspecific autophagy (**Fig. 3C**). We conclude that Atg24 is essential for mitophagy in *M. oryzae*.

Next, we decided to determine whether MoAtg24 is required for macroautophagy and/or any other types of selective autophagy. Lipidation of RFP-MoAtg8 was measured. We found that MoAtg24 is not essential in MoAtg8 lipidation (**Fig. S3A**). Furthermore, the colocalization of RFP-MoAtg8 with vacuoles in *Moatg24*Δ was comparable to that in the WT strain (**Fig. S3B**). Selective autophagy is not well characterized in *M. oryzae*, although pexophagy was previously shown to occur in *M. oryzae*.[23] Next, we examined the requirement of MoAtg24 in pexophagy. The WT and *Moatg8*Δ strains served as positive and negative controls, respectively, in this experiment. The *Moatg24*Δ mutant displayed degradation of Pex14 after shifting cells from BM-O (medium containing oleate) to MM-N (nitrogen starvation medium; **Fig. S3C**). Overall, these results suggested that MoATG24 is a mitophagy-specific gene that is not required for either nonspecific autophagy or other types of selective autophagy such as pexophagy.

The PX and BAR domains of MoAtg24 are required for its mitochondrial localization during mitophagy

To further characterize the function of MoAtg24 in mitophagy, different truncated forms of MoAtg24 were generated, and tagged with GFP (**Fig. 4A**). The PX domain of MoAtg24 was found to be essential for mitochondrial membrane localization, since the PX domain deletion variant, $MoAtg24_{1-190}$-GFP displayed cytosolic localization, instead of associating with mitochondria (**Fig. 4B**). The C terminus of MoAtg24 was predicted to contain a BAR domain, and $MoAtg24_{190-495}$-GFP also displayed cytosolic localization. To understand how MoAtg24 was translocated to the mitochondrial membrane, PtdIns3P was observed using GFP-2xFYVE, because the PX domain binds PtdIns3P in many systems.[24] In the absence of oxidative stress, about 15% of total mitochondria colocalized with GFP-2xFYVE puncta, whereas this colocalization increased to nearly 100% under ROS stress conditions (**Fig. S4**). We conclude that the mitochondrial targeting of Atg24 during oxidative stress is likely mediated by the PX-PtdIns3P interaction on the mitochondrial membrane in Magnaporthe.

Mitophagy occurs in foot cells during conidiation

Next, we investigated the potential relationship between mitophagy and Magnaporthe conidiation. First, we examined whether mitophagy occurs naturally during conidiation by using a time-course analysis. We found that Mito-GFP (to visualize mitochondria) could be clearly observed in the vacuoles in the foot cells (**Fig. 5B and E**; n = 30). However, a vacuolar GFP signal was absent in aerial hyphae (**Fig. 5C and F**; n = 30). In contrast, Mito-GFP in the *Moatg24*Δ mutant could not be delivered into the vacuoles in foot cells, due to the loss of mitophagy (**Fig. 5I**). These results indicate that mitophagy plays an important role in the foot cells during Magnaporthe conidiation.

In yeast, ScAtg32 is a mitophagy-specific receptor, which localizes to mitochondria and recruits ScAtg8 and ScAtg11 to the mitochondria.[15-17] To examine whether *Moatg24*Δ defects could be rescued with yeast ScAtg32, we expressed GFP-ScAtg32 under a strong, constitutive promoter (the *RP27* promoter) in *Moatg24*Δ. As expected, GFP-ScAtg32 colocalized with mitochondria in Magnaporthe (**Fig. S6**). Increased conidiation was observed in *Moatg24*Δ expressing the *$RP27_{PRO}$:GFP-ScAtg32* construct by microscopy (**Fig. 6A**). After two days of light induction, the *Moatg24*Δ strain expressing GFP-ScAtg32 produced a comparable number of conidia to that of WT (**Fig. 6B**). However, the *Moatg24*Δ strain expressing GFP-ScAtg32 produced a significantly lower number of conidia compared with WT after five days of light induction (**Fig. 6B**). To understand the difference between conidiation upon short (two days) vs. long (five days) photo-induction, we observed the conidiation more carefully. We found that the conidia produced in *Moatg24*Δ expressing GFP-ScAtg32 collapsed early and failed to mature (**Fig. 6C**).

Since mitochondrial function has been linked to cellular ROS levels in recent studies,[16] we tested the sensitivity of *Moatg24*Δ to increased ROS levels in Magnaporthe. *Moatg24*Δ showed increased sensitivity to menadione and paraquat compared with the WT (**Fig. S5A**). Furthermore, exogenously added antioxidants such as NAC or GSH could only partially suppress the conidiation defects in *Moatg24*Δ (**Fig. S5B**). We concluded that MoAtg24-assisted mitophagy is crucial for regulating the redox homeostasis during conidiation in the blast fungus.

Discussion

Although well studied in mammalian cells and unicellular yeasts, the function of mitophagy has not been explored in great detail in filamentous fungi.[15] Here, we provide evidence that clearly demonstrates the existence of mitophagy in a filamentous fungus, Magnaporthe, and also its potential function in conidiation and regulation of oxidative stress. Mitophagy in *M. oryzae* depends on MoAtg24, a conserved sorting nexin, which provided a means to study the physiological function of mitophagy in Magnaporthe.

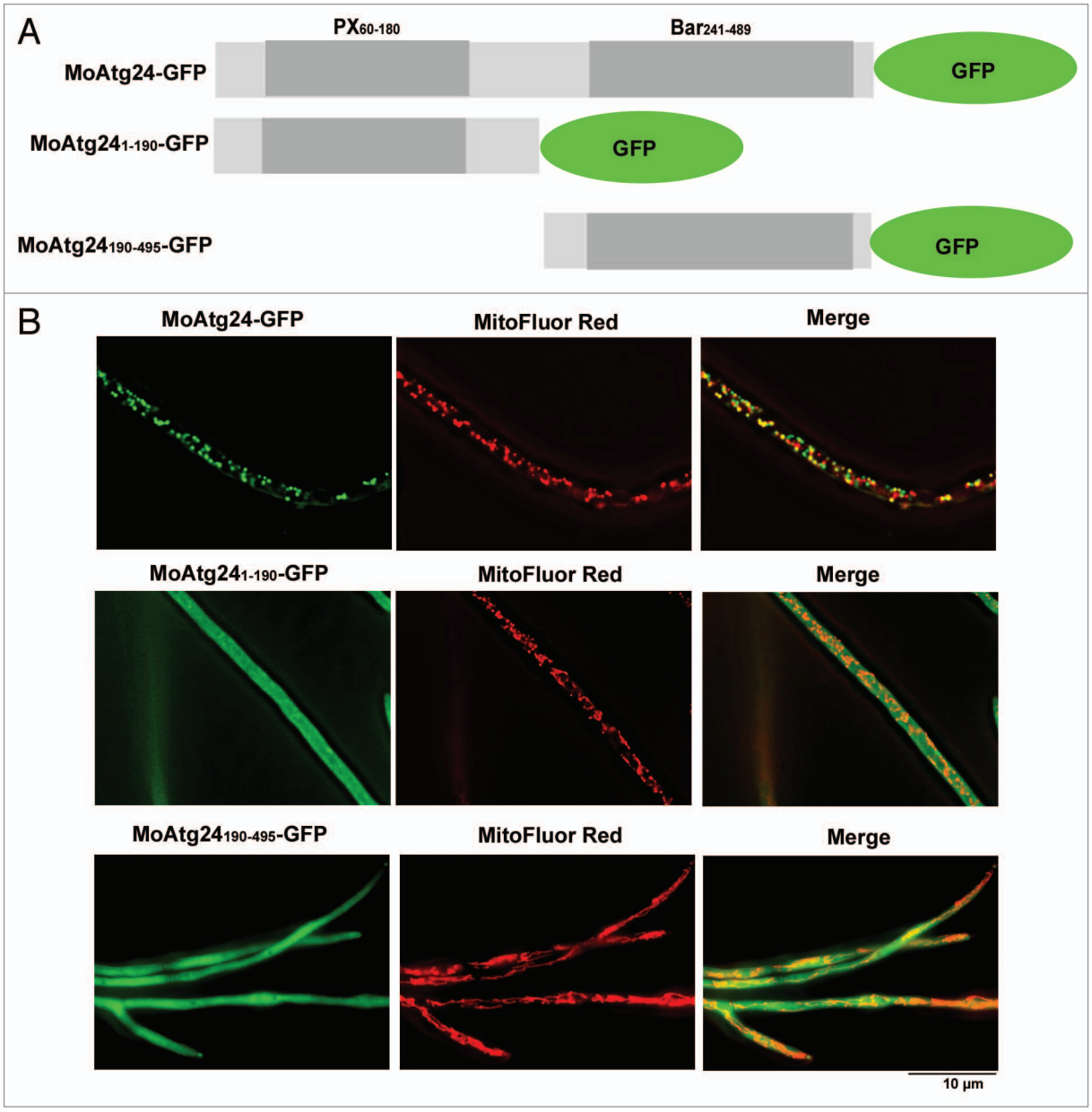

Figure 4. PX and BAR domains are required for mitochondrial anchoring of MoAtg24. (**A**) Schematic representation of construction of truncated versions of MoAtg24, tagged with GFP. (**B**) Confocal microscopy image of the strain expressing a truncated MoAtg24-GFP, co-stained with MitoFluor Red to visualize mitochondria.

Our extensive study using cell biology and biochemical analyses provides evidence that mitophagy could be significantly induced during growth transition from glycerol to nitrogen starvation. Mitophagy is very different from nonselective macroautophagy, which typically engulfs cytosolic materials including mitochondria.[21,22] Mitophagy was selectively mediated by mitochondrially-localized MoAtg24, which in turn could be induced by ROS and nitrogen starvation. We speculate that MoAtg24 reflects an aspect of adaptive evolution as the yeast mitophagy receptor ScAtg32 is not conserved in filamentous fungi including Magnaporthe.

Yeast ScAtg32 contains two functional motifs that play an

Figure 5 (See opposite page). Mitophagy during Magnaporthe conidiation. Mito-GFP-expressing WT or *Moatg24*Δ were grown on PA medium in the dark for 2 d and exposed to light to induce conidiation. Confocal microscopy was performed at 20 h post photo-induction, focusing on foot cells (FC) and aerial hyphae (AH). (**A–C**) and (**D–F**) depict two cases of FC and the connecting AH showing differential mitophagy during conidiation. (**B and C**) shows enlarged FC and AH, respectively, from (**A**). (**E and F**) show enlarged FC and AH, respectively, from (**D**). (**G–I**) Mitophagy is undetectable in the *Moatg24*Δ mutant. (**H and I**) show enlarged FC and AH, respectively, from the boxed regions in (**G**). Vacuoles based on DIC images were identified and marked by arrowheads in fluorescent images.

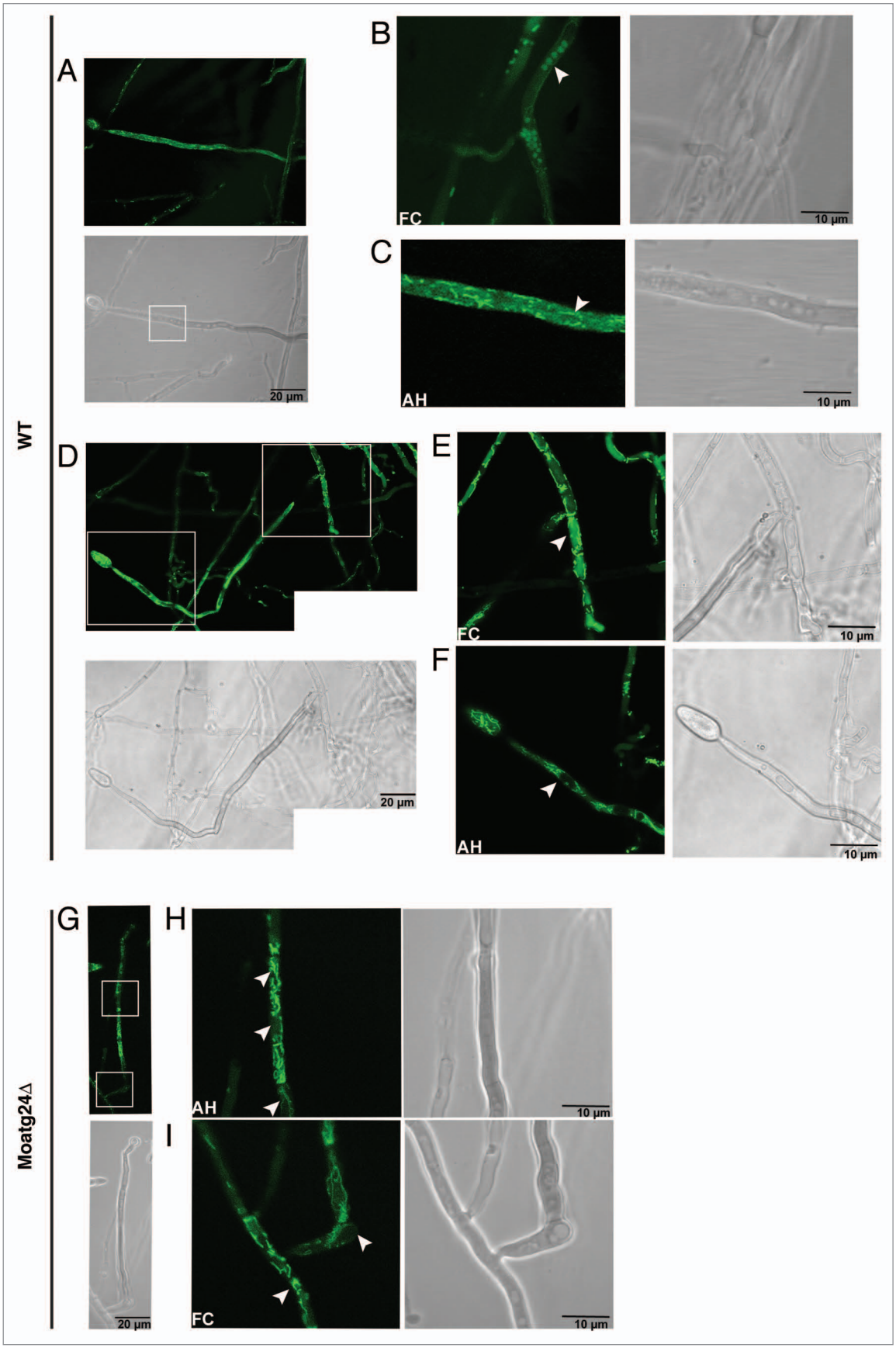

Figure 5. For figure legend, see page 6.

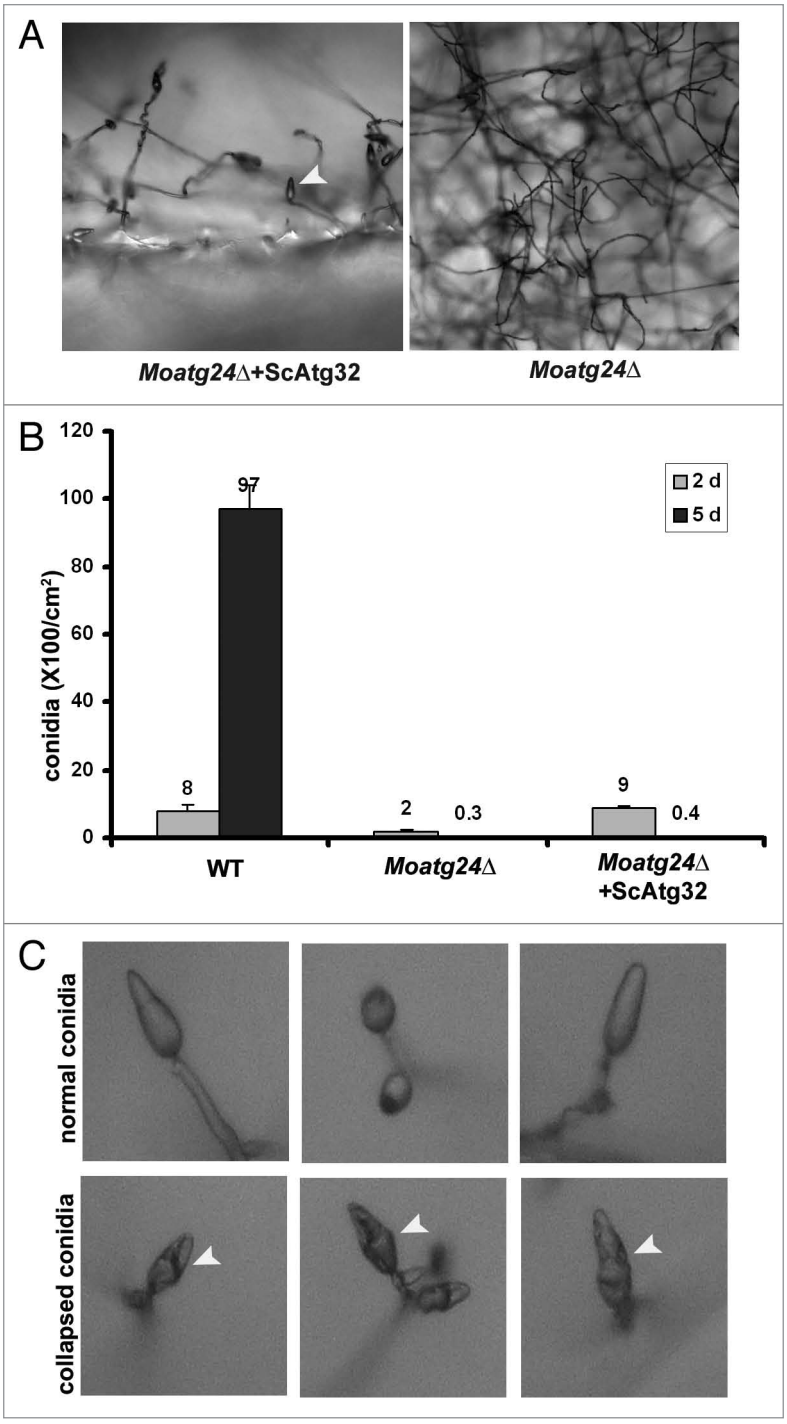

Figure 6. GFP-ScAtg32 partially restored conidiation in *Moatg24*Δ. (**A**) The *Moatg24*Δ mutant expressing GFP-ScAtg32 shows improved conidiation. (**B**) Bar chart depicts quantification of conidiation in the WT, *Moatg24*Δ or *Moatg24*Δ expressing GFP-ScAtg32 strains. Mean values (± SE) presented as percentage points were derived from three independent experiments (3 colonies for each sample). (**C**) Details of conidia formation defects in *Moatg24*Δ expressing GFP-ScAtg32. Arrowheads denote collapsed conidia.

essential role in mitophagy: the transmembrane domain mediates its localization on mitochondria, and the WXXI/L motif interacts with ScAtg8.[15,16] We showed that *M. oryzae* Atg24 contains the PX and BAR domains, which enable mitochondrial localization. Furthermore, Atg24 interacts physically with Atg17 to initiate autophagosome formation in yeast.[25] More interestingly, a WXXL motif could also be found in the N-terminal region of Atg24. Based on this comparison, the underlying mechanism for the cargo selectivity during mitophagy appears to be likely conserved in unicellular yeast and filamentous fungi: A mitochondrially-localized receptor could interact with (and recruit) an essential autophagy machinery component(s), onto the surface of mitochondria.

Another interesting observation was that mitophagy only occurs in foot cells. The function of mitophagy in foot cells during conidiation appears to be more complex than previously thought, but provides numerous questions that would certainly form the focus of future studies. The role of foot cells in conidiation could be extended from physical support and transport of nutrients to cell signaling that directly controls conidiation.[6-8] A more interesting aspect was the lack of mitophagy in aerial hyphae, although foot cells and aerial hyphae are interconnected. This observation indicates a high degree of compartmentalization in the signaling pathways and energy regulation in Magnaporthe. Future studies would certainly be directed at exploring such distinct regulation at a critical stage during asexual reproduction in the devastating rice blast pathogen.

A direct relationship between mitophagy and ROS was unearthed in this study. Exogenously added menadione and paraquat could generate mitochondria ROS specifically.[26,27] In other words, *Moatg24*Δ shows increased sensitivity specifically to mitochondrial ROS, but not to exogenous peroxides/H_2O_2. This observation confirms the role of MoAtg24 in mitophagy. Last, we speculate that MoAtg24 serves some additional function on mitochondria given that *Moatg24*Δ shows increased sensitivity to paraquat in comparison to *Moatg8*Δ.

In conclusion, the sorting nexin Atg24 in Magnaporthe showed a likely adaptive function in mitochondrial targeting as an important step toward mitophagic regulation of organellar integrity, and functions toward likely modulation of nutrient and/or redox homeostasis.

Materials and Methods

Fungal strains and growth conditions

The M. *oryzae* wild-type strain B157 was kindly provided by the Directorate of Rice Research (Hyderabad, India). All *M. oryzae* strains used in this study are described in Supplemental Data. *M. oryzae* strains were maintained and cultured on

Prune-agar (PA) medium, Basal medium (BM) or Complete medium (CM) as described previously.[11]

To quantitatively analyze conidiation, colonies were cultured on PA medium in darkness for 2 d, and then shifted to constant illumination at room temperature for 5 d. The surface of the colonies was scraped and fungal mass collected in Falcon™ conical tubes. The fungal biomass in suspension was vortexed for 30 s to detach conidia from aerial hyphae and then filtered through two layers of Miracloth (EMD Millipore, 475855-1R) to separate mycelia, hyphae and conidia. Conidia were washed twice with fresh autoclaved water and finally resuspended in sterile water. The number of conidia was counted using a hemocytometer.

Plasmid constructs and fungal transformants

To generate *Moatg24*Δ, the 5′ UTR and 3′ UTR were amplified and ligated sequentially into the *Agrobacterium* Transfer-DNA vector pFGL44[11] to flank the Hygromycin-resistance cassette. The resultant plasmid was then transferred into *M. oryzae* to induce a locus-specific knockout. The Mito-GFP/MTS-GFP construct has been described in our previous report.[28] To construct MoAtg24-GFP, eGFP was fused in frame to the last 1 kb of the *MoAtg24* ORF and the plasmid transformed into *M. oryzae*, such that the eGFP was fused to the MoAtg24 coding sequence at its genomics locus. Truncated forms of MoAtg24-GFP were made by amplifying the requisite fragments of MoAtg24 and fusing with eGFP, and were individually expressed in *M. oryzae* under control of the *TrpC* promoter.

Mitophagy, pexophagy and autophagy analysis

For mitophagy assays, the Mito-GFP-expressing strain was grown in complete medium (CM; 1 g/L yeast extract, 6 g/L casein hydrolysate, and 10 g/L sucrose) for two days, followed by 30 h growth in basal medium with glycerol (BM-G; 1.6 g/L yeast nitrogen base, 2 g/L asparagine, 1 g/L NH_4NO_3, and 1.5% V/V glycerol). Mycelia were then starved by culturing in minimal medium lacking nitrogen containing 3 mM PMSF (MM-N; 0.5 g/L KCl, 0.5 g/L $MgSO_4$, 1.5 g/L KH_2PO_4, 0.1% (v/v) trace elements, 10 g/L glucose, pH 6.5) for 6 h.[11] Vacuolar staining with CellTracker Blue CMAC (final concentration 10 μM; Molecular Probes, C2110) was performed for 30 min at room temperature (25°C) prior to microscopy observation. For biochemical assays, mycelia were then starved by culturing in MM-N for 12 h. CM-grown mycelia were washed and then subjected to nitrogen starvation (cultured in MM-N for 4, 6 or 12 h) to induce nonselective autophagy. Autophagy was analyzed following the methods described previously.[11] For pexophagy assays, strains were grown in CM for two days, followed by 20 h growth in basal medium with oleate (BM-O; 1.6 g/L yeast nitrogen base, 2 g/L asparagine, 1 g/L NH_4NO_3, and 1% V/V oleate). Mycelia were then subjected to nitrogen starvation by culturing in MM-N (with PMSF, 3 mM) for 12 h and processed accordingly for the requisite biochemical analysis.

Foot cells

To observe aerial hyphae and foot cells in detail, a mycelial plug was placed onto a thin layer of 1% agar cast on a glass slide, and then cultured in the dark. After growth for 2 d, the slides were shifted to constant illumination to induce conidiation. After 12–24 h light induction the conidiating structures were documented using bright-field microscopy.

Fluorescence microscopy

M. oryzae cells expressing fluorescent protein-fused chimera were grown for 2 d in CM or starved in MM-N. To label mitochondria, we incubated cells in requisite selection medium with 1 μM MitoFluor Red 589 (Molecular Probes, M22424) at room temperature for 30 min, followed by washing with fresh medium and further incubation in medium at room temperature for 30 to 60 min. Epiluorescence microscopy or confocal microscopy was performed as described previously.[11]

Immunoblotting

For total protein extraction, mycelia grown under requisite conditions were ground into a fine powder in liquid nitrogen and resuspended in 0.5 ml extraction buffer (10 ml Tris/Cl pH 7.5; 150 mM NaCl; 0.5 mM EDTA and 1 mg/ml protease inhibitor cocktail). Lysates were cleared up by centrifugation at 13,000 g for 20 min at 4°C. Total protein concentration was measured using the Bio-Rad Protein Assay (500-0006). Samples were resolved by 10% SDS-PAGE followed by western blotting with anti-RFP (rabbit; 1:2,000; Clontech, R10367), anti-porin (mouse; 1:2,000; Invitrogen, 459500), or anti-Pex14 (rabbit; 1:2,000; Agrisera, AS08372). Secondary antibodies were either anti-rabbit (1:10,000; Sigma-Aldrich, A0545) or anti-mouse polyclonal (1:10,000; Sigma-Aldrich, A9044) followed by detection using the enhanced chemiluminescence kit (Amersham Biosciences, RPN2108).

Disclosure of Potential Conflicts of Interest

No potential conflicts of interest were disclosed.

Acknowledgments

We thank the Fungal Pathobiology group for useful discussion and suggestions. This study was funded through grants from the Temasek Life Sciences Laboratory and the Temasek Foundation.

Supplemental Materials

Supplemental materials may be found here:
www.landesbioscience.com/journals/autophagy/article/26057

References

1. Ou SH. Rice Diseases. Surrey, UK 1985
2. Talbot NJ. Having a blast: exploring the pathogenicity of Magnaporthe grisea. Trends Microbiol 1995; 3:9-16; PMID:7719639; http://dx.doi.org/10.1016/S0966-842X(00)88862-9
3. Xue CY, Li L, Seong K, Xu JR. Fungal pathogenesis in the rice blast fungus *Magnaporthe grisea* In: Talbot NA. ed Plant-pathogen interactions Oxford OX: Blackwell Publishing, 2004:138-41
4. Wilson RA, Talbot NJ. Under pressure: investigating the biology of plant infection by *Magnaporthe oryzae*. Nat Rev Microbiol 2009; 7:185-95; PMID:19219052; http://dx.doi.org/10.1038/nrmicro2032
5. Kim S, Park SY, Kim KS, Rho HS, Chi MH, Choi J, Park J, Kong S, Park J, Goh J, et al. Homeobox transcription factors are required for conidiation and appressorium development in the rice blast fungus *Magnaporthe oryzae*. PLoS Genet 2009; 5:e1000757; PMID:19997500; http://dx.doi.org/10.1371/journal.pgen.1000757
6. Cole GT. Models of cell differentiation in conidial fungi. Microbiol Rev 1986; 50:95-132; PMID:3523190
7. Springer ML, Yanofsky C. A morphological and genetic analysis of conidiophore development in *Neurospora crassa*. Genes Dev 1989; 3:559-71; PMID:2524423; http://dx.doi.org/10.1101/gad.3.4.559
8. Wessels J, De Vries O, Asgeirsdottir SA, Schuren F. Hydrophobin genes involved in formation of aerial hyphae and fruit bodies in *Schizophyllum*. Plant Cell 1991; 3:793-9; PMID:12324614

9. Bayry J, Aimanianda V, Guijarro JI, Sunde M, Latgé JP. Hydrophobins--unique fungal proteins. PLoS Pathog 2012; 8:e1002700; PMID:22693445; http://dx.doi.org/10.1371/journal.ppat.1002700
10. Schafer DA, Gill SR, Cooper JA, Heuser JE, Schroer TA. Ultrastructural analysis of the dynactin complex: an actin-related protein is a component of a filament that resembles F-actin. J Cell Biol 1994; 126:403-12; PMID:7518465; http://dx.doi.org/10.1083/jcb.126.2.403
11. Deng YZ, Ramos-Pamplona M, Naqvi NI. Autophagy-assisted glycogen catabolism regulates asexual differentiation in *Magnaporthe oryzae*. Autophagy 2009; 5:33-43; PMID:19115483; http://dx.doi.org/10.4161/auto.5.1.7175
12. Liu X-H, Gao H-M, Xu F, Lu J-P, Devenish RJ, Lin F-C. Autophagy vitalizes the pathogenicity of pathogenic fungi. Autophagy 2012; 8:1415-25; PMID:22935638; http://dx.doi.org/10.4161/auto.21274
13. Asakura M, Ninomiya S, Sugimoto M, Oku M, Yamashita S, Okuno T, Sakai Y, Takano Y. Atg26-mediated pexophagy is required for host invasion by the plant pathogenic fungus *Colletotrichum orbiculare*. Plant Cell 2009; 21:1291-304; PMID:19363139; http://dx.doi.org/10.1105/tpc.108.060996
14. He M, Kershaw MJ, Soanes DM, Xia Y, Talbot NJ. Infection-associated nuclear degeneration in the rice blast fungus *Magnaporthe oryzae* requires non-selective macro-autophagy. PLoS One 2012; 7:e33270; PMID:22448240; http://dx.doi.org/10.1371/journal.pone.0033270
15. Youle RJ, Narendra DP. Mechanisms of mitophagy. Nat Rev Mol Cell Biol 2011; 12:9-14; PMID:21179058; http://dx.doi.org/10.1038/nrm3028
16. Okamoto K, Kondo-Okamoto N, Ohsumi Y. Mitochondria-anchored receptor Atg32 mediates degradation of mitochondria via selective autophagy. Dev Cell 2009; 17:87-97; PMID:19619494; http://dx.doi.org/10.1016/j.devcel.2009.06.013
17. Kanki T, Wang K, Cao Y, Baba M, Klionsky DJ. Atg32 is a mitochondrial protein that confers selectivity during mitophagy. Dev Cell 2009; 17:98-109; PMID:19619495; http://dx.doi.org/10.1016/j.devcel.2009.06.014
18. Kershaw MJ, Talbot NJ. Genome-wide functional analysis reveals that infection-associated fungal autophagy is necessary for rice blast disease. Proc Natl Acad Sci U S A 2009; 106:15967-72; PMID:19717456; http://dx.doi.org/10.1073/pnas.0901477106
19. Titorenko VI, Terlecky SR. Peroxisome metabolism and cellular aging. Traffic 2011; 12:252-9; PMID:21083858; http://dx.doi.org/10.1111/j.1600-0854.2010.01144.x
20. Richter C, Gogvadze V, Laffranchi R, Schlapbach R, Schweizer M, Suter M, Walter P, Yaffee M. Oxidants in mitochondria: from physiology to diseases. Biochim Biophys Acta 1995; 1271:67-74; PMID:7599228; http://dx.doi.org/10.1016/0925-4439(95)00012-S
21. Yorimitsu T, Klionsky DJ. Autophagy: molecular machinery for self-eating. Cell Death Differ 2005; 12(Suppl 2):1542-52; PMID:16247502; http://dx.doi.org/10.1038/sj.cdd.4401765
22. Xie Z, Klionsky DJ. Autophagosome formation: core machinery and adaptations. Nat Cell Biol 2007; 9:1102-9; PMID:17909521; http://dx.doi.org/10.1038/ncb1007-1102
23. Deng YZ, Qu ZW, He YL, Naqvi NI. Sorting nexin Snx41 is essential for conidiation and mediates glutathione-based antioxidant defense during invasive growth in *Magnaporthe oryzae*. Autophagy 2012; 8:1058-70; PMID:22561104; http://dx.doi.org/10.4161/auto.20217
24. Gillooly DJ, Morrow IC, Lindsay M, Gould R, Bryant NJ, Gaullier JM, Parton RG, Stenmark H. Localization of phosphatidylinositol 3-phosphate in yeast and mammalian cells. EMBO J 2000; 19:4577-88; PMID:10970851; http://dx.doi.org/10.1093/emboj/19.17.4577
25. Cheong H, Yorimitsu T, Reggiori F, Legakis JE, Wang C-W, Klionsky DJ. Atg17 regulates the magnitude of the autophagic response. Mol Biol Cell 2005; 16:3438-53; PMID:15901835; http://dx.doi.org/10.1091/mbc.E04-10-0894
26. Frei B, Winterhalter KH, Richter C. Menadione-(2-methyl-1,4-naphthoquinone-) dependent enzymatic redox cycling and calcium release by mitochondria. Biochemistry 1986; 25:4438-43; PMID:3092856; http://dx.doi.org/10.1021/bi00363a040
27. Cochemé HM, Murphy MP. Complex I is the major site of mitochondrial superoxide production by paraquat. J Biol Chem 2008; 283:1786-98; PMID:18039652; http://dx.doi.org/10.1074/jbc.M708597200
28. Patkar RN, Ramos-Pamplona M, Gupta AP, Fan Y, Naqvi NI. Mitochondrial β-oxidation regulates organellar integrity and is necessary for conidial germination and invasive growth in *Magnaporthe oryzae*. Mol Microbiol 2012; 86:1345-63; PMID:23043393; http://dx.doi.org/10.1111/mmi.12060